CHARACTERIZATION OF A NOVEL FIS1 INTERACTOR REQUIRED FOR PERIPHERAL DISTRIBUTION OF THE MITOCHONDRION OF *TOXOPLASMA GONDII*

Kylie Jacobs

Submitted to the faculty of the University Graduate School

in partial fulfillment of the requirements

for the degree

Doctor of Philosophy

in the Department of Microbiology and Immunology,

Indiana University

February 2021

Accepted by the Graduate Faculty of Indiana University, in partial fulfillment of the requirements for the degree of Doctor of Philosophy.

Doctoral Committee

_____
Gustavo Arrizabalaga, Ph.D., Chair

_____
Stacey Gilk, Ph.D.

December 3, 2020

_____
Brett Graham, M.D., Ph.D.

_____
Chandy John, M.D., M.S.

_____
Frank Yang, Ph.D.

Acknowledgments

Firstly, I would like to thank my parents for nurturing my love of science and supporting me as I followed my dreams. Without them, I would not be the woman and scientist I am today. To my friends, I am forever grateful for being my biggest cheerleaders and for always making me laugh on the hard days. To Wall-E, thank you for being a constant companion, unintentional weighted blanket, and making me laugh with your antics. I extend my greatest thanks to the teachers in my life that have led me down this career path. Mr. James, Dr. Fu, and Dr. Pikaart introduced me to academia and showed me the power of hard work and dedication. I would like to thank Dr. Clayton Wiley for giving me my first true research experience and to his wonderful lab for their encouragement and teaching. I extend my sincerest thanks to the IBMG program, Tara Hobson, and Brandy Wood for welcoming me to Indianapolis and always being there. To my committee, I want to thank you for pushing me, providing me with amazing ideas, and fostering my creativity in research. I am deeply grateful to my lab for giving me a home away from home and friends I will cherish for a lifetime. I owe my greatest thanks to my mentor, Dr. Gustavo Arrizabalaga, who has made me into the scientist I am today. His guidance, support, and patience are immeasurable and I am eternally grateful for everything he has taught me.

I would like to thank Dr. Isabelle Coppens at Johns Hopkins for performing transmission electron microscopy, Dr. Diego Huet for providing DiCre∆*ku80* SOD2-GFP IMC1-TdTomato parasites. I would also like to thank Dr. Peter Bradley

for generously providing reagents and correspondence. This work was by grants from the National Institutes of Health to Gustavo Arrizabalaga (R01AI123457 and R21AI138255) as well as a fellowship from NRSA training grant T32AI060519 to Kylie Jacobs.

Kylie Jacobs

CHARACTERIZATION OF A NOVEL FIS1 INTERACTOR REQUIRED FOR PERIPHERAL DISTRIBUTION OF THE MITOCHONDRION OF *TOXOPLASMA GONDII*

Toxoplasma's singular mitochondrion is extremely dynamic and undergoes morphological changes throughout the parasite's life cycle. While intracellular, the mitochondrion is maintained in a lasso shape that stretches around the parasite periphery and is in close proximity to the pellicle, suggesting the presence of membrane contact sites. Upon egress, these contact sites disappear, and the mitochondrion retracts and collapses towards the apical end of the parasite. Once reinvaded, the lasso shape is quickly reformed, indicating that dynamic membrane contact sites regulate the positioning of the mitochondrion. We discovered a novel protein (TgGT1_265180) that associates with the mitochondrion via interactions with the fission related protein Fis1. Knockout of TgGT1_265180, which we have dubbed LMF1 for Lasso Maintenance Factor 1, results in a complete disruption of the normal mitochondrial morphology. In intracellular LMF1 knockout parasites, the mitochondrial lasso shape is disrupted, and instead it is collapsed as normally only seen in extracellular parasites. Additionally, proper mitochondrial segregation is disrupted, resulting in parasites with no mitochondrion and extra mitochondrial material outside of the parasites. These gross morphological changes are associated with a significant reduction of parasite propagation and can be rescued by reintroduction of a wildtype copy of LMF1. Co-immunoprecipitations and Yeast

Two-Hybrid predict interactions with the parasite pellicle. Therefore, we hypothesize that LMF1 mediates contact between the mitochondrion and the pellicle in a regulatable fashion, and that the LMF1-dependent morphodynamics are critical for parasite propagation. Current studies are focused on characterizing the consequences of mitochondrial collapse and identifying proteins that interact with LMF1 to position the mitochondrion to the periphery of the parasite.

Gustavo Arrizabalaga, Ph.D., Chair

Table of Contents

List of Tables

List of Figures

List of Abbreviations

acTub	Acetylated tubulin
AIDS	Acquired Immunodeficiency Syndrome
ANOVA	Analysis of variance
Ato	Atovaquone
ATRX1	Apicoplast thioredoxin 1
cDNA	Complementary deoxyribonucleic acid
CDPK	Calcium-dependent protein kinase
CERT	Ceramide transport protein
comp	Complement
CRISPR	Clustered Regularly Interspaced Short Palindromic Repeats
CTS	C-terminal sequence
DAPI	4’,6’-diamidino-2-phenylindole
DD	Destabilization domain
DHFR	Dihydrofolate reductase
DLP	Dynamin-like protein
DMEM	Dulbecco’s modified Eagle medium
DMSO	Dimethylsulfoxide
DNA	Deoxyribonucleic acid
Dnm1	Dynamin 1
Drp	Dynamin-related protein
E	Early
ER	Endoplasmic reticulum
ERMES	ER-Mitochondria Encounter Structure
FBS	Fetal bovine serum
FHA	Fork-head associated
Fis1	Fission 1
GC	guanylyl cyclase
GDP	Guanosine diphosphate
GFP	Green fluorescent protein
grp75	Glucose-regulated protein 75
GTP	Guanosine triphosphate
HA	Hemagglutinin
HFF	Human foreskin fibroblast
HPT	Hypoxanthine-xanthine-guanine phosphoribosyl transferase
I	Intermediate
IFA	Immunofluorescence assay
ILP1	Inner membrane localizing protein 1

IMC	Inner membrane complex
IMM	Inner mitochondrial membrane
IP	Immunoprecipitation
IP_3R	Inositol 1, 4, 5-triphosphate receptor
KO	Knockout
L	Late
LMF1	Lasso Maintenance Factor 1
LOK1	Loss of kinetoplast 1
LOPIT	Localization of Organelle Proteins by Isotope Tagging
MCS	Membrane contact site
Mdv1	Mitochondrial division 1
MFNL	Mitofusin-like
Mon	Monensin
mtDNA	Mitochondrial DNA
myc	Myelocytomatosis peptide
Myx	Myxothiazol
OMM	Outer mitochondrial membrane
PAM	Protospacer adjacent motif
Par	Parental
PBS	Phosphate buffered saline
PCR	Polymerase chain reaction
PrBS	Predicted biological score
PTM	Posttranslational modification
PV	Parasitophorus vacuole
Pyr	Pyrimethamine
RNA	Ribonucleic acid
Rop1	Rhoptry 1
SAG1	Surface antigen 1
SDS-PAGE	Sodium docecyl sulfate polyacrylamide gel electrophoresis
SERCA	Sarco/endplasmic reticulum Ca2+-ATPase
sgRNA	Small guide RNA
SID	Selected interaction domain
SOD2	Superoxide dismutase 2
TM	Transmembrane
TPR	Tetratricopeptide repeat
UPRT	Uracil phosphoribosyltransferase
UTR	Untranslated region
VDAC1	Voltage-dependent anion channel 1
Veh	Vehicle
WT	Wild-type

Y2H	Yeast two-hybrid

Chapter 1: Introduction

Natural history of *Toxoplasma gondii*

In 1908, two researchers were studying *Leishmania* in a small rodent species called the gundi when they discovered a new parasite. Nicolle and Manceaux at the Pasteur Institute in Tunisia named the genus of this novel organism *Toxoplasma* for its morphology, with *toxo* meaning “bow” and *plasma* meaning “life” (1, 2). However, the researchers had identified the host, *Ctenodactylus gundi*, incorrectly thus creating the species name *gondii* rather than *gundi*. Almost simultaneously, Dr. Alfonso Splendore working in Brazil identified the same parasite in rabbits. After *Toxoplasma gondii* was given its official nomenclature, it was identified in various other species, including birds, and was eventually isolated and identified in a human sample, as well (1).

Toxoplasma gondii was classified into the phylum Apicomplexa, which contains a number of parasites of both health and agricultural importance, such as *Plasmodium spp.,* the causative agent of malaria (3–5). Apicomplexa are obligate, intracellular parasites that infect a wide variety of host species and have unique organelles that contribute to this infectivity. The apical complex, the structure for which the phylum is named, coordinates secretion events essential for motility, invasion, and maintenance of the intracellular niche (5, 6). Within the Apicomplexa, *Toxoplasma* is subcategorized as a coccidian, which includes those apicomplexan parasites that are shed in the feces of the definitive host. These include *Eimeria* and *Cryptosporidium*, both diarrheal agents. In the over 110 years since its discovery, *Toxoplasma gondii* is considered the model organism of the over 6,000

species identified and named Apicomplexans due to its genetic tractability and ease of culturing.

Life cycle of *Toxoplasma gondii*

Toxoplasma has two major life cycles: the sexual cycle, which only occurs in felines, and the asexual cycle, which occurs in any other warm-blooded animal such as livestock and humans. In the gut of the feline, ingested parasites can invade the intestinal epithelium. After invasion, parasites will differentiate into schizonts and eventually will develop into merozoites. These merozoites then undergo a few rounds of division before they differentiate into either macrogametes or microgametes, the *Toxoplasma* life stage that allows for sexual reproduction. Macrogametes fuse with microgametes to form diploid oocysts, which are shed in the cat's feces (7). These oocysts sporulate and become extremely infectious and are able to remain stable in the environment for over a year (8). These sexual stages only occur in the gastrointestinal system of felids due to the lack of delta-6-desaturase in the small intestine, producing higher than normal levels of linoleic acid (9). Prey species, such as rodents and birds, can ingest these infectious oocysts in the environment and develop into tissue cysts. Thus, felines can acquire the parasite consuming infected prey animals or by consuming environmental oocysts, thus completing the sexual cycle of *Toxoplasma gondii.*

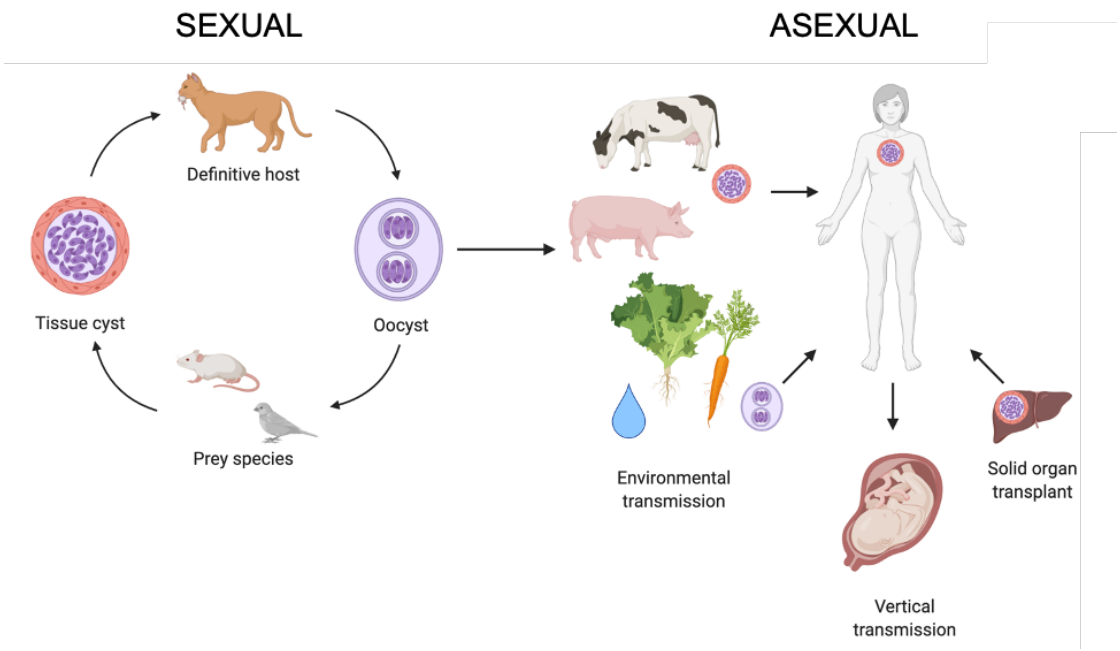

Figure 1. Life cycle of *Toxoplasma gondii*. Diagram showing the sexual and asexual stages of the parasite life cycle. The sexual stage of the parasite life cycle occurs in felines, where the parasite sexually recombines in the gut and is excreted as infectious oocysts. Oocysts in the environment can infect any warm-blooded animal, including prey species, and form tissue cysts. Cats will ingest infected prey, which will reinitiate the sexual life cycle. Humans can be infected through direct ingestion of oocysts, through routes of food contamination in meat and produce, transplacentally from the mother, or through solid organ transplant from a seropositive patient. Created with BioRender.com.

The infectious environmental oocyst can also be consumed by other warm-blooded species including humans initiating the asexual cycle. Oocyst-driven infections in humans are typically due to ingestion of oocyst contaminated water supplies, or unwashed produce, and from oocysts in cat litter boxes, garden beds or sand boxes. Once ingested, the parasites escape the oocyst and disseminate throughout the new host as tachyzoites, the fast replicating form of the asexual life cycle (10). Tachyzoites are able to infect almost any nucleated cell, with tropism for the central nervous system, muscle tissue, and cardiac tissue. When

recognized by the immune response of the host, the tachyzoite differentiates into the bradyzoite, which is encased in a thick cyst wall and replicates very slowly (10). Warm-blooded animals can be also infected through carnivorism of infected animals. Accordingly, humans can become infected by eating undercooked or raw meat that contains these tissue cysts, thus restarting the asexual cycle in a new host. In both cases, the parasites will disseminate and form chronic tissue cysts that will persist throughout the host's life. If a woman is infected for the first time while she is pregnant, the parasite can be vertically transmitted from mother to fetus. This transmission can cause a number of birth defects, miscarriage, and even still birth (11, 12). Transmission can also occur during solid organ transplant from an infected individual to a seronegative individual (13). These many routes of infection and infectivity of numerous hosts and cell types contributes to the ubiquitous nature of this parasite.

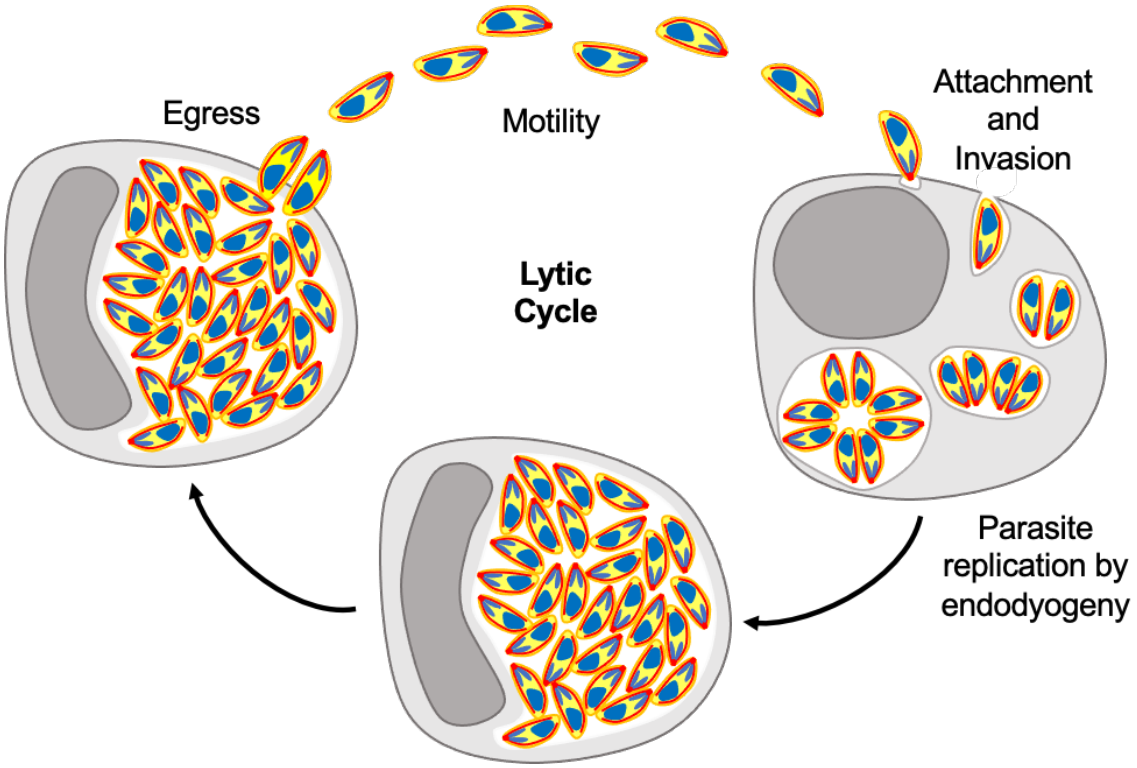

Figure 2. Lytic cycle of *Toxoplasma gondii* tachyzoites. Diagram depicting the asexual lytic cycle in which free tachyzoites attach to a host cell and actively invade to form a parasitophorous vacuole. Within that vacuole, the parasite replicates through a process called endodyogeny, which causes the parasite number to double after each round of replication. After several rounds of replication, the parasites undergo a controlled egress and are able to move to the next cell.

During the tachyzoite stage of asexual infection, the parasite propagates through multiple rounds of a lytic cycle in which the parasite invades, divides, and undergoes egress from a host cell (Fig. 2). Briefly, extracellular tachyzoites actively attach to a host cell and secrete factors that enhance the attachment and drive invasion. *Toxoplasma* then actively invades the host cell and forms a parasitophorous vacuole around itself through an invagination of the host cell plasma membrane and pinching off the membrane at the moving junction (5, 14). Once within this vacuole, the parasite is able to initiate division. *Toxoplasma*

divides through a process called endodyogeny, where two daughter parasites form within a single mother parasite (15). Daughters form cytoskeletal components into which newly formed and divided organelles can partition. Of these organelles, the mitochondrion is the last to migrate along the daughter IMC and integrate into the almost fully formed daughters (16). At the end of endodyogeny, the daughters emerge from the mother, themselves in the mother plasma membrane. Because two daughters form in each mother, the parasite number doubles each round of division, which occurs every 6-12 hours in tissue culture (Fig. 2)(15, 17, 18). As the parasite divides, the parasitophorous vacuole (PV) grows and occupies the majority of the host cell cytoplasm, at which point *Toxoplasma* can initiate a controlled egress to release tachyzoites into the extracellular space (19, 20). Parasites then migrate and attach to a new host cell to start the lytic cycle over.

Toxoplasmosis

Toxoplasma gondii is the causative agent of toxoplasmosis, a disease characterized by extensive tissue damage and can be life-threatening in immunocompromised individuals. Approximately one-third of the world is infected chronically with *Toxoplasma,* causing approximately 750 deaths each year (21, 22). In the immunocompetent person, toxoplasmosis presents with mild, flu-like symptoms and lasts for a couple of weeks. This acute infection will be forced into a chronic stage of infection by the host immune system, inducing the formation of tissue cysts that persist throughout the host's life. However, in those who are immunosuppressed, such as those being treated with certain chemotherapies and

patients with AIDS, a primary infection or the reactivation of encysted parasites can lead to severe tissue damage, seizures, and in some cases death (23). In these individuals, the immune system is not effective enough to ameliorate the acute infection and the parasite is able to constantly divide and lyse cells, causing significant tissue damage.

Pregnant mothers who are infected for the first time during pregnancy or have a reactivation of the acute infection while pregnant can pass toxoplasmosis to the fetus. Fetal infection is relatively rare, but the risk of infection from an acutely infected mother increases to 60-81% during the third trimester from 20% during the first trimester (24). However, infection *in utero* can cause a number of birth defects including mental retardation, seizures, hydrocephalus, miscarriage, and even still birth (11). Currently, the accepted treatment to prevent congenital infection is spiramycin, a macrolide antibiotic that has been observed to decrease the frequency of vertical transmission (25). However, if congenital infection is confirmed through PCR of amniotic fluid, then the course of treatment includes pyrmethamine, sulfadiazine, and folinic acid (26). Since pyrmethamine is relatively toxic and teratogenic, it is not recommended during the first trimester and still has significant risks for birth defects throughout pregnancy (11, 26). Infants infected during the first trimester tend to have more severe symptomology, whereas those infected later in pregnancy are usually born asymptomatic with developmental defects later on (11, 27). One of these defects that affects infants in long-term infection is chorioretinitis, which is the inflammation of the lining of the retina (28). In these cases, *Toxoplasma* can cause scarring of the retinal tissue, which some

reactivation along the borders of the scar (29). Ocular toxoplasmosis can reactivate throughout the host's life and the cause of this reactivation is currently unknown. Interestingly, South American countries have a much higher prevalence of ocular toxoplasmosis, with ~20% of seropositive cases resulting in ocular infection compared to 1-2% of infections in the United States (30).

Toxoplasma gondii cell biology

Toxoplasma gondii is part of the kingdom Alveolata, which include species designated as alveolates. Alveolates contain alveolar "sacs" that are flattened vesicles that reside under the plasma membrane, creating a structural support system. Alveolata includes dinoflagellates and apicomplexans, which both have flattened membranous sacs, non-photosynthetic plastid organelles, and a microtubule organizing center or cone (4, 31). In apicomplexans, the relic plastid organelle is the apicoplast (Figure 3, blue) which is important for isoprenoid production, fatty acid synthesis, and potentially completes the citric acid cycle from the mitochondrion through a citrate shunt (32, 33). Apicomplexans are such named for the apical complex, which is a structure at the apical end of the parasite that includes the microtubule organizing center, called the conoid in *Toxoplasma*. From this conoid, 22 subpellicular microtubules emanate and extend 2/3 the length of the parasite and are important for maintaining structure, rigidity, and allowing movement (6, 34). Sitting between these microtubules and the parasite plasma membrane is the inner membrane complex (IMC), which is made up of alveolar sacs stitched together (15, 17, 35). The plasma membrane and the IMC make up

the parasite pellicle (Fig. 3). Beneath the IMC is a network of intermediate filaments that make up the subpellicular network (36).

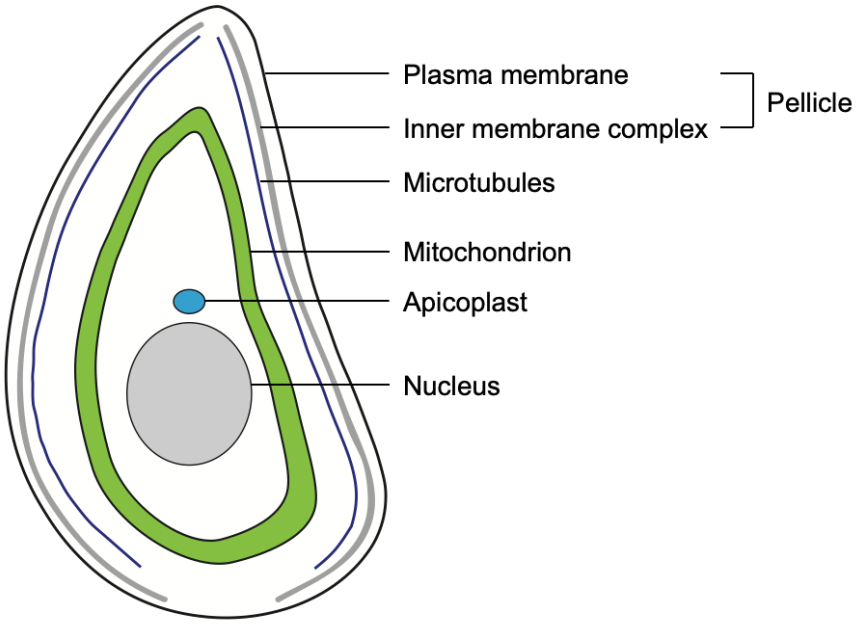

Figure 3. Cellular structures of *Toxoplasma gondii.* Schematic indicating the shape of the mitochondrion and its proximity to the microtubules, IMC, and plasma membrane.

During parasite division, daughter parasites first start to form their own IMCs that provide a scaffold for organelle partitioning between the two new parasites. As these new IMCs form, organelles are continuously incorporated into the forming daughters through a highly coordinated process. Some organelles are made *de novo*, such as the micronemes and dense granules. Other organelles, such as the apicoplast and the mitochondrion, are formed from the mother organelle and divided between daughters (16, 18). During this process, the parasite mitochondrion begins to form branches that extend into the forming daughter parasites to establish the typical lasso shape (16). Interestingly, this incorporation of the mitochondrion into the daughters occurs very late in endodyogeny and the

mitochondria are not fully integrated into the new parasites until they are already emerging from the mother parasite (16). Until this point, the mitochondrion is completely excluded from the daughter parasites. Currently, there is a knowledge gap in what proteins are involved in the branching of new mitochondrial material, forming membrane contact sites with the IMC for proper mitochondrial segregation, and what factors are involved in mitochondrial division.

Mitochondrial dynamics and division

The mitochondrion is most well-known for being the powerhouse of the cell and an important hub for metabolism. Essential functions of the mitochondrion are highly dependent on the structure of the mitochondrion, its biogenesis, and quality control. The mitochondrion is also involved in essential signaling mechanisms, transport of proteins and nutrients throughout the cell, and forming contact sites with other organelles to mediate lipid and calcium transport (37–39). Two such important mitochondrial dynamic processes are fusion and fission of mitochondria. Mitochondrial fusion is the process of two or more mitochondria coming together to form an elongated network of mitochondrial material (Fig. 4). One instance in which this process occurs is after treatment with a DNA damaging agent, like cycloheximide, which can damage both nuclear DNA and mitochondrial DNA (mtDNA) (40). Once damaged, mitochondria will fuse to promote DNA mixing to complement and repair the damaged DNA fragments. In another example, growing *Saccharomyces cerevisiae* in anaerobic conditions results in fused mitochondria (41). In contrast, mitochondria also undergo mitochondrial fission to produce more

mitochondria, to promote mitophagy of damaged mitochondria, and in response to drugs that affect mitochondrial respiration, such as oligomycin (42, 43). Additionally, *S. cerevisiae* mitochondria show a fragmented, punctate phenotype in aerobic environments where respiration is more favorable (41).

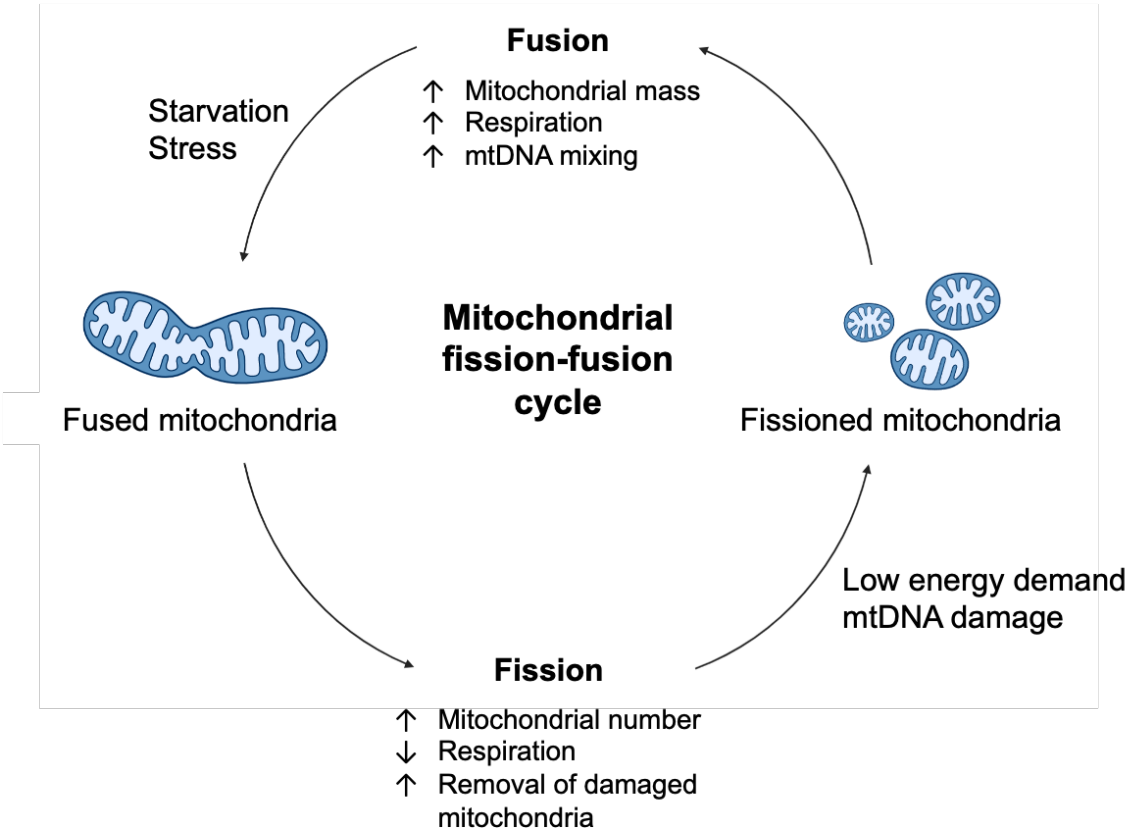

Figure 4. Schematic of mitochondrial fission-fusion cycle. Diagram indicating mitochondrial fusion, shown as multiple mitochondria coming together to make an elongated mitochondrion, and fission, where the mitochondria divides to make more mitochondria. Created with BioRender.com.

Mitochondria are constantly altering their shape and undergoing both fission and fusion events. In yeast, mitochondrial fission is initiated by an outer mitochondrial membrane protein called Fission 1, or Fis1. Fis1 is a tail-anchored outer mitochondrial membrane protein that recruits adaptor proteins, like

mitochondrial division 1 (Mdv1), to the mitochondria (44). Once recruited, a dynamin related protein such as dynamin 1 (Dmn1) is able to bind to the adaptor and initiate oligomerization. Dmn1 oligomerizes to form a ring and, once GTP is hydrolyzed to GDP and inorganic phosphate, begins to constrict the mitochondrion (45, 46). In yeast, the endoplasmic reticulum is then recruited to these sites of mitochondrial constriction and the ER tubules wrap around preconstricted sites to initiate final scission (38, 47). This eventually leads to complete fission and the production of two mitochondria. This process requires three components: a protein anchored to the outer mitochondrial membrane (OMM), adaptor protein(s), and a dynamin-related protein (45).

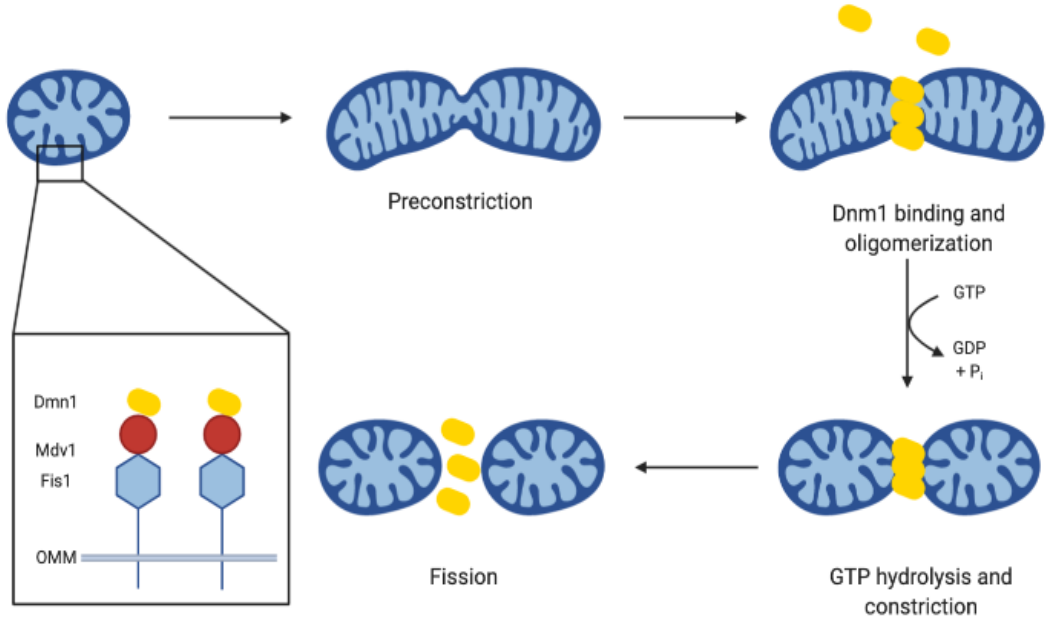

Figure 5. Model of mitochondrial fission in yeast. Diagram of the process of a mitochondrion dividing into two. First, the mitochondrion starts to constrict, and Fis1 (blue hexagon) recruits adaptors like Mdv1(red circle) to form a platform for Dmn1 (yellow) at the site of constriction. Dmn1 oligomerizes to form a contractile ring and upon GTP hydrolysis, the ring constricts further, eventually leading to fission of the mitochondrion. Created with BioRender.com.

In *Toxoplasma gondii,* there is one singular, large mitochondrion that extends to the parasite periphery, producing a lasso shape in intracellular parasites. Because there is only one mitochondrion, it is unlikely that there is a mitophagy process, which is corroborated by the lack of homologs to mitophagy proteins of other system. Additionally, there are no traditional homologs to proteins involved in fusion, indicating that the parasite's mitochondrion does not undergo this part of the fission-fusion cycle or it does so with non-canonical factors. However, the mitochondrion of *Toxoplasma* still continues to change its shape throughout the parasite lytic cycle. In intracellular parasites, the mitochondrion is a large loop. During division, the mitochondrion encircles the forming daughter parasites and begins to form branches that extend into the daughters during the last stages of division before the daughter egresses from the mother (16). These branches migrate along the daughter cytoskeletons to reform the traditional lasso shape. After multiple division cycles, the parasite undergoes a controlled egress from the host cell. In the extracellular environment, the mitochondrion begins to retract from the parasite periphery to form a sperm-like morphology, with a large balled portion of mitochondrial material and a tail extending towards the basal end of the parasite (48). As *Toxoplasma* remains extracellular, the percentage of parasites with sperm-like mitochondria increases and the mitochondria eventually collapse into a ball at the apical end of the parasite. Upon reinvasion into a new host cell, the lasso reforms and division can continue (48). In addition to mitochondrial morphology changes throughout the parasite lytic cycle, the mitochondrion of *Toxoplasma gondii* also alters its morphology in the presence of

certain stressors, such as drug treatment and amino acid starvation (49–51). Treatment with the anti-coccidial drug monensin results in global disruption of membranes and, specifically, a punctation of the mitochondrion seen by F_1B ATPase staining (49, 52) (Fig. 6B). In *Toxoplasma,* there are very few homologs to fusion or fission proteins and there are no homologs to the adaptor proteins identified in yeast (Fig. 5). *Toxoplasma gondii* contains three identified dynamin-related proteins (Drps): DrpA, DrpB, and DrpC. DrpA and DrpB are involved in apicoplast division and biogenesis of secretory organelles, respectively (53, 54). TgDrpC is an atypical GTPase because it lacks a conserved GTPase Effector Domain, which is typically required for function. Our lab recently showed that TgDrpC localizes to cytoplasmic puncta that redistribute to the growing edge of the daughter cells during division and that loss of TgDrpC stalls division and leads to rapid deterioration of multiple organelles (55). This association with growing daughters during endodyogeny was recently corroborated by Amiar et al. (56). Interestingly, our lab showed that TgDrpC interacts with proteins that exhibit homology to those involved in vesicle transport, including the AP2 adapter complex, which was confirmed by Ross Waller's group while investigating AP2 interacting proteins (Toxoplasmosis Congress 2019, Colombia). Based on these results, TgDrpC appears to contribute to various processes including vesicle trafficking, organelle stability and division. Whether mitochondrial division is part of its function remains unclear but its association with the edge of the IMC late in division when the mitochondrion enters the daughter parasites could suggest an interaction with the mitochondrion during fission. This is supported by the results

of Melatti et al. in which a dominant negative allele of DrpC halts mitochondrial division (57). Nonetheless, despite significant efforts to define the mechanisms and proteins driving mitochondrion division in *Toxoplasma* significant knowledge gaps remain.

Toxoplasma has one Fis1 homolog (TGGT1_263323) that contains a C-terminal transmembrane domain and two tetratricopeptide repeat (TPR) domains, that are necessary for adaptor recruitment and binding (Fig. 5A) (58, 59). A striking aspect of monensin treatment of *Toxoplasma* is the disruption of mitochondrial morphology, producing what appears to be a fragmented organelle. A survey of the *Toxoplasma* database (ToxoDB) to identify homologs involved in mitochondrial dynamics revealed that the genome of *Toxoplasma* is rather bereft of proteins that participate in the fusion and fission processes. However, we were able to identify a protein (TGGT1_263323) with homology to the fission 1 (Fis1) protein from higher eukaryotes. TGGT1_263323, referred to hereafter as Fis1, is a 154 amino acid protein and contains two tetratricopeptide (TPR) domains, a C-terminal transmembrane (TM) domain followed by a three amino acid C-terminal sequence (CTS). In previous work focused on the characterization of membrane anchor domains in *Toxoplasma*, our lab showed through transient transfection of an N-terminal HA tagged Fis1 that it localized to the mitochondrion (60). In order to further characterize the localization and function of Fis1, our lab established a parasite strain stably expressing an N-terminally HA epitope-tagged version of Fis1 under the control of the SAG1 promoter (Fig. 6B, top panel). Immunofluorescence assay (IFA) of intracellular parasites of this strain (RHΔ*hpt*+HAFis1) confirmed that

Fis1 localized to the parasite mitochondrion by co-localization with F_1B ATPase protein, which is located in the inner mitochondrial membrane (IMM) (Fig. 6B). This strongly suggests that, as expected for Fis1 proteins, Fis1 localizes to the outer mitochondrial membrane.

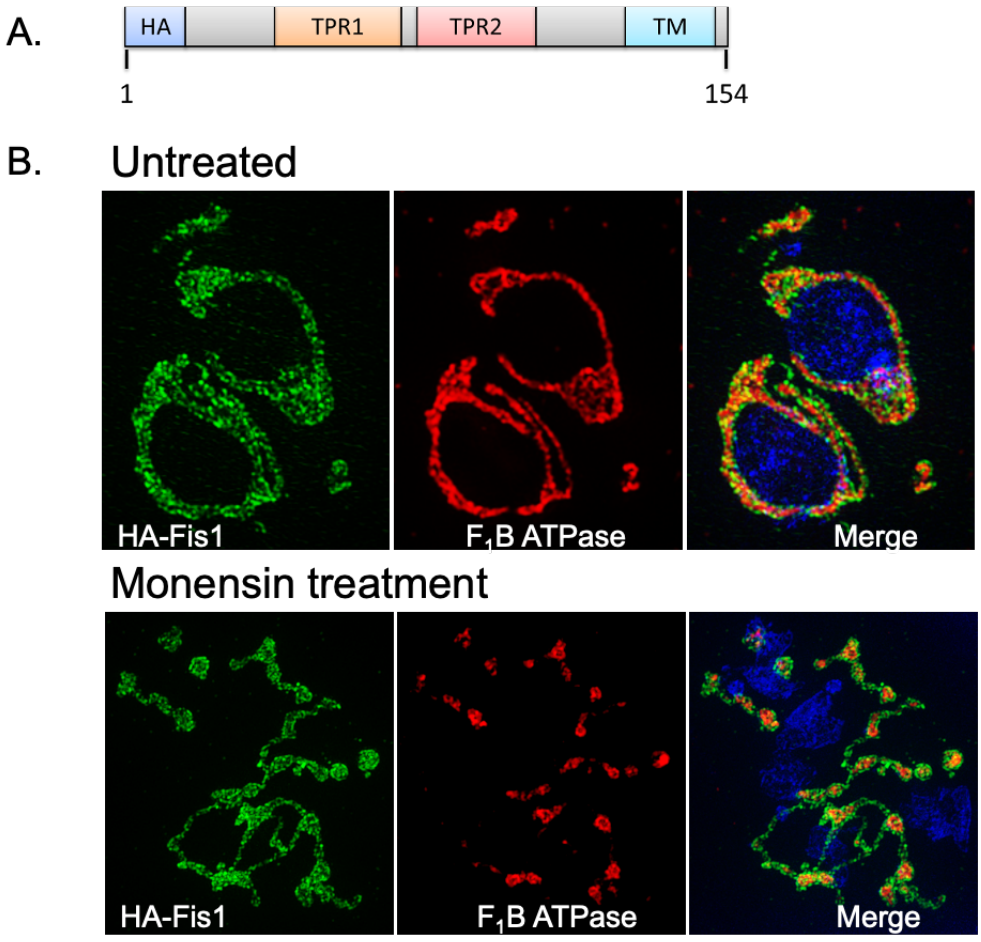

Figure 6. Fis1 localizes to the Toxoplasma outer mitochondrial membrane, which remains intact after monensin treatment. To determine the subcellular distribution of the fission protein homolog Fis1, a parasite strain expressing an ectopic copy of Fis1 including an N-terminal HA epitope tag was generated. (A) Illustration shows the exogenously expressed epitope-tagged Fis1. Protein domains in Fis1 are indicated: tetratricopeptide repeat domains TPR1 and TPR2 and transmembrane (TM) domain. (B) Intracellular parasites of the (HA)Fis1-expressing strain were analyzed by IFA using antibodies against the HA tag to detect Fis1 (in green) and against the Toxoplasma F_1B ATPase protein to delineate the inner mitochondrial membrane (in red) using an OMX 3D-SIM

superresolution imaging system. In the second panel, intracellular parasites were treated for 8 h with monensin (1 ng/mL). Bar, 2 μm (61).

Our lab has demonstrated that multiple organelles, including the mitochondrion, are affected by treatment with the anti-coccidial drug, monensin. Monensin is a Na^+/H^+ ionophore than causes autophagy and mitochondrial fragmentation in *Toxoplasma gondii* (49, 62). Since we established that Fis1 localizes to the OMM, we were able to observe the effects of monensin on both the outer and inner mitochondrial membranes. After 8 hours of treatment with 1ng/mL monensin, the inner mitochondrial membrane became punctate (Fig. 6B, red), as observed previously (49, 61). However, the OMM remained intact and connected the inner mitochondrial fragments like beads on a string (Fig. 6B, green). Therefore, the previous observation of mitochondrial punctation in the presence of monensin is actually a constriction of the mitochondrion (Fig. 6B).

Our previous studies have shown that the TM domain of Fis1 is sufficient for mitochondrial targeting (60). To determine whether the TM is necessary for mitochondrial localization our lab established a parasite strain that endogenously replaced the TM and CTS of Fis1 with a HA tag using homologous recombination (Fig. 7A). Intracellular parasites of this strain were co-stained with antibodies against HA to detect Fis1ΔTM and against F_1B ATPase to visualize the mitochondrion (Fig. 7B). Eliminating the TM of the endogenous Fis1 shifted its localization from the mitochondrion to the cytoplasm (Fig. 7B). Thus, proper Fis1 localization to the OMM is dependent on its C-terminal transmembrane domain and CTS.

When analyzing the localization of the truncated endogenous Fis1 it was noted that the morphology of the mitochondrion appeared abnormal. Instead of the typical lasso seen in wildtype parasites (Figs. 3 and 7), the mitochondrion in parasites of the RHΔ*ku80*:Fis1ΔTM strain appeared to contain additional branches as well as unconnected strands, a phenotype that seemed to increase as the parasites underwent several rounds of division (Fig. 7B). In the RHΔ*ku80*:Fis1ΔTM strain, 60.4±7.5% of vacuoles had parasites with atypical mitochondrion (i.e. extraneous branches and strands). This is in contrast to the parental strain in which only 12.7±3.4% of vacuoles had parasites with atypical mitochondrion (Fig. 7C). These observations suggest that mislocalizing the endogenous Fis1 alters the typical mitochondrial morphology.

The phenotypes observed with the RHΔ*ku80*:Fis1ΔTM parasites could be due to either absence of Fis1 at the mitochondrion or a dominant negative effect from the mislocalized truncated protein. To differentiate between these possibilities, we next sought to determine how genetic ablation of Fis1 would affect the parasite's ability to respond to monensin challenge and undergo mitochondrial remodeling. Interestingly, in contrast to what is observed with mislocalized Fis1, complete lack of Fis1 did not affect the mitochondrial morphology (57, 61). Thus, it appears that Fis1 lacking the TM domain imparts a dominant negative effect on mitochondrial morphology.

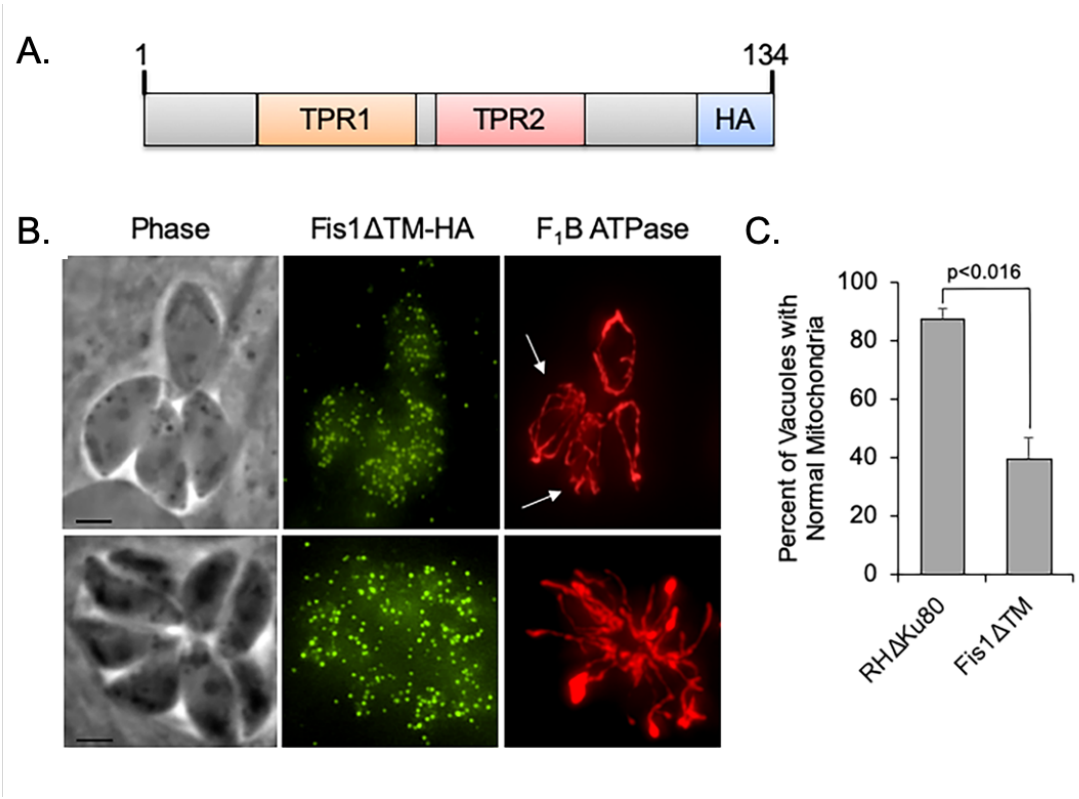

Figure 7. Mislocalization of Fis1 disrupts mitochondrial morphology. To determine the necessity of the TM domain for localization of Fis1, we engineered strains in which either an exogenous or the endogenous Fis1 lacked the transmembrane domain. (A) Schematic of endogenous Fis1 in which TM has been replaced by an HA epitope (Fis1ΔTM-HA). (B) Intracellular parasites of the strain expressing the truncated Fis1 were stained with antibodies against the HA tag (green) to detect Fis1ΔTM and antibodies against F_1B ATPase (red) to detect mitochondria. White arrows indicate abnormal appearing mitochondria. Bars, 2 μm. (C) The frequency of Fis1ΔTM-HA-expressing parasites with abnormal mitochondrial morphology (extraneous fragments or branches) was examined and compared to that of the parental Δ*ku80* strain. In three independent experiments, parasite vacuoles from 15 random fields of view were enumerated, and the data are presented as percentage of vacuoles with normal mitochondrial morphology ± SD. Student's t-test was employed for determining statistical significance (61).

Basis of inquiry

The mitochondrion of *Toxoplasma* is both metabolically and morphologically dynamic in order to adapt to the constantly changing environment. The mitochondrion is a validated drug target, but these drugs are toxic or

ineffective at treating all stages of the parasite life cycle. Therefore, it is important that new treatments are developed that can target multiple life stages and accommodate the parasite's ability to adapt. In this study, I have identified a novel protein which we have named Lasso Maintenance Factor 1 (LMF1) which is involved in maintaining the typical mitochondrial shape in intracellular parasites. Upon genetic disruption of LMF1, the *Toxoplasma* mitochondrion retracts from the parasite periphery to form sperm-like and collapsed mitochondria in intracellular parasites. The goal of this thesis is to determine the consequences of this mitochondrial morphology change in intracellular parasites and identify other proteins that may be involved in this process, both naturally upon egress and upon depletion of LMF1 (Fig. 8).

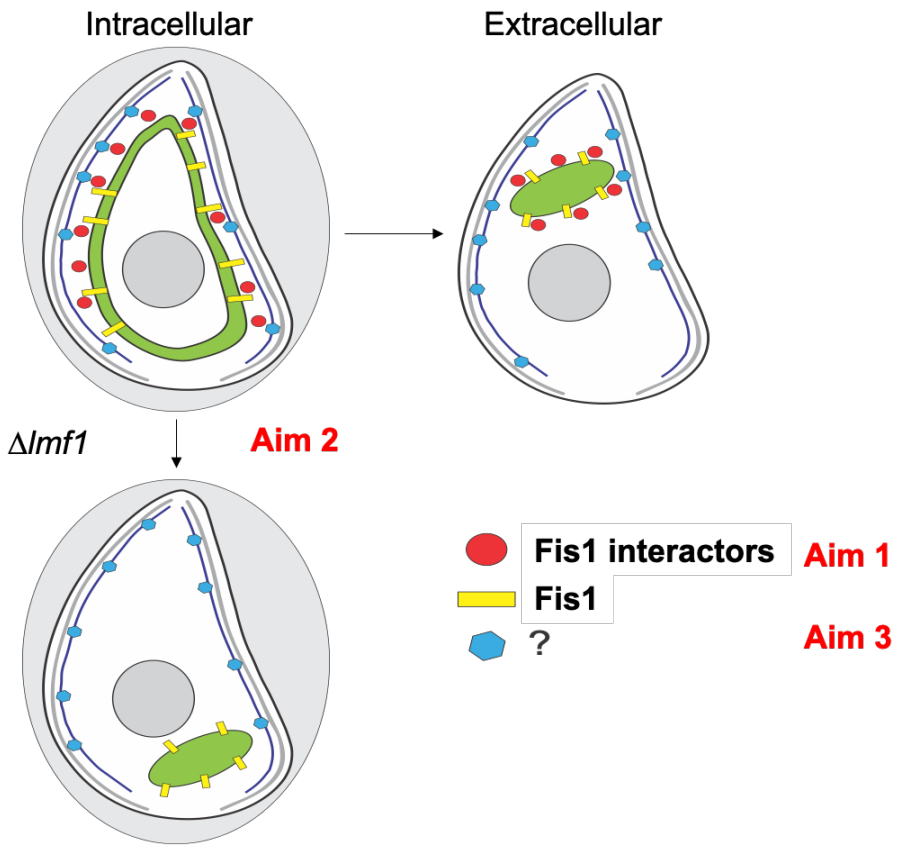

Figure 8. Model of aims of this study. Schematic of the mitochondrial morphology change observed between intracellular and extracellular forms of the parasite. Upon deletion of LMF1 or exposure to the extracellular environment, the mitochondrion (green) retracts from the IMC. Aim 1 is to identify putative Fis1 (yellow rectangle) interactors. Aim 2 is to determine the role of LMF1 (red circle) in parasite fitness. Aim 3 is to determine interacting partners of LMF1 (blue hexagon).

Aim 1: Identify Fis1 interactors

Toxoplasma gondii lacks many of the canonical factors involved in mitochondrial fission, such as the adaptor protein Mdv1 and a traditional dynamin. Therefore, I will determine putative interactors of Fis1 to investigate their role in mitochondrial dynamics and division. I will use two methods, Yeast Two-Hybrid (Y2H) and immunoprecipitation, to identify putative Fis1 interactors. Proteins found using both techniques will be investigated further, along with putative proteins of

interest from either list with good confidence of interaction by Y2H and/or 5 or more peptides in the HA-Fis1 sample, but none in the control. I will tag and localize three potential Fis1 interactors for further study.

Aim 2: Determine role of LMF1 in parasite fitness

TGGT1_265180 was identified in both Y2H and immunoprecipitation of Fis1, which our lab has now dubbed Lasso Maintenance Factor 1 (LMF1). In order to determine if LMF1 plays a role in mitochondrial dynamics or parasite survival, I propose the following: I will endogenously tag LMF1 and determine its localization in relation to Fis1 and confirm interaction with Fis1 through truncational mutations to either Fis1 or LMF1. I will knockout LMF1 using double homologous replacement of the coding sequence with a drug resistance marker. Using these knockout parasites, I will perform tissue culture assays, such as plaque and doubling assays, to determine if LMF1 plays a role in the *Toxoplasma* lytic cycle. Additionally, I will observe any changes to mitochondrial morphology using immunofluorescence microscopy and transmission electron microscopy. I will also conditionally knockdown LMF1 using a destabilization domain to better control specific levels of the protein in relation to mitochondrial morphology and parasite fitness.

Aim 3: Determine interacting partners of LMF1

In order to further identify proteins involved in mitochondrial dynamics of *Toxoplasma gondii*, I plan to identify putative interactors of LMF1 using Y2H and

immunoprecipitation analysis. Proteins common to both generated lists will be prioritized for localization and phenotypic characterization. I plan to determine the localization and determine potential interaction with LMF1 of three proteins chosen by a set of predetermined criteria.

Chapter 2: Methods

Host cell and parasite maintenance

All parasite strains were maintained via continued passage through human foreskin fibroblasts (HFF, purchased from ATCC) in normal growth medium, which consisted of Dulbecco's Modified Eagle Medium (DMEM) supplemented with 10% fetal bovine serum (FBS), 2 mM L-glutamine, and 100 units penicillin/100µg streptomycin per mL. All cultures were grown in a humidified incubator at 37ºC and 5% CO_2. Parasites used were of the strain RH lacking hypoxanthine-xanthine-guanine phosphoribosyl transferase (HPT, RH∆*hpt)* (63) and RH lacking HPT and Ku80 (RH∆*ku80*∆*hpt*, referred to as ∆*ku80* thereafter) (64, 65). For experiments involving drug treatment, the medium was supplemented with 1% FBS rather than 10%. For pyrimethamine treatment we used dialyzed serum. All drugs were purchased from Sigma. Stocks of monensin, pyrimethamine, and myxothiazol were prepared in ethanol, while atovaquone was prepared in DMSO.

Generation of transgenic parasites

(HA)Fis1 and Fis1∆TM: Parasites were engineered to express ectopic copies of full-length Fis1 (TGGT1_263323) or a truncated version lacking the putative transmembrane (TM) domain. For this purpose, PCR was utilized to amplify the Fis1 cDNA and append a hemagglutinin (HA)-tag at the N-terminus. The amplicon was flanked by NsiI and PacI restriction enzyme sites. Table 1 lists all the primers used throughout this study. Purified PCR fragments were inserted into the pHEX2 plasmid (66) using the In-Fusion HD Cloning Plus kit (Clontech).

Expression of the transgenes was controlled by the *SAG1* promoter and selection was provided by the presence of the HPT selectable marker (63). 35µg of KpnI-linearized plasmids were electroporated into parental RHΔ*hpt* parasites (67) and selection of parasites that successfully integrated the plasmid was achieved by growing parasites in medium containing 50µg mycophenolic acid and 50µg xanthine per mL. Three rounds of drug selection were followed by limited dilution cloning to establish HA-tag positive parasite lines with and without the transmembrane domain termed RHΔ*hpt*+HAFis1 and RHΔ*hpt*+Fis1ΔTM, respectively.

To generate a parasite line expressing an endogenous Fis1 lacking the TM (RHΔ*ku80*:Fis1ΔTM), a fragment of the Fis1 gene comprising the region just upstream of the TM and flanked by PacI and AvrII was PCR amplified from *Toxoplasma* genomic DNA and inserted into the pLIC-HA(3x)-DHFR plasmid (64) by In-Fusion cloning. 35µg of EcoRV-linearized plasmid was transfected into Δ*ku80* parasites (64). Resulting transfectants were selected for dihydrofolate reductase (DHFR) by growth in medium with 1µM pyrimethamine and cloned by limited dilution.

Endogenous tagging of putative Fis1 interactors: Putative Fis1 interactors TGGT1_224270 and TGGT1_287980 were endogenously tagged at their C-termini with a triple hemagglutinin tag and a DHFR resistance cassette using CRISPR/Cas9. Briefly, approximately 4kb from the pLIC-3xHA-DHFR plasmid was amplified by PCR to contain the epitope tag and DHFR with primer overhangs homologous to 42bp before the stop codon and 42 bp after the PAM site. The

pSAG1-U6-Cas9-sgUPRT sgRNA was mutated to contain a sgRNA targeted to 50-100bp downstream of the stop codon. The small guide RNA was mutated using Q5® Site-Directed mutagenesis (NEB) using primers 30 and 31 for TGGT1_287980 and primers 34 and 35 for TGGT1_224270. Approximately 1µg of the PCR amplicon and 2µg of the CRISPR/Cas9 plasmid with the correct guides were nucleofected into RHΔ*ku80* parasites and selected using 1µM pyrimethamine and cloned using limiting dilution. Positive clones were confirmed using Western blotting and IFA.

TGGT1_265180(myc): For C-terminal endogenous epitope tagging of TGGT1_265180, a PacI-flanked fragment of TGGT1_265180 just upstream of its stop codon was PCR amplified and inserted into pLIC-myc(3x)-DHFR by In-Fusion cloning. 60µg of XcmI-linearized plasmid was transfected into Δ*ku80* parasites and transfectants were selected for DHFR as described above.

Δ265180: Double homologous replacement of the TGGT1_265180 coding sequence was used to establish a knockout strain. For this purpose, we generated a knockout construct using the previously described pminiGFP vector (68). Using In-Fusion cloning we introduced a 1,400bp PCR amplicon encompassing the region upstream of the TGGT1_265180 start codon into the HindIII restriction site of pminiGFP and a 1,156bp amplicon of the region downstream of the stop codon into the NotI restriction site. In this manner, the resulting vector (p265180_KO) has a drug selection cassette, HPT, flanked by regions of homology to the sequences upstream and downstream of TGGT1_265180. 10µg of DraIII-linearized p265180_KO was transfected into *Δku80* parasites using Nucleofector™ (Lonza)

and parasites were then selected for the expression of HPT, as described above. Disruption of TGGT1_265180 was confirmed by PCR using three primer sets (Table 1). The first primer set (P1) amplifies a 637bp region present in wildtype parasites and absent in the knockout strain (Fig. 13A and B). The second primer set (P2) was designed to amplify a 1933bp fragment only present if the double homologous recombination of the knockout construct occurred at the TGGT1_265180 locus (Fig. 13A and B). The final primer set (P3) amplifies a fragment in both the wildtype and knockout strains (Fig. 13A and B).

Δ265180+265180(HA) and Δ265180+265180ΔSID(HA): For exogenous expression of TGGT1_265180, a 3700bp fragment beginning approximately 2kb upstream of the TGGT1_265180 start codon and ending at the penultimate codon was PCR amplified from genomic DNA. This PCR amplicon was inserted into the PacI site of pLIC-HA(3x)-DHFR by In-Fusion cloning. The same method was used to create a plasmid lacking the predicted SID, thus truncating the gene. These plasmids were used as templates to amplify an 8kb fragment that included the TGGT1_265180 gene under the control of its own promoter, a triple hemagglutinin tag, and the DHFR drug selection cassette. Primers used included overhangs homologous to the remnants of the Δ*ku80* site on each side of a double-stranded cut created by CRISPR/Cas9. The 8kb PCR fragment was gel extracted using the NucleoSpin Gel and PCR Clean-up kit (Macherey-Nagel) and eluted in P3 Buffer (Lonza) for nucleofection. The pSAG1-Cas9-U6-sgUPRT plasmid, generously provided by the Sibley lab (69), was mutated to contain a guide RNA targeted to the Ku80 site. TGGT1_265180 knockout and parental parasites were transfected

with 1µg of either the full-length (265180-HA) or truncated (265180ΔSID-HA) PCR amplicons and 2µg of pSAG1-Cas9-sgKu80 using the Nucleofector™ (Lonza). Parasites were selected for the presence of DHFR, as described above. Immunofluorescence and Western blot (see below) was used to confirm expression and localization of the exogenous copies of TGGT1_265180.

LMF1-2xHA-DD-DHFR: For conditional knockdown of LMF1, the same PCR primers and amplified sequence were used to insert into the pLIC-HA(2x)-DD-DHFR plasmid using InFusion cloning. Approximately 65 µg of Xcm1-linearized plasmid was transfected into DiCreΔ*ku80* SOD2-GFP IMC1-TdTomato parasites, generously provided by Dr. Diego Huet (70). Transfectants were cloned through selection in both pyr and SHLD-1 and confirmed as described above.

LMF1-HA+IMC10-myc: For endogenous tagging of IMC10 C-terminus with a myc epitope tag, a 2.6kb fragment was amplified from the pLIC-myc(3x)-HPT plasmid that included the triple myc epitope tag and HPT drug selection cassette. Primer overhangs for this amplicon corresponded to 42bp before the stop codon of IMC10 and 42bp after the PAM sequence designed for CRISPR/Cas9 (Table 1). This fragment was PCR amplified and gel extracted using the NucleoSpin Gel and PCR Clean-up kit (Macherey-Nagel) before eluting in P3 Buffer (Lonza). We designed primers to mutate the pSAG1-Cas9-U6-sgUPRT plasmid to contain a guide RNA targeted to a site no greater than 100bp downstream of the IMC10 stop sequence. This mutagenesis was achieved using Q5® Site-Directed mutagenesis (NEB) and plasmids with the correct guide RNA sequence were confirmed by sequencing. Approximately 2µg of pSAG1-Cas9-sgIMC10 plasmid and 1µg of the

PCR amplicon containing the epitope tag and drug selection marker were nucleofected into RHΔ*ku80* LMF1-HA parasites. Positive clones were selected for in the presence of MPA/XAN and were confirmed using IFA and Western blots, as described previously.

Immunofluorescence microscopy analysis

For IFA, infected HFFs were fixed with 3.5% formaldehyde, quenched with 100 mM glycine, and blocked and permeabilized in 3% bovine serum albumin (BSA) and 0.2% Triton x-100 (TX-100) in PBS. Samples were then incubated with primary antibodies in PBS/3% BSA/0.2% TX-100 for one hour, washed five times with PBS, and incubated with Alexa Fluor conjugated secondary antibodies in PBS/3% BSA for one hour. Coverslips were washed with PBS and mounted on glass slides with 3 µL DAPI containing Vectashield. For 3D-SIM microscopy coverslips were stained with a liquid DAPI solution in PBS, washed, and inverted on a glass slide with Vectashield mounting medium without DAPI. Image acquisition and processing was performed on either a Nikon Eclipse 80i microscope with NIS-Elements AR 3.0 software or a Leica DMI6000 B microscope with LAS X 1.5.1.13187 software. 3D-SIM was performed utilizing the OMX 3D-SIM super-resolution system located within the Light Microscopy Imaging Center at Indiana University Bloomington (http://www.indiana.edu/~lmic/microscopes/OMX.html). The system is equipped with four Photometrics Cascade II EMCCD cameras that permit imaging four colors

simultaneously and is controlled by DV-OMX software. Images processing was completed using the Applied Precision softWoRx software.

Primary antibodies used in this study included rabbit anti-HA (Cell Signaling Technology), rabbit anti-myc (Cell Signaling Technology), rabbit polyclonal antibody against the MORN1 protein (71), mouse monoclonal antibody 5F4 (detects F_1B ATPase, P. Bradley, unpublished), and rabbit anti-acetyl-K40-α-tubulin (EMD Millipore ABT241), all used at 1:1,000, with the exception of 5F4 which was used at 1:5,000. Secondary antibodies included Alexa Fluor 594 or Alexa Fluor 488 conjugated goat anti-rabbit and goat anti-mouse (Invitrogen), all used at 1:2,000.

Phenotypic characterization of parasite strains

For drug effects on mitochondrial morphology infected HFFs on coverslips were vehicle or drug treated with monensin (1 ng/mL), atovaquone (100 nM), pyrimethamine (1 μM), or myxothiazol (50 ng/mL) for 12 hours. To allow for recovery, drug medium was washed away and replaced with normal growth medium for an additional 12 hours. IFA was performed as above using F_1B ATPase antibodies to monitor the mitochondrion. Samples were blinded and at least 100 vacuoles per sample were inspected. Experiments were performed in experimental and biological triplicates.

Plaque and doubling assays were performed with 12-well plates using standard methods (72). Briefly, for the plaque assays 500 freshly egressed parasites were added to confluent HFF monolayers. After four days of incubation,

cultures were fixed with methanol for 5 minutes and stained with Crystal Violet. Plaques were imaged using a ProteinSimple imaging system and number of plaques were counted on a light microscope. Experiments were performed in experimental and biological triplicates. LMF1-HA-DD parasites maintained in 50nM SHLD-1 were allowed to infect cells grown in 12-well tissue culture plates at a concentration of 500 parasites per well for two hours. After the two-hour invasion period, wells were washed four times with warm PBS and media was replaced with media containing 0, 50, 150, and 300nM SHLD-1. Plates were left untouched for six days before fixation and visualization. These experiments were done in experimental triplicate and biological quadruplicate.

Mitochondrial morphology was quantitated by counting the number of lassoed, sperm-like, and collapsed mitochondrion for approximately 100 parasites, along with vacuoles that contained amitochondriate parasites or extraparasitic mitochondrial material. These results are shown as a percentage of total parasites and was repeated for biological triplicates. LMF1-HA-DD mitochondrial morphologies in 0, 50, 150, and 300nM SHLD-1 were quantitated as the percentage of parasites with these morphologies over ten fields of view for three replicates.

Yeast two-hybrid screening

Yeast two-hybrid screening was performed by Hybrigenics Services, S.A.S., Paris, France (http://www.hybrigenics-services.com). The coding sequence for Fis1 (aa 2-118; XM_018781322.1) was PCR-amplified and cloned

into pB66 as a C-terminal fusion with the Gal4 DNA-binding domain (Gal4-Fis1). The construct was checked by sequencing and used as a bait to screen a random-primed *Toxoplasma* cDNA library constructed into pP6. pB66 derives from the original pAS2ΔΔ vector (73) and pP6 is based on the pGADGH plasmid (74). 46 million clones (5-fold the complexity of the library) were screened using a mating approach with YHGX13 (Y187 ade2-101::loxP-kanMX-loxP, matα) and CG1945 (matα) yeast strains as previously described (73). 247 His+ colonies were selected on a medium lacking tryptophan, leucine, and histidine. The prey fragments of the positive clones were amplified by PCR and sequenced at their 5' and 3' junctions. The resulting sequences were used to identify the corresponding interacting proteins in the GenBank database (NCBI) using a fully automated procedure. A confidence score (PBS, for Predicted Biological Score) was attributed to each interaction as previously described (75).

To determine interactors of LMF1 by Y2H, the coding sequencing of full length LMF1 (aa 1-452) was sent to Hybrigenics Services for the same screening as done for Fis1. The bait was analyzed and generated 257 positive clones over 96 million interactions through selection in 0.5mM 3-Aminotriazol (76, 77).

Immunoprecipitation assays

To confirm the results of the Fis1 yeast two-hybrid screening, we performed one immunoprecipitation assay using RHΔ*hpt*+HAFis1, with the parental RHΔ*hpt* parasites as a negative control. Extracellular parasites from 10 T175 culture flasks per strain were spun down, washed twice with cold PBS, and resuspended in

Pierce Co-IP Lysis buffer (Fisher Scientific) with Protease/Phosphatase Inhibitor Cocktail (100X, Cell Signaling Technology). After one hour of lysis at 4°C, the samples were sonicated three times for 15 seconds, with one-minute rest period between each sonication. After sonication, samples were pelleted and the supernatant transferred to Pierce™ Anti-HA Magnetic Beads (Fisher Scientific). Samples were placed on a rocker at 4°C for 2.5 hours before beads were washed once with Pierce Co-IP Lysis buffer and twice with PBS. Beads were resuspended in 8M urea and sent for LC/MS-MS analysis. Results were narrowed down to proteins that had at least 4 peptides in the RHΔ*hpt*+HAFis1 sample and none in the RHΔ*hpt* control. This shortened list was then compared to the list of putative interactors obtained through yeast two-hybrid.

The above was repeated with LMF1-HA to determine interactors, with the following modifications. RHΔ*ku80* was used as the control line since it is the parental strain for the LMF1-HA parasites. This was repeated three times and the total number of peptides for each putative interactor were summed and divided by the number of peptides in the control sample to yield the fold change. Proteins that had a fold change of 4 or greater and less than 4 peptides in the control samples are listed in Table 5.

Parasites were co-tagged with LMF1-HA and IMC10-myc to confirm interaction by reciprocal co-immunoprecipitation. Briefly, one T175 flask of intracellular LMF1-HA+IMC10-myc parasites were scraped into PBS and washed before resuspending the sample pellet in Pierce Co-IP Lysis Buffer (Fisher Scientific) with Protease/Phosphatase Inhibitor cocktail, as described above. After

sonication, samples were incubated in Pierce™ Anti-HA magnetic beads for two hours at 4°C before washing the beads and eluting the bound protein by boiling the beads in 1X Laemmli Sample Buffer with 5% BME. Samples collected from the input solution (before beads), unbound (after incubation with beads), and wash (first wash in lysis buffer) were also resuspended to a final concentration of 1X Laemmli Sample Buffer with 5% BME. Samples were then used for Western blotting to probe for both HA and myc signal.

Western blot analysis

Extracellular parasites were pelleted and resuspended in 2X Laemmli Sample Buffer (Bio-Rad) with 5% 2-mercaptoethanol (Sigma-Aldrich). Samples were boiled for 5 minutes at 95°C before separation on a gradient 4-20% SDS-PAGE gel (Bio-Rad). Samples were then transferred to nitrocellulose membrane using standard methods for semi-dry transfer (Bio-Rad). Membranes were probed with rabbit anti-HA (Cell Signaling Technologies), mouse anti-c-myc (Cell Signaling Technologies), or mouse anti-SAG1 (Thermo Fisher) at a dilution of 1:5000 for 1 hour. Membranes were then washed and probed with either goat anti-mouse horseradish peroxidase or goat anti-rabbit horseradish peroxidase (Sigma-Aldrich) at a dilution of 1:10000 for 1 hour (GE Healthcare). Proteins were detected using SuperSignal West Femto substrate (Thermo Fisher) and imaged using the FluorChem R system (Biotechne). All original western blots are shown in supplemental dataset 2.

For comparative analysis of LMF1 protein levels in RHΔ*ku80*:Fis1ΔTM parasites to that of RHΔ*ku80*, parasites were centrifuged and washed once with PBS. Parasites were counted using a hemocytometer and the parasite pellets were resuspended at appropriate volumes to equilibrate the concentration of parasites. The subsequent immunoblots were then probed for anti-SAG1 as a loading control. ImageJ was used for densitometry analysis of the detected protein band and compared to SAG1 signal. The ratio of LMF1 protein levels (normalized to the SAG1 levels in the same sample) of RHΔ*ku80*:Fis1ΔTM to RHΔ*ku80* was determined and represented as a percentage. These were done in biological triplicate and the described percentage is an average of these replicates. These methods were also performed for LMF1-HA-DD parasites maintained in 0, 150, and 300nM SHLD-1 for two passages before collection. Levels of LMF1 were compared to SAG1 levels in each sample using densitometry and ImageJ analysis.

In order to analyze the potential interaction between LMF1 and IMC10, samples from reciprocal co-IP experiments split into two and were run on a gel, as described above. The two resulting blots were either probed for rabbit anti-HA, to identify the presence of LMF1, or mouse anti-myc to observe IMC10. Because mouse antibody was used for IMC10, the heavy and light chain are visible on the Western blot (Fig. 22B) at 50 kDa and 25 kDa, respectively.

Transmission electron microscopy

To observe the ultrastructural defects seen in the LMF1 knockout parasites, both wildtype (RHΔ*ku80*)- and knockout (Δ*lmf1*)-infected host cells were sectioned

and analyzed by transmission electron microscopy (TEM). Briefly, samples were fixed with 2.5% glutaraldehyde in 0.1 mM sodium cacodylate 24 hours post-infection. After fixation, samples were incubated in 1% (w/v) osmium tetroxide and 2% (w/v) potassium ferrocyanide for one hour at 4°C. These samples were then extensively dehydrated in ethanol before embedding in an epoxy-resin mix. These sections were stained first with 3% (w/v) uranyl acetate in water, followed by lead citrate, before being examined with a Philips CM120 EM (Eindhoven, the Netherlands) under 80 kV(78).

Statistical analysis

Statistics were performed with either JMP14.0 or Prism software.

Table 1. Primers used in this study

Use	Primer #	Name	Primer Sequence
Split N-terminal HA tag	1	RC #1	GTTTTTTGACGAGTATGCATATGTATCCTTACGATGTTCC
Ectopically express HA-Fis1	2	RC #2	CGATGTTCCAGATTATGCCGAAGACTCCAACTTCAG
	3	RC #3	GCACAACGGTGATTAATTAATTATTTTGATAGCGTCCACAA
Ectopically express HA-Fis1ΔTM	4	RC #4	CGATGTTCCAGATTATGCCGAAGACTCCAACTTCAG
	5	RC #5	GCACAACGGTGATTAATTAATTAAAGCACGGAGCCAATGAG
Create Fis1 sgRNA for CRISPR	6	RC #6	ACTGGAGTCGGTTTTAGAGCTAGAAATAGCAAG
	7	RC #7	TTGAGTATGCAACTTGACATCCCCATTTAC
Endogenously tag TGGT1_265180 C-terminus with myc, HA, or HA-DD	8	TgME49_265180 Tag.FOR	TTCCAATCCAATTTAATTAATGAGTACGCAGTGAGCCTTCG
	9	TgME49_265180 Tag.REV	CCACTTCCAATTTTAATTAACCAAAATCGAACCTTTCCGATGT
Ectopically express 265180-HA* and 265180ΔSID-HA under native promoter	10	FIP1 EE.HA.DHFR.FOR	TTCCAATCCAATTTAATTAATTATCTCCTTTGCGGACGCTAGG
	11	FIP1 no SID.REV	CCACTTCCAATTTTAATTAACTGCTTCGCGTCACTGC
Knockout of TGGT1_265180 coding sequence	12	Fis1.KO.5UTR.FOR	CGGTATCGATAAGCTTTTTTCGTTGAATCATATCCGCTTTGTCT
	13	Fis1.KO.5UTR.REV	CGTGCTGATCAAGCTTTCTCGTACAGTGCTCACAAAAAACGC
	14	Fis1.KO.3UTR.FOR	AGTTCTAGAGCGGCCGCATGGCGCCCCGGTTATCGGCTG
	15	Fis1.KO.3UTR.REV	ACCGCGGTGGCGGCCGCAGCGGTATACTAGAGGTCAGCGTACT

Confirmation of TGGT1_265180 knockout	16	Fis1 KO P1.FOR	TCAAGCAGACGGAGAGGC
	17	Fis1 KO P1.REV	CGACGGACTGTCCATACGT
	18	Fis1 KO P2-3.FOR	CAACTCACTGACCGCGGT
	19	Fis1 KO P3.REV	CAGAAGGGCTGTTGCGAG
Targeting to Ku80 site	20	IMC2A-CmR [Ku80].F	GTCCCCGGTTCGCCTCAGCACACACACACATGACGTACATCGAAGCTGGGTACCCTGTACTTCC
	21	IMC2A-CmR [Ku80].R	GTAATGTCGGAATAGTTCCCATCAGAAACAATGGAGCTATCCGCGTCCCATTCGCCATTCAG
Endogenously tag IMC10 with myc using CRISPR/Cas9	22	IMC10.Cas9.myc. FOR	GCCAGCGGAGTAGGATTGGGCGAAGAGGCACAGATCAGCGCCTTAATTAAAATTGGAAGTGGAGG
	23	IMC10.Cas9.myc. REV	CATGCCCTGTCCCTAAAAATTAGTTCCCTTTCTCAGTTGTAGGTTTTCCCAGTCACGACG
	24	IMC10.Q5.FOR	ACAACACACAGTTTTAGAGCTAGAAATAGC
	25	IMC10.Q5.REV	GGGACGTCTCAACTTGACATCCCCATTTAC
Analysis of interactors by Y2H	26	FIP1 cDNA.FOR	TTCCAATCCAATTTAATTAAATGGATGCGGTGATGGTTGT
	27	FIP1 cDNA.REV	CCACTTCCAATTTTAATTAATCACCAAAATCGAACCTTTCCGATG
Endogenous tagging of TGGT1_287980 using CRISPR/Cas9	28	287980.Cas9.HA. FOR	GACGAGGCACCCGAGGGGATGGAAAAACGGGAGGACGAGGCGTTAATTAAAATTGGAAGTGGAGG
	29	287980.Cas9.HA. REV	CACAGGCGTCAGATGCATCTCTCCTGCTTCTTGTGGTGACTGGTTTTCCCAGTCACGACG
	30	287980.Q5.FOR	TTCGTCATCGGTTTTAGAGCTAGAAATAGC
	31	287980.Q5.REV	CCCCAGAGGCAACTTGACATCCCCATTTAC
Endogenous tagging of TGGT1_224270 using CRISPR/Cas9	32	224270.Cas9.HA. FOR	CACACACAGCGTGTCTGAGGAATGCCACCAACGCACTTTGGTTAATTAAAATTGGAAGTGGAGG
	33	224270.Cas9.HA. REV	GTCTCTCATCTCAGCATTCTCTCTTCCGCTCGTTCAGCTGGTTTTCCCAGTCACGACG
	34	224270.Q5.FOR	GAGGGGAACTGTTTTAGAGCTAGAAATAGC

	35	224270.Q5.REV	TTTCTCTTTCAACTTGACATCCCCATTTAC

All sequences are 5’ to 3’. * Used TgME49_265180 Tag.REV as the reverse primer for ectopic expression of 265180-HA.

Chapter 3: Results

Fis1 and its interactors

Mislocalization of the endogenous Fis1 results in a dominant negative phenotype in terms of mitochondrial morphology. We hypothesize that this is the result of mislocalization of Fis1 interactors required at the mitochondrion for normal morphology. To identify these potential interactors, we employed a Yeast Two-Hybrid (Y2H) interaction screen. Using full-length Fis1 as bait, 46 million clones were screened for Y2H interaction and 247 were selected for identification. The putative interactors were then given a confidence score based on the likelihood of interaction with Fis1 (76, 77). This resulted in 24 potential interactors with a global Predicted Biological Score (PrBS) from A (highest confidence) to D (lowest confidence) (76, 77) (Table 2).

Of these putative interactors, we identified three that may be of interest based on predicted domains and functions. The first is TGGT1_224270, which is a hypothetical protein that had a PrBS of C (good confidence of interaction), is predicted to have three WD40 domains and two transmembrane domains. WD40 domains contain approximately 40 amino acids and generally terminate these regions with tryptophan (W) and aspartate (D) dipeptide to form propeller-like β-sheets (79). WD40 domains function in numerous cellular processes, but are most commonly seen in protein-protein or protein-DNA interactions. Fis1 adaptor proteins in yeast commonly contain these domains and, for that reason, we decided that TGGT1_224270 warranted further investigation (58, 59). We endogenously tagged the C-terminus with a triple hemagglutinin tag and DHFR

resistance cassette. The resulting parasites showed mitochondrial localization of this putative Fis1 interactor (Figure 9A).

A second interesting interactor is TGGT1_287980, which is designated as a putative FHA-domain containing protein on ToxoDB. This protein is predicted to have a forkhead-associated domain (FHA), which can be found in many regulatory proteins (80). These domains recognize phosphopeptides and has been found to modulate various signaling mechanisms and may also be involved with protein-protein interactions with phosphorylated residues (80). For these reasons, we also decided to tag TGGT1_287980 using similar methods of tagging used above. Interestingly, TGGT1_287980 was found to localize to the IMC in both the daughter and mother parasites (Figure 9B). The last interactor that we investigated further is TGGT1_304990, which has a PrBS of D and a CRISPR fitness score of -5.5, indicating moderate confidence of interaction with Fis1 and essentiality for parasite survival, respectively. In addition to 4 transmembrane domains, TGGT1_304990 has a predicted guanylate-binding domain and coiled-coil domain. Guanylate-binding domains are found within proteins in the dynamin superfamily and mechanistically are involved with membrane remodeling and scission (81). As stated earlier, *Toxoplasma* has 3 predicted Drps that do not appear to have involvement in mitochondrial division. Therefore, it is possible that TGGT1_304990 could act as a noncanonical dynamin for mitochondrial division. Current attempts to tag this protein have identified it as an ER-resident protein, which is corroborated by the LOPIT results for this protein produced by the Waller lab (82).

Table 2. Putative Fis1 interactors determined by Y2H[a]

ToxoDB Gene ID	Product Description	Global PrBS[b]	CRISPR Score[c]
TGME49_215520	hypothetical protein	A	0.61
TGME49_218560	acetyl-coA carboxylase ACC2	B	-3.06
TGME49_222800	glycogen synthase, putative	B	-0.70
TGME49_265180	hypothetical protein	B	-1.65
TGME49_224270	hypothetical protein	C	-3.75
TGME49_293840	hypothetical protein	C	-3.62
TGME49_201390	hypothetical protein	D	1.86
TGME49_226050	hypothetical protein	D	0.13
TGME49_237015	hypothetical protein	D	2.40
TGME49_246720	hypothetical protein	D	0.24
TGME49_247700	AP2 domain transcription factor AP2XII-4	D	-5.12
TGME49_284620	hypothetical protein	D	-1.02
TGME49_286470	AGC kinase	D	-1.74
TGME49_287980	FHA domain-containing protein	D	-3.15
TGME49_297770	hypothetical protein	D	-0.56
TGME49_299670	hypothetical protein	D	0.35
TGME49_304990	guanylate-binding protein, N-terminal domain-containing protein	D	-5.50
TGME49_321370	hypothetical protein	D	-2.58
TGME49_321450	Myb family DNA-binding domain-containing protein	D	-4.21

[a] Proteins that also appear in the Fis1 immunoprecipitation experiments are highlighted in orange and those that also appeared in the Fis1 Y2H are highlighted in green.

[b] Predicted biological score (PrBS) are confidence scores, with A indicating the highest confidence of interaction and D being the lowest confidence of interaction (73, 77).

[c] CRISPR Score from genome-wide screen with phenotype scores ranging from approximately -7 (essential) to 3 (dispensible) (83).

Table 3. Potential Fis1 interactors determined by immunoprecipitation[a]

ToxoDB Gene ID	Product Description	Total Peptides	Fold Change[b]	Fisher's Exact Test ($p < 0.05$)
TGGT1_263323	Fis1	35	INF	< 0.00010
TGGT1_241170	hypothetical protein	32	INF	< 0.00010
TGGT1_248520	hypothetical protein	31	INF	< 0.00010
TGGT1_265180	LMF1	28	INF	< 0.00010
TGGT1_305270	hypothetical protein	17	INF	< 0.00010
TGGT1_356400	cAMP-dependent protein kinase	7	INF	0.0015
TGGT1_410610	hypothetical protein	11	INF	< 0.00010
TGGT1_227850	peptidyl-prolyl cis-trans isomerase, cyclophilin-type domain-containing protein	10	INF	< 0.00010
TGGT1_305940	peptidyl-prolyl cis-trans isomerase, cyclophilin-type domain-containing protein	7	INF	0.0015
TGGT1_211670	S1 RNA binding domain-containing protein	7	INF	0.0015
TGGT1_212090	hypothetical protein	6	INF	0.0039
TGGT1_213670	hypothetical protein	6	INF	0.0039
TGGT1_210370	hypothetical protein	4	INF	0.025
TGGT1_225150	hypothetical protein	4	INF	0.025
TGGT1_274060	2-oxoglutarate/malate translocase OMT	4	INF	0.025
TGGT1_244840	zinc knuckle domain-containing protein	4	INF	0.025

TGGT1_320490	N-acyl-phosphatidylethanolamine-hydrolyzing phospholipase D family protein	3	INF	0.062
TGGT1_284560	ribosomal protein RPL9	3	INF	0.062
TGGT1_266470	hypothetical protein	3	INF	0.062
TGGT1_228170	GRA44	3	INF	0.062
TGGT1_227560	putative IWS1 transcription factor	2	INF	0.16
TGGT1_204050	subtilisin SUB1	2	INF	0.16
TGGT1_320020	transporter, major facilitator family protein	2	INF	0.16
TGGT1_314750	hypothetical protein	2	INF	0.16
TGGT1_203630	ribosomal protein RPL44	2	INF	0.16
TGGT1_312622	DUF803 domain-containing protein	2	INF	0.16
TGGT1_232350	lactate dehydrogenase LDH1	2	INF	0.16
TGGT1_210095	hypothetical protein	14	14	< 0.00010
TGGT1_410590	cAMP-dependent protein kinase	11	11	0.00028
TGGT1_210095	hypothetical protein	10	10	0.00066
TGGT1_215775	rhoptry protein ROP8	14	7	0.00011
TGGT1_252360	rhoptry kinase family protein ROP24 (incomplete catalytic triad)	14	7	0.00011
TGGT1_227810	rhoptry kinase family protein ROP11 (incomplete catalytic triad)	27	6.8	< 0.00010
TGGT1_209985	cAMP-dependent protein kinase	13	6.5	0.00024
TGGT1_262960	putative U1 snRNP-associated protein Usp106	25	6.2	< 0.00010
TGGT1_231080	ribosomal protein RPL38	6	6	0.018
TGGT1_290700	hypothetical protein	5	5	0.039
TGGT1_309120	ribosomal protein RPL4	4	4	0.084
TGGT1_226240	putative bud site selection protein	4	4	0.084
TGGT1_289690	glyceraldehyde-3-phosphate dehydrogenase GAPDH1	4	4	0.084

[a] Fis1, the bait protein, is highlighted in blue. Proteins that also appeared in the Fis1 Y2H are highlighted in orange.
[b] Fold change was determined by dividing the total peptides of each putative interactor in the HAFis1 sample by the control sample. INF fold change indicates there were no peptides in the control sample.
[c] p-value of t-test results comparing HAFis1 to control sample.

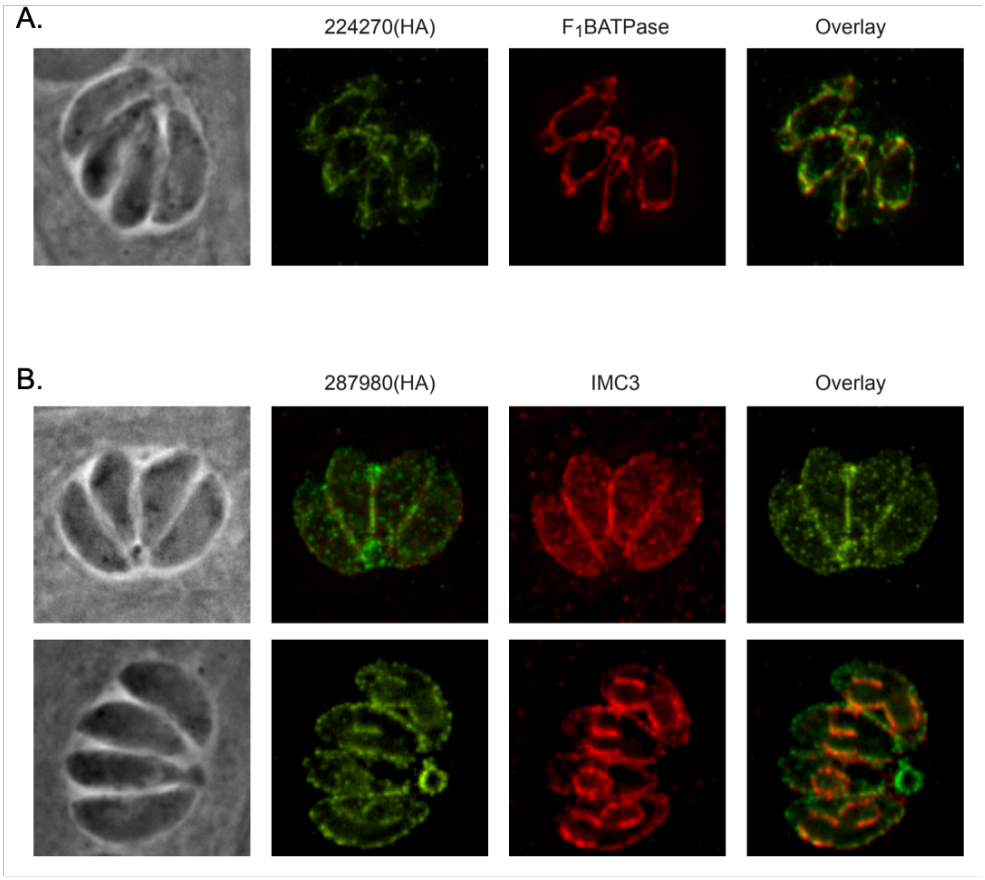

Figure 9. Localization of putative Fis1 interactors. To determine the localization of two putative interactors, each was tagged at their C-termini with a 3xHA epitope tag and DHFR drug resistance cassette. (A) TGGT1_224270 was tagged and is shown in green to co-localize with F_1B ATPase (red), indicating mitochondrial localization. (B) TGGT1_287980 was found to localize to the IMC, which is corroborated by the IMC3 costaining. The top panel shows TGGT1_287980 (green) in nondividing parasites, with localization to the mother parasite IMC and the residual body. In dividing parasites (second panel), TGGT1_287980 also colocalizes with the forming daughters and residual body.

To narrow down these putative interactors, we immunoprecipitated the exogenous HA tagged Fis1 using HA conjugated beads and analyzed the precipitated complex by mass spectroscopy. As a control, we used the parental RHΔ*hpt* strain, which does not express the hemagglutinin tag. Through this analysis, we identified 11 putative interactors that had at least 5 peptides in the Fis1 sample and no peptides in the control sample (Table 3). Among these only one was also identified in the Y2H interaction screen, TGGT1_265180.

Localization of TGGT1_265180

To determine the localization of TGGT1_265180, we introduced a C-terminal myc epitope tag to the endogenous gene. IFA assays of the resulting strain show that, like Fis1, TGGT1_265180 is localized to the mitochondrion of intracellular parasites and persists during parasite division (Fig. 11A and B). To determine whether it was localized within the mitochondrion or associated with the outer mitochondrial membrane, we performed IFA after permeabilization with various concentrations of digitonin, a detergent, using detection of F_1B ATPase to monitor mitochondrial permeabilization (Fig. 11C). When using 0.01% digitonin we can detect both F_1B ATPase and TGGT1_265180 (Fig. 11C). By contrast, using 0.005% digitonin allows for detection of TGGT1_265180 but not F_1B ATPase. This result mimics what is seen with Fis1 (Fig. 10) and thus, like Fis1, TGGT1_265180 likely associates with the outer mitochondrial membrane (OMM) and faces the cytoplasm of the parasite (Fig. 11C). Association with the OMM was confirmed by treatment with monensin. After treating TGGT1_265180(myc) expressing

parasites with monensin, we observed a similar pattern to that of Fis1 in which fragments containing the IMM marker F_1B ATPase are surrounded and connected by TGGT1_265180 (Fig. 11D). Thus, TGGT1_265180 localizes to the OMM as expected for a *bona fide* interactor of Fis1.

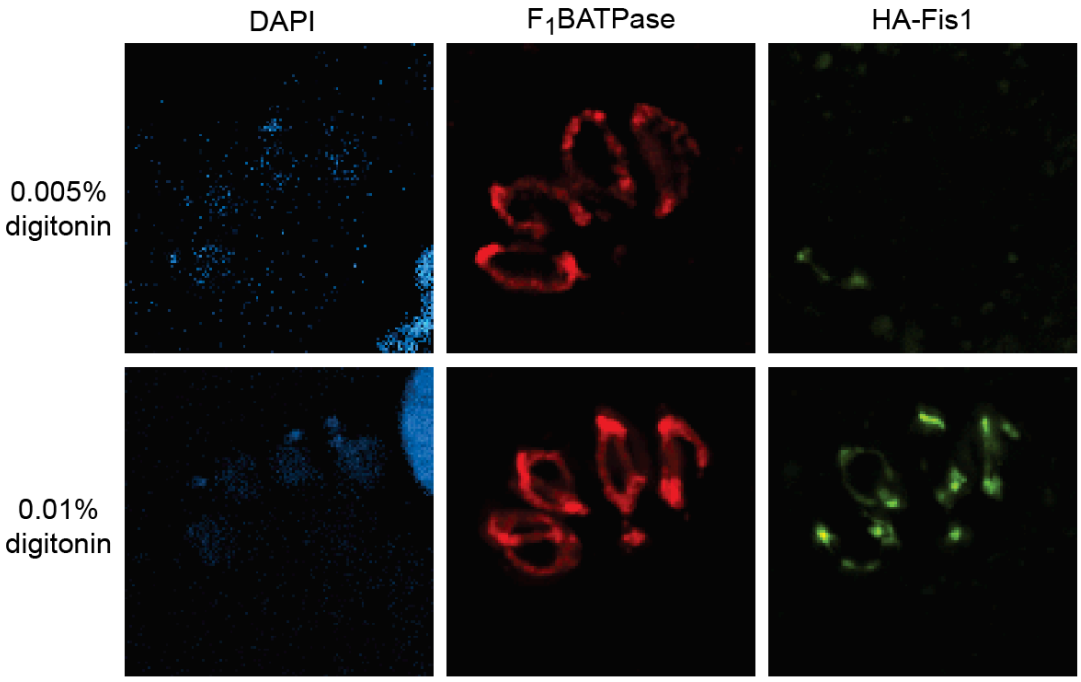

Figure 10. Fis1 localizes to the OMM by partial permeabilization. Intracellular parasites of the HA-Fis1 expressing strain were fixed and permeabilized with either 0.005% or 0.01% digitonin before staining for the IMM protein F_1B ATPase (green) and HA (red). Fis1 can be detected when F_1B ATPase remains inaccessible to the antibodies suggesting that it is associated with the OMM (61).

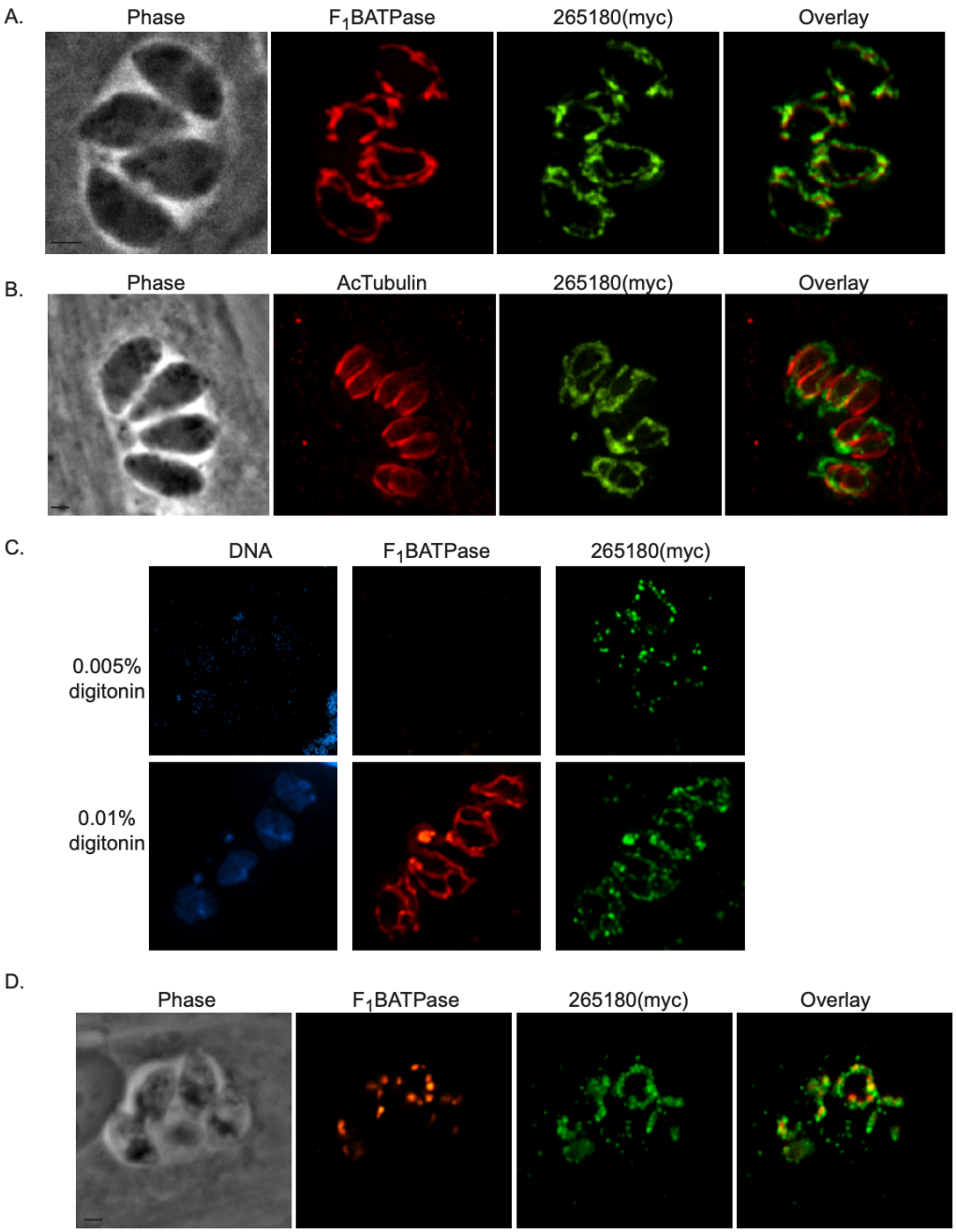

Figure 11. Fis1 interactor TGGT1_265180 localizes to the outer mitochondrial membrane. To investigate the localization of TGGT1_265180, we introduced sequences encoding an N-terminal myc tag to the endogenous locus. (A) Intracellular parasites of the TGGT1_265180(myc)-expressing strain were stained for mitochondrial F_1B ATPase (red) and myc (green). (B) Intracellular parasites of the same strain were stained for myc (green) and acetylated tubulin (red), which clearly demarcates daughter parasites during division. (C) Intracellular parasites of the TGGT1_265180(myc)-expressing strain were fixed and permeabilized with either 0.005% or 0.01% digitonin before staining for the IMM protein F_1B ATPase (red) and myc (green).

TGGT1_265180 can be detected when F_1B ATPase remains inaccessible to the antibodies, suggesting that it is associated with the OMM. (D) TGGT1_265180(myc) parasites were treated with 5 mM monensin for 5-h. Mitochondrial morphology was monitored by IFA for TGGT1_265180(myc) (green) and F_1B ATPase (red). Bars, 2 μm (61).

Localization of TGGT1_265180 is partially dependent on proper Fis1 localization

Despite its association with the OMM, TGGT1_265180 has no predicted trans-membrane domains or posttranslational modifications that would suggest membrane interaction. Therefore, we hypothesize the localization of TGGT1_265180 occurs via protein-protein interaction. To test this idea, we transfected parasites with an ectopic copy of either full length or truncated TGGT1_265180 carrying a C-terminal HA epitope tag and under the control of the TGGT1_265180 promoter (Fig. 12A). The truncated form lacks the C-terminal 92 amino acids, which represent the region of the protein that was identified through the Y2H screen as interacting with Fis1, referred to as the Selected Interaction Domain (SID). As expected, the full-length ectopic copy localized to the mitochondrion (Fig. 12A). However, deletion of the SID resulted in the mislocalization of the protein to the cytoplasm (Fig. 12A). These data indicate that the C-terminal SID is necessary for proper mitochondrial localization.

To investigate if localization of TGGT1_265180 to the mitochondrion is mediated through an interaction with Fis1, we added a myc epitope tag to the endogenous TGGT1_265180 in the strain in which Fis1 lacks its TM (RHΔ*ku80*:Fis1ΔTM) and is mislocalized to the cytoplasm. In this strain, TGGT1_265180 does not colocalize with the mislocalized Fis1 but appears to

accumulate towards the basal end of the parasites in a pattern that does not resemble normal mitochondrial localization (Fig. 12B). To further analyze the localization of TGGT1_265180 in the RHΔ*ku80*:Fis1ΔTM parasite line, we co-stained for F_1B ATPase (Fig. 12C). While we observed some overlap between the TGGT1_265180 and F_1B ATPase signals, TGGT1_265180 was also detected away from the mitochondrion (Fig. 12C, white arrows). Interestingly, we observed that the TGGT1_265180(myc) signal, as detected through IFA, appeared to be much weaker in the Fis1ΔTM strain than in the parental one (Fig. 12C). To quantitate this observation, we performed Western blots from both strains probing for TGGT1_265180(myc) (Fig. 12D). This analysis corroborated that indeed the levels of endogenous TGGT1_265180 are significantly reduced when Fis1 is no longer localized to the mitochondrion (Fig. 12D). We quantitated the levels of TGGT1_265180 in both strains with densitometry of three independent Western blots using the surface antigen SAG1 as a loading control and determined that the level of TGGT1_265180 in the RHΔ*ku80*:Fis1ΔTM is 23.2$\pm$8.7% of that in the parental strain. In conjunction, these results indicate that TGGT1_265180 associates with the mitochondrion via its C-terminus and that its localization and stability is at least in part dependent on Fis1.

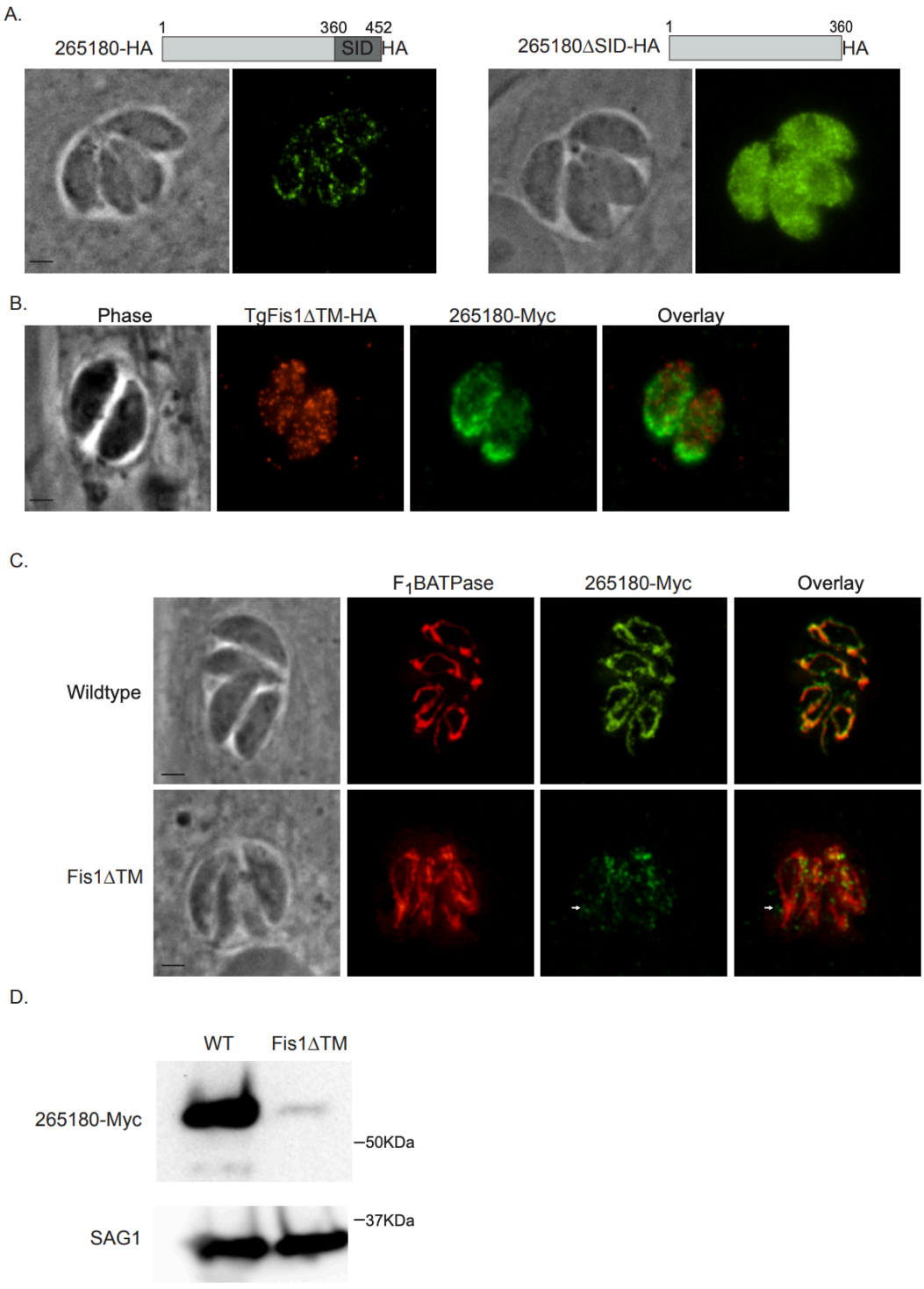

Figure 12. Association of TGGT1_265180 with the mitochondrion depends on Fis1. To investigate how TGGT1_265180 associates with the mitochondrion, we tested the roles of its C terminus and Fis1 on its localization. (A) Parasites were transfected with an exogenous copy of C-terminally HA-tagged wild-type TGGT1_265180 or with N-terminally HA-tagged TGGT1_265180 lacking the selected interaction domain (SID). The SID is the region of TGGT1_265180 that

was identified as interacting with Fis1. Intracellular parasites expressing TGGT1_265180-HA (left) or TGGT1_265180ΔSID-HA (right) were stained for HA. (B) Intracellular Fis1ΔTM-HA parasites expressing an endogenous copy of C-terminally myc-tagged TGGT1_265180 were probed for HA to detect Fis1 (red) and for myc to detect TGGT1_265180 (green). (C) Wild-type or Fis1ΔTM-HA parasites endogenously expressing TGGT1_265180-Myc were stained for F_1B ATPase (red) and myc (green) to monitor localization of TGGT1_265180. Bars, 2 μm. (D) Representative Western blot of extract from wild-type (WT) and Fis1ΔTM parasites expressing TGGT1_265180-Myc probed for myc (top blot) and SAG1 (bottom blot) as a loading control (61).

TGGT1_265180 knockout affects parasite fitness in tissue culture

Based on a genome-wide CRISPR screen, TGGT1_265180 was assigned a relative fitness phenotype score of -1.65, which indicates that, while its absence would negatively affect parasite fitness, it is likely not essential, making its genetic disruption possible (83). Accordingly, we employed double homologous recombination to replace the coding sequence of TGGT1_265180 with a drug selection marker and confirmed proper integration of the knockout construct by PCR (Fig. 13A and B). To test the effect of the knockout on parasite propagation we used a standard growth assay in which the same number of either parental or mutant parasites were allowed to infect human fibroblasts and form plaques over a five-day period. We observed a significant propagation defect in the Δ*265180* parasites, which manifests in both less and smaller plaques in comparison to the parental strain. To quantitate this defect, we counted the number of plaques formed by the parental and knockout strains in three separate experiments each with experimental triplicates (Fig. 13C). The average number of plaques by the Δ*265180* was 30.2$\pm$9.0% of that detected for the parental strain.

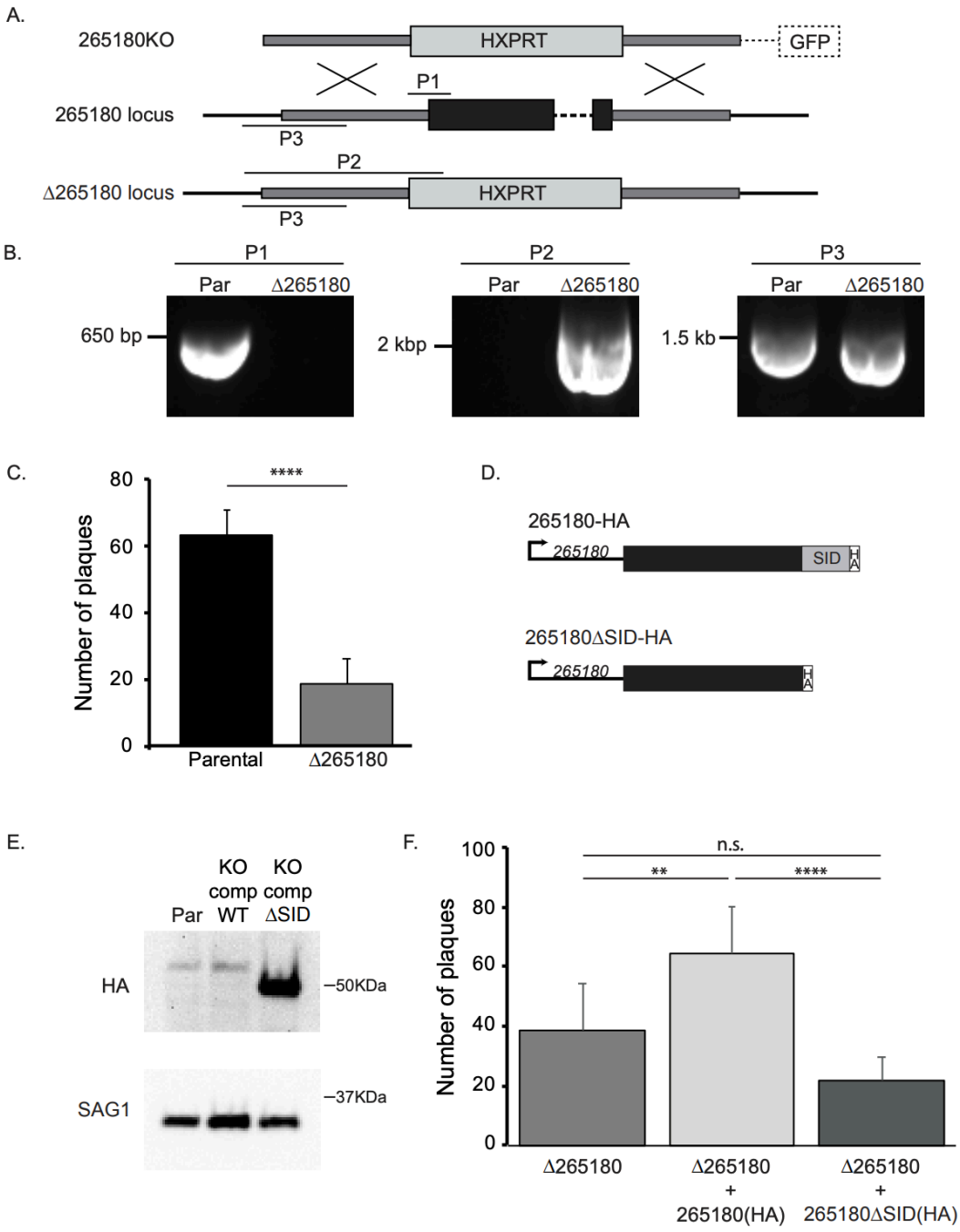

Figure 13. Knockout of TGGT1_265180 affects parasite propagation. To investigate the role of TGGT1_265180 in parasite fitness, we established knockout and complemented strains. (A) Schematic of strategy implemented to disrupt the TGGT1_265180 by replacing the coding sequences by the selectable marker HPT. On top is the vector used to drive the gene replacement, which includes HPT flanked by areas of homology to the TGGT1_265180 locus (dark gray boxes) and a downstream copy of GFP that is not integrated upon the desired double homologous recombination and can be used as a negative

selectable marker. Endogenous TGGT1_265180 is depicted in the middle with coding sequences represented by a black box. The bottom drawing shows the expected result from gene replacement in the knockout strain. P1, P2, and P3 indicate the PCR amplicons that were used to confirm integration. P1 would be detected only from parental parasites, P2 only from knockout parasites, and P3 from both. (B) PCR products from reactions to detect P1, P2, and P3 in the parental strain and the established Δ*265180* clone. (C) Average number of plaques per well for either parental or knockout strains after 4-day incubation period. Plaque assays were done in biological and technical triplicates, with error bars representing SD. Statistical analysis was performed by Student's t-test (****, $p<0.0001$). (D) Diagrams depict the two constructs used for complementation: TGGT1_265180-HA and TGGT1_265180ΔSID-HA. SID is the selected interaction domain identified through the two-hybrid screen. (E) Representative Western blot of a strain in which the endogenous TGGT1_265180 includes a HA epitope tag (parental [Par]), and the knockout strain complemented with wild-type TGGT1_265180-HA (KO comp WT) or with TGGT1_265180ΔSID-HA (KO comp ΔSID) probed for HA (top blot) and for SAG1 (bottom blot) as a loading control. (F) Average number of plaques per well for each strain after 4-day incubation period. Plaque assays were done in biological and technical triplicates, with error bars representing SD. Statistical analysis was performed by one-way ANOVA (****, $p<0.0001$; **, $p<0.0019$; n.s., not significant) (61).

To confirm that the phenotype observed was due to the disruption of the target gene and not a secondary effect, we complemented the Δ*265180* strain with an exogenous copy of the TGGT1_265180 including a C-terminal HA epitope tag driven by its own promoter. As the knockout strain lacks Ku80 and does not effectively allow for random integration, the exogenous copy was directed to the remnants of the Ku80 locus using CRISPR/Cas9. In addition to complementing with the wildtype TGGT1_265180, we transfected the knockout strain with the truncated version TGGT1_265180ΔSID, which does not localize to the mitochondrion (Fig. 13D). Western blot showed that both complemented strains expressed proteins of the expected size (Fig. 13E). Interestingly, while the wildtype complement expression level is similar to that of the endogenous levels, the

truncated copy appears to be expressed at a much higher level (Fig. 13E). Plaque assays of both the Δ*265180*+265180(HA) and Δ*265180*+265180ΔSID(HA) strains were performed in parallel to the knockout strain (Fig. 13F). The average number of plaques by the Δ*265180*+265180(HA) was 64.5±15.8, which is significantly higher than both the knockout and truncated complement strains (Fig. 13F). Δ*265180*+265180ΔSID(HA) had a lower average number of plaques (21.6±8.0) than that of the knockout (38.8±15.3), but this difference was not statistically significant. These results indicate that proper localization of TGGT1_265180 is necessary to rescue the growth phenotype seen in tissue culture.

TGGT1_265180 knockout disrupts the normal morphology of the mitochondrion

As TGGT1_265180 is associated with the mitochondrion we assessed mitochondrial morphology in the knockout parasites. In intracellular parasites, the mitochondrion maintains what is referred to as a lasso shape that abuts the periphery of the parasite (Figs. 6 and 14A, top panel) (48). However, based on staining with antibodies against F_1B ATPase, the mitochondrion of Δ*265180* parasites exhibit an altered mitochondrial morphology, with the bulk of the mitochondrial material concentrated at one end of the parasite (Fig. 14A). By contrast disruption of TGGT1_265180 did not affect the morphology of the apicoplast, rhoptries, or endoplasmic reticulum (Fig. 15). Introduction of the wild type TGGT1_265180 to the knockout strain complements the mitochondrial phenotype (Fig. 14B). In contrast, the truncated TGGT1_265180ΔSID, which is not

localized to the mitochondrion, does not rescue the collapsed mitochondrion phenotype (Fig. 14C).

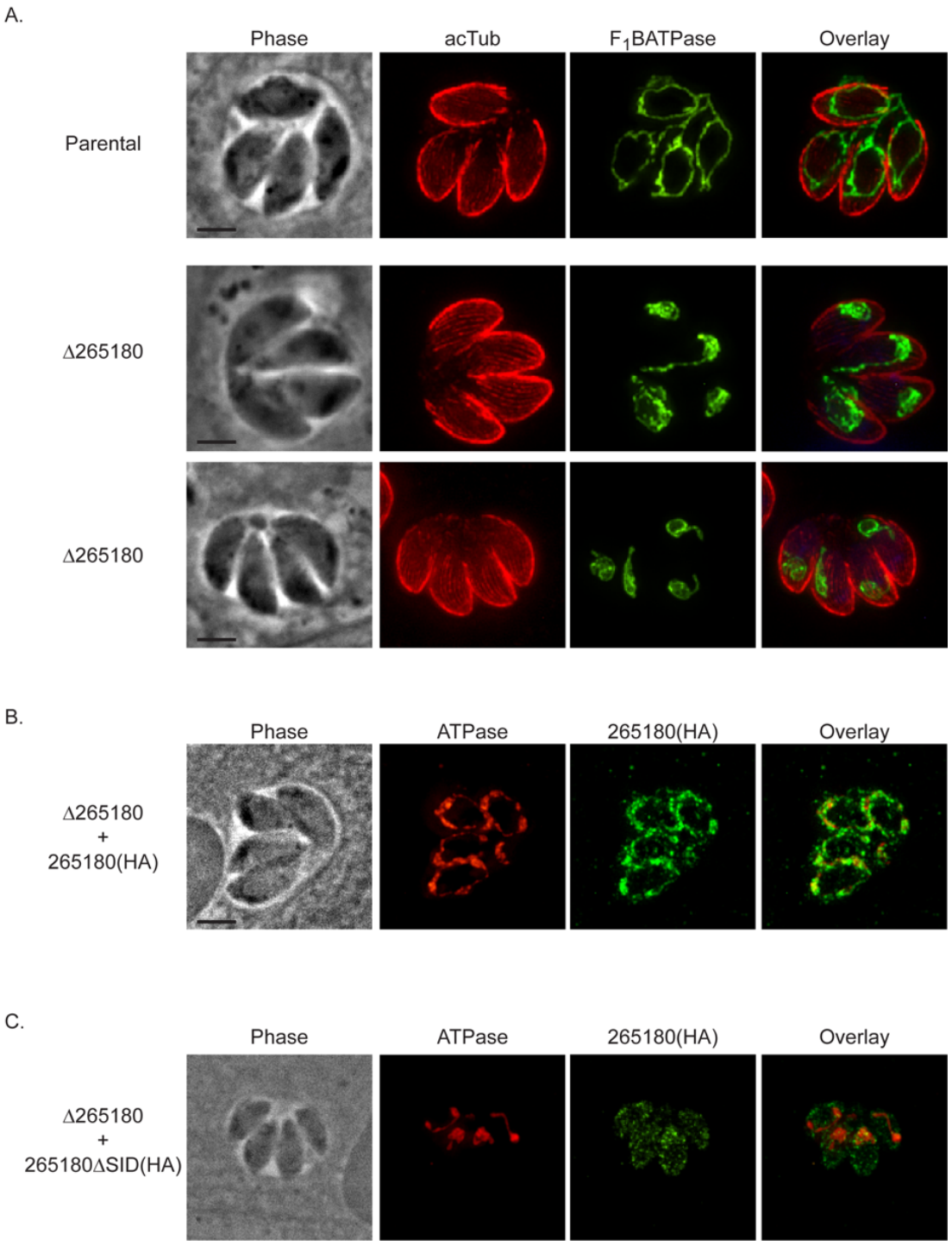

Figure 14. Mitochondrial morphology is disrupted by the absence of TGGT1_265180. To determine the effect of TGGT1_265180 ablation on the

mitochondrion, knockout and complemented parasites were analyzed by IFA. (A) Intracellular parasites of the parental or Δ*265180* strain were stained for F1B ATPase (green) to monitor mitochondrion and for acetylated tubulin (acTub) to detect the parasite cytoskeleton (red). (B and C) IFA of knockout parasites (Δ*265180*) transformed with either the wild-type [265180(HA)] or truncated [265180ΔSID(HA)] TGGT1_265180 with antibodies against F_1B ATPase (red) and HA (green). Bars, 2 μm (61).

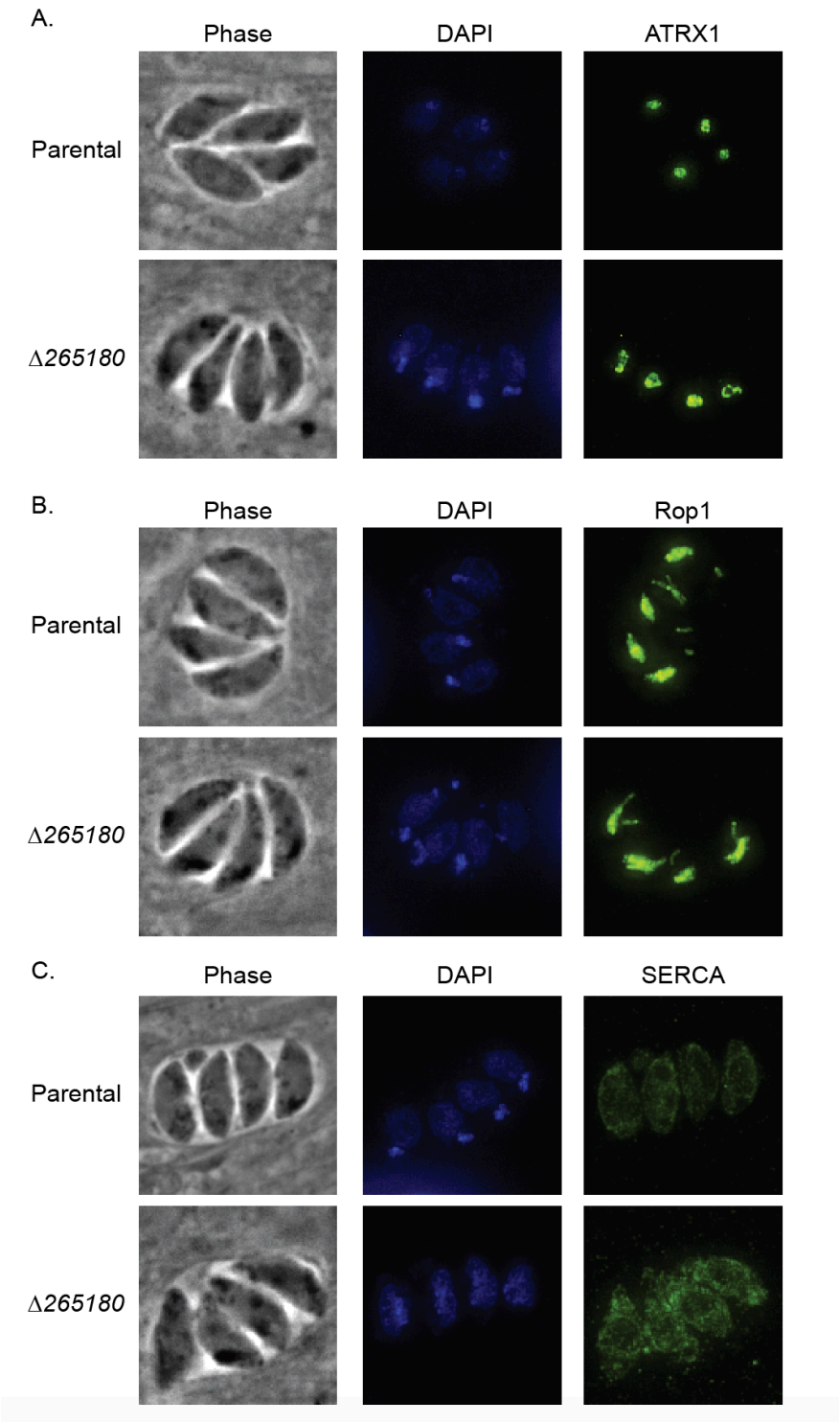

Figure 15. Genetic ablation of TGGT1_265180 has no apparent effect on the apicoplast, rhoptries, or ER. Intracellular parasites of the parental and the Δ*265180* strains were stained with DAPI to visualized DNA and with antibodies against (A) ATRX1 to visualize the apicoplast, (B) Rop1 to visualize the rhoptries, and (C) SERCA to visualize the endoplasmic reticulum (61).

The phenotype of the knockout and the complemented strains was quantitated by determining the percentage of parasites with normal and abnormal mitochondrion morphology. Normally, the *Toxoplasma* mitochondrion retracts from the periphery of the parasite during egress and changes its morphology to what has been described as sperm-like and collapsed (48). Interestingly, we observed all three morphologies normally associated with extracellular parasites (lasso, sperm-like, and collapsed) in intracellular parasites of the Δ*265180* strain (Fig. 16A). With the parental strain, the proportion of mitochondrial morphologies in intracellular parasites is 84.7±2.1% lasso, 15.3±2.1% sperm-like, and 0% collapsed. By contrast, intracellular parasites of the Δ*265180* strain, the mitochondrial distribution is 6.0±2.6% lasso, 50.0±2% sperm-like, and 44.0±4.4% collapsed (Fig. 16B). Just as it was the case for the plaquing phenotype, introduction of a wild type copy of TGGT1_265180 partly rescues the morphological phenotype with 48.5±4.4% of parasites exhibiting lasso-shaped mitochondrion, 49.2±3.9% sperm-like, and only 2.3±0.6% collapsed. Additionally, the truncated copy had a similar morphological distribution to that of the knockout strain (2.7±2.3% lasso, 56.0±10.1% sperm-like, and 41.4±12.4% collapsed) and was significantly different from the distributions of the parental and complement strains, which is consistent with defects seen in plaquing (Fig. 16B). Thus, TGGT1_265180 plays a crucial role in maintaining proper morphology of the mitochondrion. Consequently, we have dubbed this new gene Lasso Maintenance Factor 1 (LMF1).

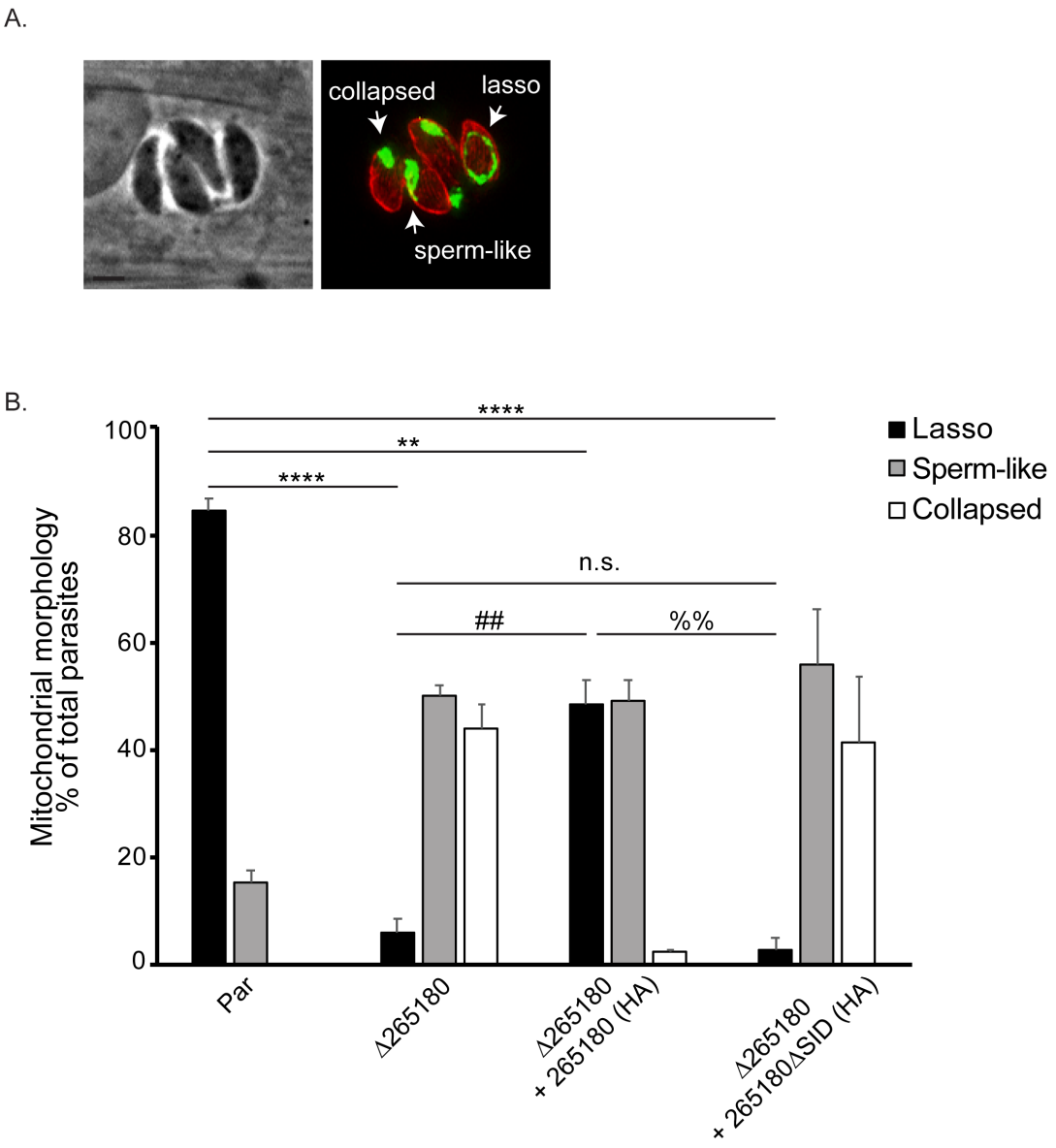

Figure 16. Intracellular parasites lacking TGGT1_265180 do not maintain their mitochondrion in the lasso conformation. To determine the penetrance of the mitochondrial phenotype observed in the Δ*265180* strain, the different morphological patterns observed were quantitated. (A) Intracellular parasites of the Δ*265180* strain stained for F_1B ATPase (green) and acetylated tubulin (red) exhibiting three distinct mitochondrial morphologies: lasso, collapsed, and sperm-like. Bar, 2 μm. (B) Percentage of parasites with each of the three different morphologies for the parental (par), knockout (Δ*265180*), and complemented [Δ*265180*+265180(HA) and Δ*265180* +265180ΔSID(HA)] strains. Data are average of biological triplicates, at least 50 vacuoles per sample were inspected. Error bars are ± SD. Statistics shown are ANOVA of percentage of parasites with lasso shape for each strain. ****, $p<0.001$; **, $p<0.004$; ##, $p<0.003$; %%, $p<0.002$; n.s., not significant. Bars, 2 μm (61).

Disruption of LMF1 results in defects in mitochondrial segregation between daughter parasites

During our analysis of mitochondrial morphology in the LMF1 mutant strain we noted various aberrant phenotypes that likely relate to parasite and mitochondrial division. *Toxoplasma* divides through a process called endodyogeny, where two daughter parasites form within a mother parasite (10, 15). This results in a doubling in the number of parasites in a vacuole after each round of replication. We noted that vacuoles of the LMF1 strain often had abnormal number of parasites (i.e. not 2, 4, 8, etc). We found that approximately 25.3±5.1% of vacuoles in Δ*265180* parasites had odd numbers compared to 5.8±2.9% in wildtype parasites and 13.7±3.1% in the complemented strain (Fig. 17A). Interestingly, we also noticed numerous vacuoles in which some parasites lacked a mitochondrion based on absence of F_1B ATPase staining (Fig. 17B, white arrows). When quantified, 16.2±4.0% of vacuoles contained at least one parasite that did not have mitochondrial material compared to 0.3±0.6% of RHΔ*ku80* parasites were amitochondriate (Fig. 17B). As with the other phenotypes, exogenous expression of wildtype LMF1 complemented the phenotype with 6.0±1.7% of vacuoles containing amitochondriate parasites. In addition to amitochondriate parasites, disruption of LMF1 also results in an accumulation of mitochondrial material outside of parasites (Fig. 17C, white arrows). We determined that 30.9±4.0% of vacuoles had extraparasitic mitochondrial material, which is three times greater than that of the parental parasite line (10.6±3.2%).

Interestingly, this particular phenotype was not complimented, as 28.3±2.1% of Δ*265180*+265180(HA) vacuoles contained extraparasitic material (Fig. 17C).

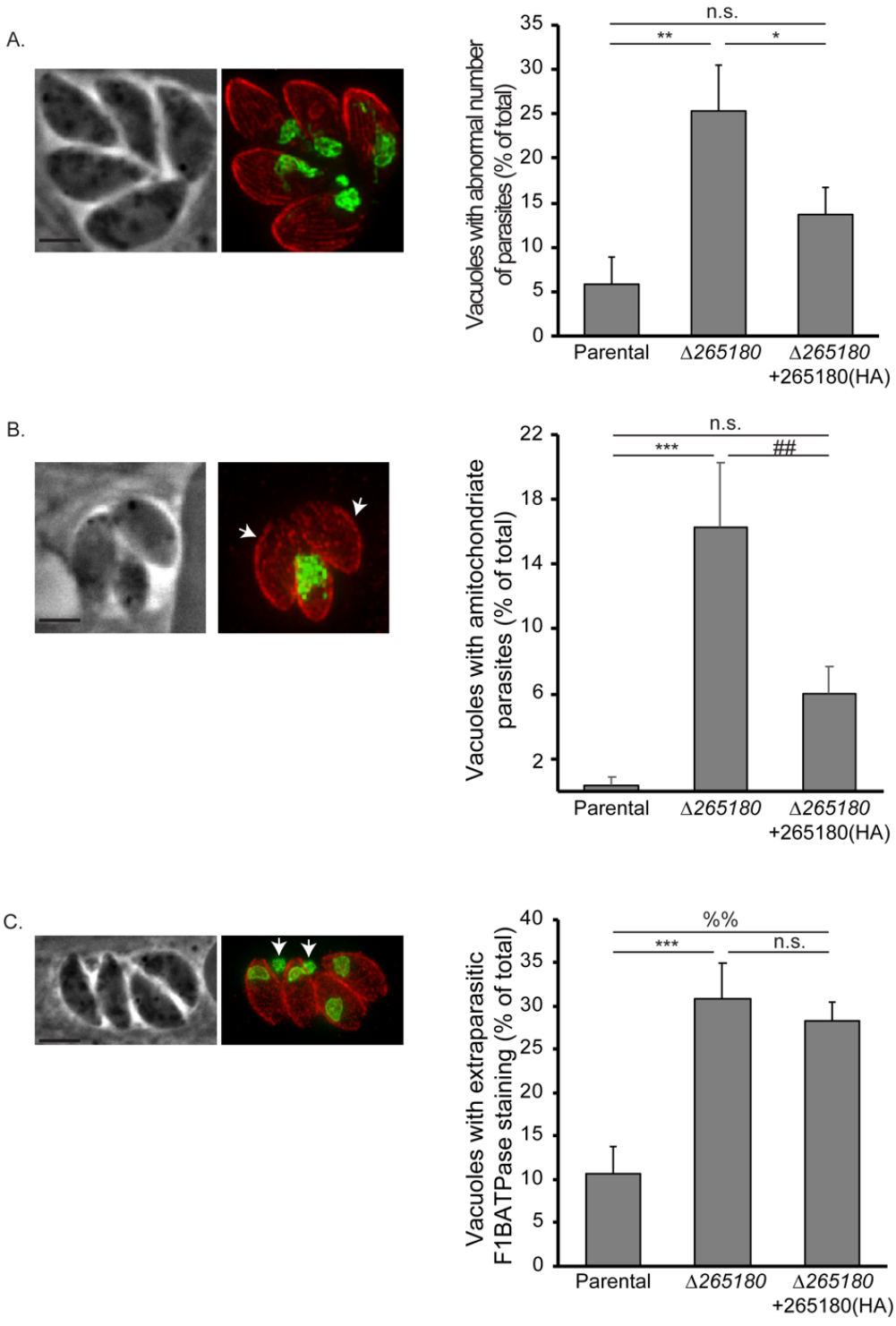

Figure 17. Parasites lacking TGGT1_265180 exhibit various division-related phenotypes. IFA of knockout parasites stained for F_1B ATPase (green) and acetylated tubulin (red) reveal various aberrant phenotypes. (A) The images on the left show a Δ*265180* vacuole containing five parasites rather than either four or eight as expected. The graph shows the percentage of vacuoles with

abnormal number of parasites for the three strains. (B) Images show vacuole with amitochondriate parasites (arrows) based on the absence of F_1B ATPase signal. The graph shows the percentage of vacuoles with at least one amitochondriate parasite for each strain. (C) Images show a vacuole that contains parasites with F_1B ATPase signal outside the parasite and within the parasitophorous vacuole (arrows). Bars, 2 μm. The graph shows the percentage of vacuoles with this phenotype. For all graphs, n=3 ± SD with at least 50 vacuoles per sample inspected. Statistical analysis was done with one-way ANOVA and a Tukey posthoc test. ***, $p<0.0006$; **, $p<002$; *, $p<0.02$; ##, $p<0.006$; %%, $p<0.001$; n.s., not significant (61).

We hypothesize that these phenotypes (abnormal number of parasites, amitochondriate parasites, and extraparasitic mitochondria) are the result of aberrant segregation of the mitochondrion into the daughter cells during endodyogeny. Accordingly, we co-stained parental and knockout parasites for acetylated tubulin to detect daughter cells and for F_1B ATPase to monitor the mitochondrion (Fig. 18). During the early (E) stages of division, wildtype parasite mitochondria surround the forming daughters (Fig. 18A, top panel). As endodyogeny progresses to an intermediate (I) stage, the mitochondrion remains excluded from the daughters (Fig. 18A, middle panel). When the daughters have almost fully formed (late (L) stages), branches of mother mitochondria incorporate into the daughter parasites before emerging from the mother (Fig. 18A, bottom panel). When LMF1 is disrupted, the mitochondrion does not have the typical lasso shape and appears to associate with one of the two daughters instead of surrounding both (Fig. 18B, top panel, E). As the daughters continue to form in the LMF1 deficient parasites, the mitochondrial material remains associated with one daughter or is completely excluded from the budding daughters (Fig. 18B, second panel, I). During the final stages of endodyogeny, some daughters seem to have

received mitochondrial material, whereas others have not. This correlates to an accumulation of mitochondrial material outside of the parasites (Fig. 18B, bottom three panels, L). Therefore, disruption of LMF1 leads to defects in mitochondrial segregation during endodyogeny, which agrees with the aberrant phenotypes observed with mitochondrial shape and localization (Figs. 16 and 17).

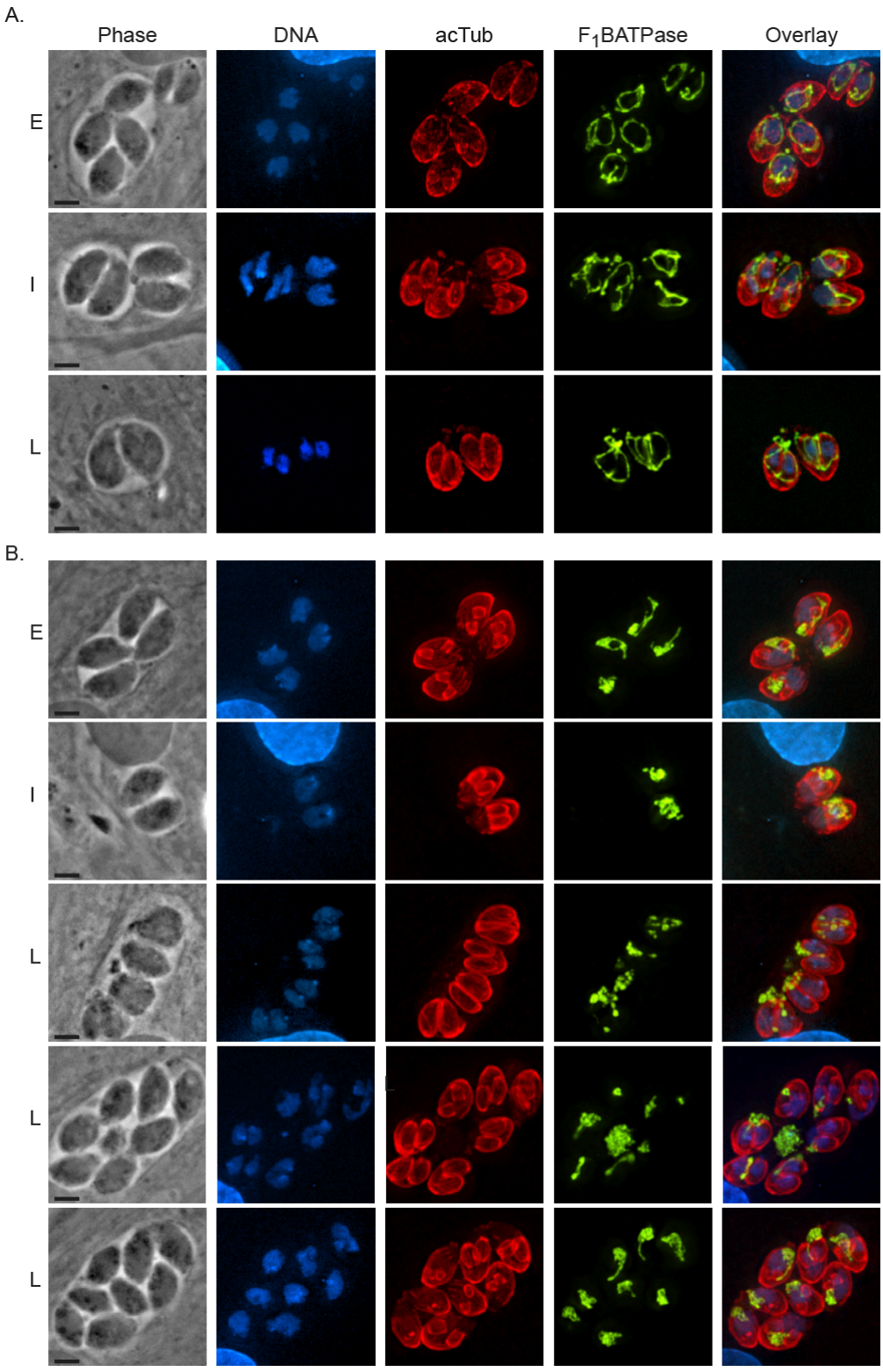

Figure 18. TGGT1_265180 disruption results in mitochondrial segregation defects. To examine mitochondrial dynamics during parasite division, IFAs of

parasites during early (E), intermediate (I), and late (L) stages of endodyogeny were conducted. (A) IFAs of intracellular wild-type parasites. (B) IFAs of intracellular Δ*265180* (also known as LMF1) knockout parasites. In both panels A and B, the stage of division was determined by DAPI staining (blue) and acetylated tubulin (red), which demarcate budding daughters. Mitochondrial morphology was observed by staining with F_1B ATPase, shown here in green. Bars, 2 μm (61).

Ultrastructural analysis of LMF1 knockout by EM

We have shown that LMF1 knockout causes defects in mitochondrial morphology and segregation with little observable defects in other organelles (Fig. 19). However, we wanted to confirm these results and inspect the morphology of the mitochondrion of parasites lacking LMF-1 at the ultrastructural level. Accordingly, in collaboration with Dr. Isabelle Coppens at Johns Hopkins University, we performed transmission electron microscopy of parental and knock out parasites. Through this ultrastructural analysis we identified a number of defects in parasite and mitochondrial structure. One noticeable phenotype is the presence of elongated mitochondria (Fig. 19A, yellow arrows) or multiple mitochondrial fragments within each parasite (Fig. 19A, second panel). Defects in mitochondrial morphology were consistent throughout the knockout LMF1 samples, but were not present in the parental RHΔ*ku80* sections. These data confirm that loss of LMF1 causes a disruption of the normal mitochondrial shape.

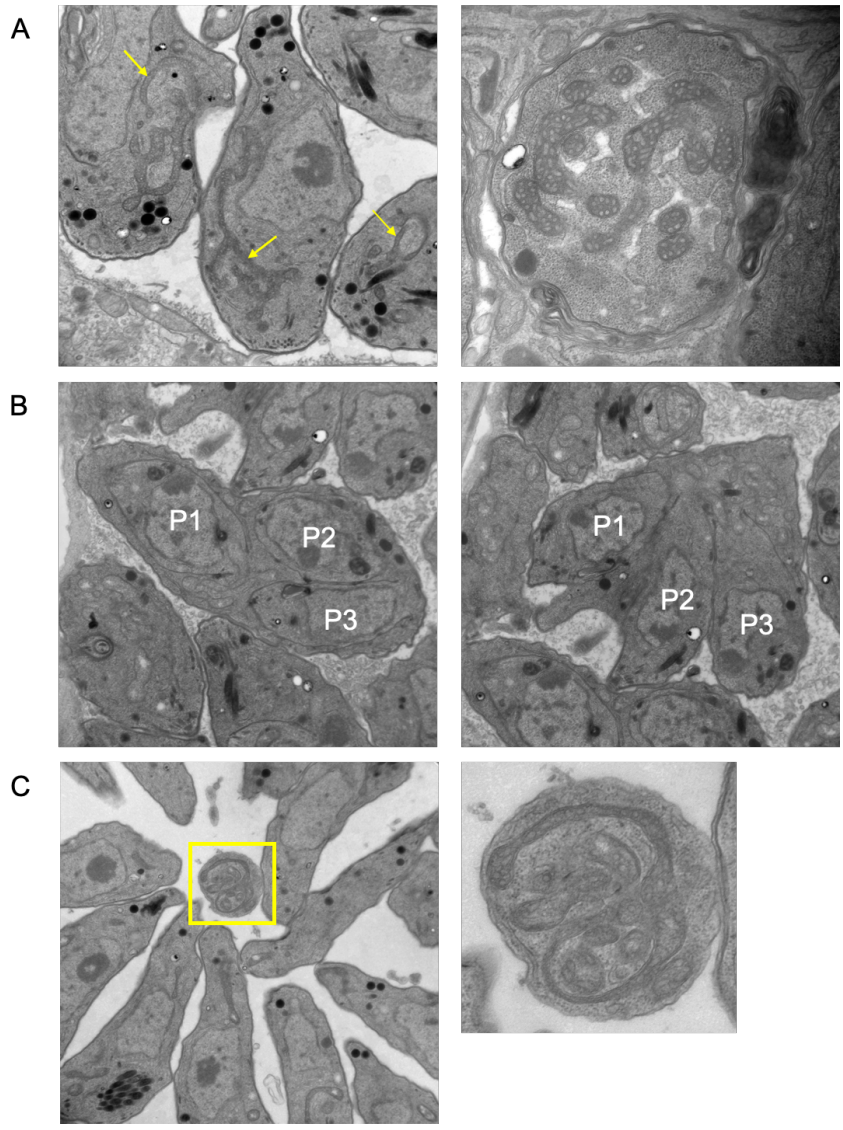

Figure 19. Ultrastructural analysis of LMF1-deficient parasites reveals mitochondrial segregation errors, abnormal mitochondria, and endopolygeny. Transmission electron microscopy (TEM) of LMF1 knockout parasites showed a number of defects including (A) elongated mitochondria (demarcated by yellow arose) and multiple mitochondrial fragments (second panel) (B) endopolygeny (each parasite nucleus is indicated) and (C) mitochondrial material left within the residual body, demarcated by the yellow box and second panel.

In addition to the mitochondrial shape defects seen, there were also a number of defects in parasite division. One defect observed is the presence of more than two daughter parasites within a single mother parasite, called

endopolygeny (Fig. 19B). This abnormal number of daughter parasites may account for the increase in odd numbers of parasites per vacuole seen in LMF1 knockout parasites (Fig. 17A). Additionally, a whole mitochondrion can be seen in the residual body of a vacuole in Figure 19C. This is reminiscent of the extraparasitic mitochondrial material that was observe by immunofluorescence in these parasites (Fig. 17C). Further analysis of these sections and gold labeling of LMF1 are needed to better understand how this protein, or lack thereof, is involved in the putative membrane contact site between the mitochondrion and the parasite pellicle.

Conditional knockdown of LMF1

We were able to show that complete genetic ablation of LMF1 results in mitochondrial collapse and various division and growth defects. In order to better observe what happens when the mitochondrion retracts from the periphery upon loss of LMF1, we endogenously tagged LMF1 with an HA epitope tag and a destabilization domain (DD) to conditional regulate LMF1 levels. In the presence of a ligand called SHLD-1, this DD domain is stabilized and the protein is able to function normally. However, when SHLD-1 is taken away, the protein is sent for proteasomal degradation (Fig 20A). We applied this system LMF1 for in parasites that stably express SOD2-GFP, to demarcate the mitochondria, and IMC1-TdTomato, to show the IMC. These SOD2-GFP IMC1-TdTomato parasites, generously provided to us by Dr. Diego Huet (70), allow to monitor mitochondrial morphology throughout the lytic cycle. After establishing the LMF1-HA-DD system

in the GFP/TdTomato-expressing strain we monitored the levels of protein and mitochondrial morphology in the parental strain and in the LMF1-HA-DD strain grown in 0, 50, 150 and 300 nM SHLD-1 (Fig.20B and C). LMF1-HA-DD parasites were maintained in their respective SHLD-1 concentrations for two passages before collecting samples for Western blot. After two passages in the absence of SHLD-1, LMF1 is very lowly expressed compared to parasites maintained in 150nM and 300nM SHLD-1 (Fig. 20B). When compared to their respective loading controls, there is an apparent increase in protein levels as the SHLD-1 concentration is also increased (Fig. 20B). We also examined the mitochondrial morphology of these parasites in either 0nM SHLD-1 or 150nM SHLD-1 and found that the absence of SHLD-1 causes mitochondrial collapse, whereas parasites maintained in 150nM are able to retain the lasso shape. Based on these data, we have shown that LMF1 is able to be conditionally regulated and its protein expression is dose-dependent on SHLD-1.

Interestingly, the parental GFP/TdTomato-expressing parasites exhibit approximately half lasso mitochondria and half sperm-like (46.87$\pm$2.45% and 50.21$\pm$4.08%, respectively), which is different than the parental RHΔ*ku80* line (Fig. 21A). This is possibly due to the large GFP tag on SOD2 causing interference in mitochondrial morphology. Nonetheless, we observe significant differences in mitochondrial morphology in the LMF1-HA-DD strain depending on the amount of SHLD-1 present. When comparing between parental and LMF1-HA-DD parasites at the four concentrations of SHLD-1 we found that both 0 and 50nM SHLD-1 had significantly lower levels of lasso mitochondria with only 4.72$\pm$5.19% and

17.08±7.99% of parasites having this morphology, respectively (Fig. 21A). This is significantly less than the parental, which exhibits 46.87±2.46% of parasites with lasso mitochondrion. The percentage of LMF1-HA-DD parasites with lasso mitochondrion is not significantly different from the parental when grown at 150nM and 300nM SHLD-1 (Fig. 21B). Thus, stabilization of LMF-1 by SHLD-1 recovers the normal morphology of the mitochondrion, which confirms the important role of LMF-1 on mitochondrial morphology.

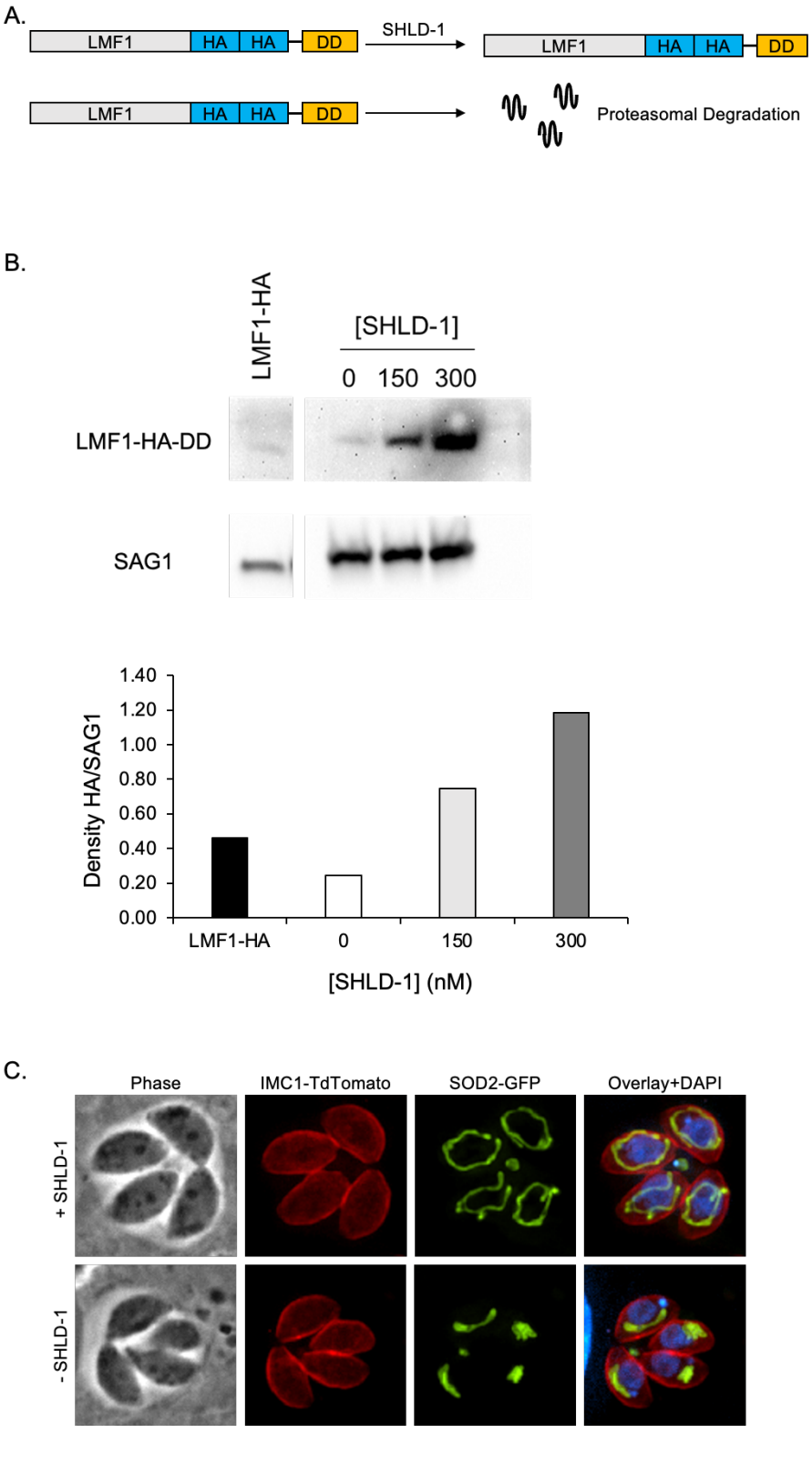

Figure 20. Conditional knockdown of LMF1 causes a SHLD-1 dose-dependent mitochondrial collapse and growth defect. (A) Schematic of LMF1 stabilization and degradation in the presence and absence of SHLD-1,

respectively. (B) Representative Western blot showing regulation of LMF1 levels by varying concentrations of SHLD-1. Graph shows the density of the HA band over the density of the respective SAG1 band of the Western blot above (n=1). (C) LMF1 depletion results in mitochondrial collapse, shown in green, with no effects on parasite pellicle structure, shown in red.

Our previous data on Δ*lmf1* suggests that mitochondrial collapse results in defects in mitochondrial segregation and parasite fitness. Based on this, we performed plaque assays to determine if altering levels of LMF-1 with different concentrations of SHLD-1 affected parasite growth. Briefly, parasites of the LMF1-HA-DD strain were maintained in 0nM, 50nM, 150nM, or 300nM SHLD-1 for three passages before the same number of parasites were allowed to invade a confluent monolayer. After the plate has incubated for six days, the plate was fixed and stained with crystal violet to show the intact monolayer compared to the unstained plaques. Our data showed that LMF1-HA-DD parasites in the absence of SHLD-1 only disrupted 2.12±2.83% of the monolayer, which significantly differed from parasites maintained in 150nM SHLD-1 (12.93±9.20%) (Fig. 21B). Interestingly, parasites maintained in 300nM of the ligand showed decreased parasite growth compared to the 150nM, though this result was not significant (Fig. 21B). These data suggest that not only does the level of SHLD-1 affect LMF1-HA-DD mitochondrial morphology in a dose-dependent manner, but it also affects parasite growth as well.

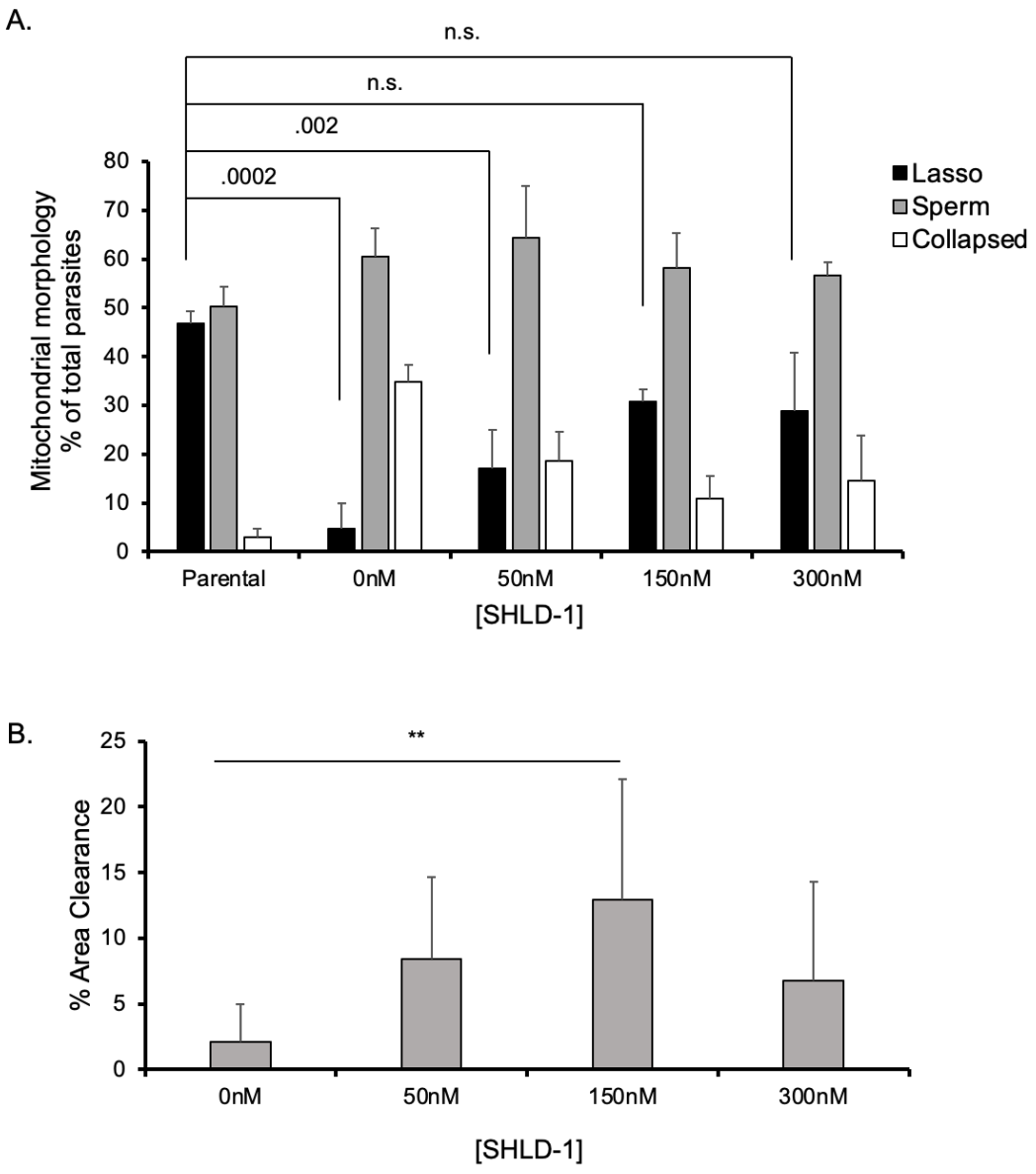

Figure 21. Conditional knockdown of LMF1 results in mitochondrial shape change and decreased growth in tissue culture in a SHLD-1 dose-dependent manner. (A) Frequency of lasso, sperm-like, and collapsed mitochondrial morphologies were quantified for parental parasites strain (DiCredku80 SOD2-GFP IMC1-TdTomato), and LMF1-HA-DD in varying concentrations of SHLD-1. Mitochondrial morphology was quantified as ten fields of view per replicate over three biological replicates. (B) LMF1-HA-DD parasites were cultured in four concentrations of SHLD-1 over two passages before performing plaque assay. The percent area cleared was determined by ImageJ and the values shown are the mean % area clearance $\pm$ SD (One-way ANOVA, n=4; **p< 0.001).

Mitochondrial position throughout lytic cycle

Previous studies have shown that mitochondrial retraction from the pellicle of *Toxoplasma* is directional, with greater than 90% of extracellular sperm-like mitochondria containing the majority of the mitochondrial material at the apical end of the parasite (48). Since the mitochondrion of LMF1 knockout parasites is always collapsed regardless of whether the parasite is inside or outside the cell, we monitored mitochondrial position throughout the parasite lytic cycle. Mitochondrial position in parasites with either sperm-like or collapsed mitochondrion was classified as either apical or basal using the IMC, which does not cover the apical periphery of the parasite, as a reference (Fig. 22A, second panel). For sperm-like the classification was based on the position of the bulk of the mitochondrion (i.e., the head of the sperm). In intracellular Δ*lmf1* parasites, there was no significant difference in the frequency of apical and basal mitochondrial position, indicating that the position is stochastic in this environment (Fig. 22B). This position is maintained directly after mechanical egress of the parasites through a needle (Fig. 22C). These knockout parasites were then allowed to invade host cells for one hour before they were extensively washed and fixed to observe the mitochondrial position directly after parasite invasion. In this case, there was a significant difference between apical and basal localization, with a higher level of apically positioned mitochondria. This result could indicate a number of things, but the two most likely possibilities are that: 1. parasites with apically positioned mitochondria are more efficient at invasion than those with basal localization or 2. parasites with basally positioned mitochondria may be ill equipped to survive in the extracellular

environment, thus creating a lower proportion of basally localized mitochondria. The distinction between these two hypotheses has yet to be explored and is proposed for further study.

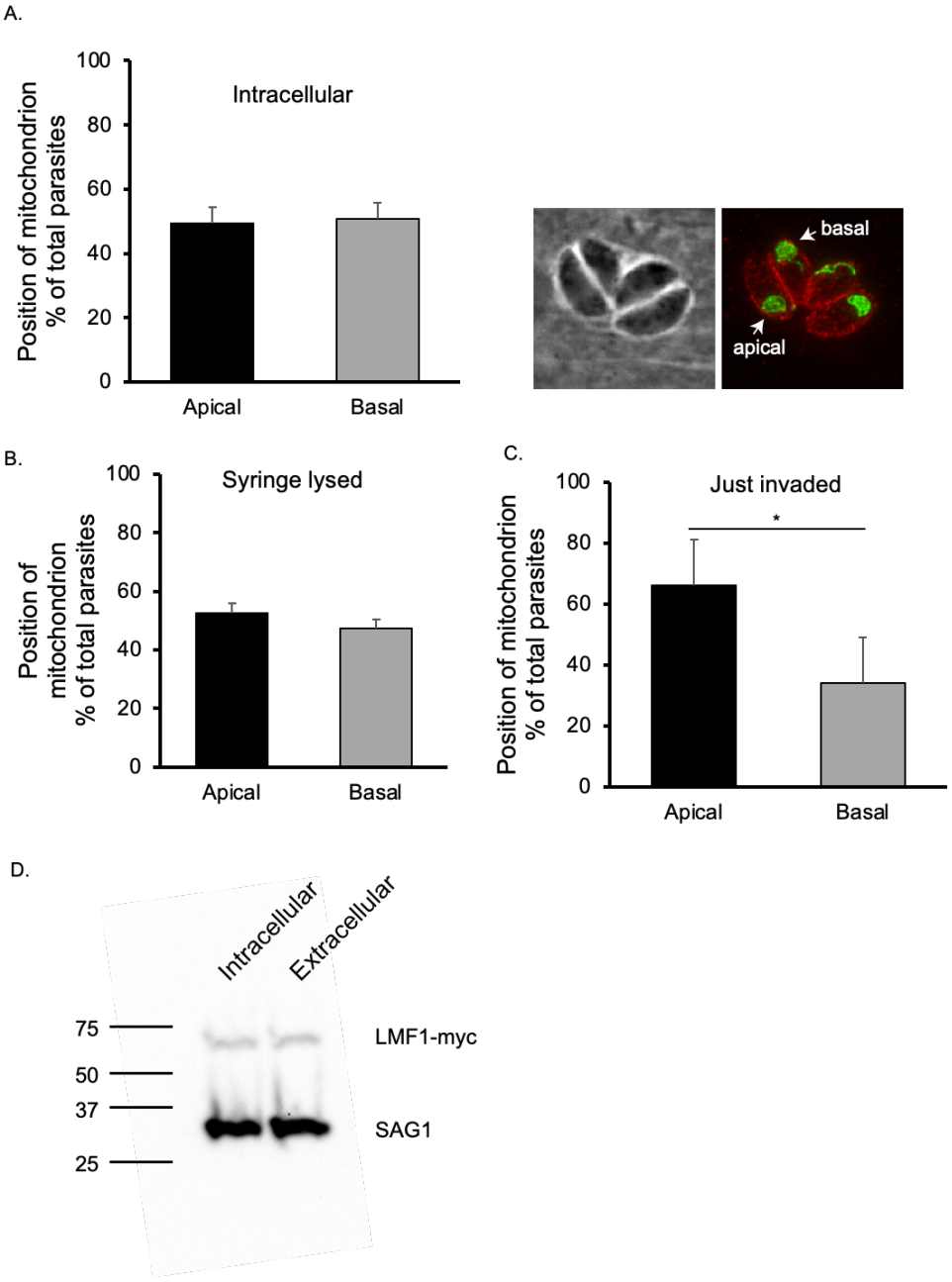

Figure 22. Mitochondrial position of LMF1 knockout parasites is stochastic after division and immediately after egress, but is preferentially apical directly after invasion. Mitochondrial position was determined to be apical or

basal based on IMC3 staining, which stains the apical 2/3 of the parasite pellicle. Parasites were determined to be apical or basal (shown in A, second panel) in (A) intracellular parasites, (B) parasites immediately after mechanical egress, and (C) after invading host cells for one hour. (D) Levels of LMF1 in intracellular and extracellular parasites were determined by Western blot and compared to the loading control, SAG1.

In order to determine if the mitochondrial retraction seen in extracellular wildtype parasites was due to a change in protein levels, protein lysate from LMF1-myc parasites that were either intracellular or extracellular for 8 hours were collected. These protein levels were compared to their respective loading control by densitometry and the difference between LMF1 protein levels in intracellular and extracellular parasites is not significant (Fig. 22D). Since there is no difference in LMF1 protein levels, it is possible that there is a differential posttranslational modification that occurs upon egress. As of now, the environmental trigger that causes mitochondrial collapse in extracellular parasites is unknown and may be tied to changes in LMF1.

LMF1 interactors

Based on the results presented in Chapter 3, we propose that LMF1 is a molecular component of a membrane contact site between the mitochondrial membrane and the parasite pellicle. This model would predict that LMF1 would interact with other proteins in both the pellicle and the mitochondrion. Accordingly, we sought to identify proteins that interact with LMF1 both in the mitochondrial membrane and in the pellicle. For this purpose, we employed both Y2H and immunoprecipitations as complementary approaches. Using the same method as

done previously for Fis1 (see Chapter 2), full-length LMF1 was analyzed for interactions by screening against a *Toxoplasma* cDNA library and analyzing over 95 million interactions. Of these, there were 257 positive clones produced, which resulted in 70 potential interactors (Table 4) (73, 77). We analyzed interactors with no known localization using a recently published proteomic database that predicts localization through Localization of Organelle Proteins by Isotope Tagging (LOPIT) and ultracentrifugation (ToxoDB) (82). Since we predict that LMF1 mediates a membrane contact site between the mitochondrion and parasite periphery, we focused on proteins predicted to localize to the mitochondrion, apical end, IMC, and parasite periphery. Using LOPIT, 3 interactors are localized to the IMC, 6 proteins associate with the apical end, 2 are associated with the mitochondrial membrane, and 3 are in the parasite periphery. Some putative interactors of note include the calcium-dependent protein kinase CDPK7, guanylyl cyclase (GC), and numerous proteins within the parasite pellicle, such as inner membrane complex 10 (IMC10) and inner membrane localizing protein 1 (ILP1). IMC10 is an inner membrane complex (IMC) resident protein that localizes to the IMC and is expressed at higher levels in the budding daughter parasites in comparison to the mother, which is similar to the expression pattern of IMC3 (84). ILP1 has a similar localization pattern to IMC10 and interestingly, IMC10 was shown to be a possible interactor of ILP1 by co-immunoprecipitation and mass spectrometry (85, 86). Therefore, it is possible that ILP1, IMC10, and LMF1 work together to form the scaffold necessary for peripheral distribution of the mitochondrion.

Since LMF1 protein levels do not differ between intracellular and extracellular parasites (Fig. 22D), it is possible that a post-translation modification is able to eliminate the membrane contact site between the mitochondrion and the pellicle in the extracellular space. LMF1 is predicted to be phosphorylated multiple times, which makes CDPK7 an interesting putative interactor. CDPK7 was found to be involved in parasite division and is essential for parasite fitness (87). Another interesting interactor is guanylyl cyclase (GC), which was recently found to change localization between intracellular and extracellular parasites. In addition to this dynamic localization, TgGC is essential for proper secretion of micronemes and conoid extrusion, both of which are necessary for egress, motility, and invasion. The signaling events that GC may regulate, including cGMP and potential lipid transport functions, are potentially rapid enough to account for the mitochondrial shape change that occurs upon egress (88, 89).

Table 4. Putative LMF1 interactors determined by Y2H[a]

ToxoDB Gene ID	Product Description	Global PrBS[b]	CRISPR score
TGME49_230210	alveolin domain containing intermediate filament IMC10	A	-4.70
TGME49_285870	SAG-related sequence SRS20A	A	1.74
TGME49_295050	tRNA ligase class II core domain (G, H, P, S and T) domain-containing protein	A	-2.96
TGME49_300140	elongation factor 1-gamma, putative	A	-3.02
TGME49_235470	myosin A	B	-3.09
TGME49_254370	guanylyl cyclase	B	-3.56
TGME49_258540	phosphoglycerate mutase family protein	B	-4.95
TGME49_201780	microneme protein MIC2	B	-1.17
TGME49_233810	Sel1 repeat-containing protein	B	-0.78
TGME49_244530	hypothetical protein	B	2.12
TGME49_313380	ILP1	C	-4.70
TGME49_205360	hypothetical protein	C	-1.59
TGME49_217680	hypothetical protein	C	0.99
TGME49_242260	hypothetical protein	C	-5.58
TGME49_257760	hypothetical protein	C	1.21
TGME49_269690	hypothetical protein	C	1.54
TGME49_278030	hypothetical protein	C	0.45
TGME49_290950	clathrin heavy chain, putative	C	-4.77
TGME49_243250	myosin H	D	-3.94
TGME49_244470	RNG2	D	-4.21
TGME49_246720	hypothetical protein	D	0.24
TGME49_252880	hypothetical protein	D	-2.09

TGME49_273560	Kinesin B	D	-0.94
TGME49_289990	hypothetical protein	D	-0.65
TGME49_213670	hypothetical protein	D	-3.88
TGME49_231930	hypothetical protein	D	-1.24
TGME49_259720	hypothetical protein	D	-4.55
TGME49_266830	Sec7 domain-containing protein	D	0.30
TGME49_202040	hypothetical protein	D	-0.20
TGME49_203520	hypothetical protein	D	-1.25
TGME49_204080	histidine acid phosphatase superfamily protein	D	-1.99
TGME49_206430	formin FRM1	D	-3.24
TGME49_218560	acetyl-coA carboxylase ACC2	D	-3.06
TGME49_223760	hypothetical protein	D	-2.75
TGME49_224870	hypothetical protein	D	-0.48
TGME49_225745	hypothetical protein	D	0.53
TGME49_227960	PCI domain-containing protein	D	-3.33
TGME49_228750	calcium dependent protein kinase CDPK7	D	-4.13
TGME49_229790	hypothetical protein	D	-4.80
TGME49_231840	hypothetical protein	D	-0.81
TGME49_247290	hypothetical protein	D	-1.16
TGME49_248680	hypothetical protein	D	-1.00
TGME49_250690	zinc finger (CCCH type) motif-containing protein	D	-1.40
TGME49_252220	tetratricopeptide repeat domain containing protein	D	-1.03
TGME49_254470	hypothetical protein	D	0.88
TGME49_255300	hypothetical protein	D	-2.99
TGME49_258070	hypothetical protein	D	-5.24
TGME49_258870	hypothetical protein	D	1.32

TGME49_267020	hypothetical protein	D	-3.27
TGME49_269200	crooked neck family 1 protein isoform 2, putative	D	-2.99
TGME49_272040	WD domain, G-beta repeat-containing protein	D	-3.80
TGME49_272695	hypothetical protein	D	0.43
TGME49_275440	dense granule protein GRA6	D	1.84
TGME49_275690	ClpB, putative	D	-4.75
TGME49_286450	dense granule protein GRA5	D	2.58
TGME49_289520	hypothetical protein	D	-4.87
TGME49_293430	hypothetical protein	D	1.48
TGME49_294350	DEAD/DEAH box helicase domain-containing protein	D	-4.32
TGME49_294620	eukaryotic initiation factor-3, subunit 8, putative	D	-4.89
TGME49_295730	tetratricopeptide repeat-containing protein	D	-3.99
TGME49_298020	DEAD-family helicase	D	-4.44
TGME49_304680	ubiquitin family protein	D	-0.95
TGME49_305240	XPA binding protein 2 family protein	D	-2.50
TGME49_306660	RNA pseudouridine synthase superfamily protein	D	-4.59
TGME49_308070	hypothetical protein	D	-2.65
TGME49_314900	LisH protein	D	-0.93
TGME49_314970	root hair defective 3 GTP-binding protein (rhd3) protein	D	-4.38
TGME49_318390	hypothetical protein	D	-0.87
TGME49_319860	DNA polymerase family B protein	D	-3.85
TGME49_215520	hypothetical protein	E	0.61

[a] Proteins that also appear in the LMF1 immunoprecipitation experiments are highlighted in orange and those that also appeared in the Fis1 Y2H are highlighted in green.

[b] Predicted biological score (PrBS) are confidence scores, with A indicating the highest confidence of interaction and E being the lowest confidence of interaction (73, 77).

[c] CRISPR Score from genome-wide screen with phenotype scores ranging from approximately -7 (essential) to 3 (dispensible) (83).

Table 5. Potential LMF1 interactors as determined by three independent immunoprecipitations[a]

ToxoDB Gene ID	Product Description	Total Peptides	Fold Change[b]	CRISPR Score[c]
TGGT1_278870	myosin F	63	INF	-3.55
TGGT1_265180	LMF1	44	INF	-1.65
TGGT1_260540	**IMC14**	11	INF	1.75
TGGT1_295360	**IMC18**	10	INF	1.13
TGGT1_311230	**hypothetical protein**	10	INF	0.74
TGGT1_219270	**multi-pass transmembrane protein GAPM2a**	9	INF	-3.53
TGGT1_230850	**TSC3**	8	INF	-0.38
TGGT1_258470	**IMC24**	6	INF	2.58
TGGT1_250820	**AC2**	5	INF	0.50
TGGT1_210370	ROP54	4	INF	1.07
TGGT1_286580	**IMC17**	36	36.0	1.38
TGGT1_220270	**IMC6**	16	16.0	-3.19
TGGT1_248700	**IMC12**	12	12.0	-0.17
TGGT1_230210	**IMC10**	34	11.3	-4.70
TGGT1_267500	**CBAP**	11	11.0	-0.72
TGGT1_222220	**IMC7**	23	7.7	-0.64
TGGT1_258410	**PhIL1**	20	6.7	1.74
TGGT1_308860	**AC3**	23	5.8	-0.37
TGGT1_252360	rhoptry kinase family protein ROP24 (incomplete catalytic triad)	11	5.5	1.34
TGGT1_313380	**ILP1**	21	5.3	-4.70

TGGT1_226570	**hypothetical protein**	4	4.0	2.46
TGGT1_252290	Cluster of putative importin alpha	4	4.0	-5.32
TGGT1_316340	**IMC22**	4	4.0	-0.27
TGGT1_232130	**TLAP2**	4	4.0	-0.82

[a] LMF1, the bait protein, is highlighted in blue. Proteins that also appeared in the LMF1 Y2H are highlighted in orange. Proteins in bold type font localize to the parasite pellicle

[b] Fold change was determined by dividing the total peptides of each putative interactor from three experiments by the number of peptides for that protein in the control sample. INF fold change indicates there were no peptides in the control.

[c] CRISPR Score from genome-wide screen with phenotype scores ranging from approximately -7 (essential) to 3 (dispensible) (83).

Since the list of interactors produced by Y2H is extensive, we sought to narrow down potential interactors by doing immunoprecipitation experiments. We pulled down LMF1-HA onto HA magnetic beads and sent these beads for mass spectrometry. Fold change was determined by dividing the total number of peptides in the LMF1-HA samples by the total number of peptides in the Ku80 control samples. This was repeated three times and the resulting putative interactors are compiled in Table 5. This list only includes proteins that were identified in at least two of the three replicates and had a fold change of 4 or greater over the control. This produced a list of 23 potential interactors, including both IMC10 and ILP1, which were also in the Y2H. Interestingly, 19 out of 23 interactors are known to localize to the parasite pellicle (shown in bold type font in Table 5). In addition to the two proteins found in both the LMF1 experiments, three proteins were from the LMF1 Y2H were also in the Fis1 Y2H (Table 5).

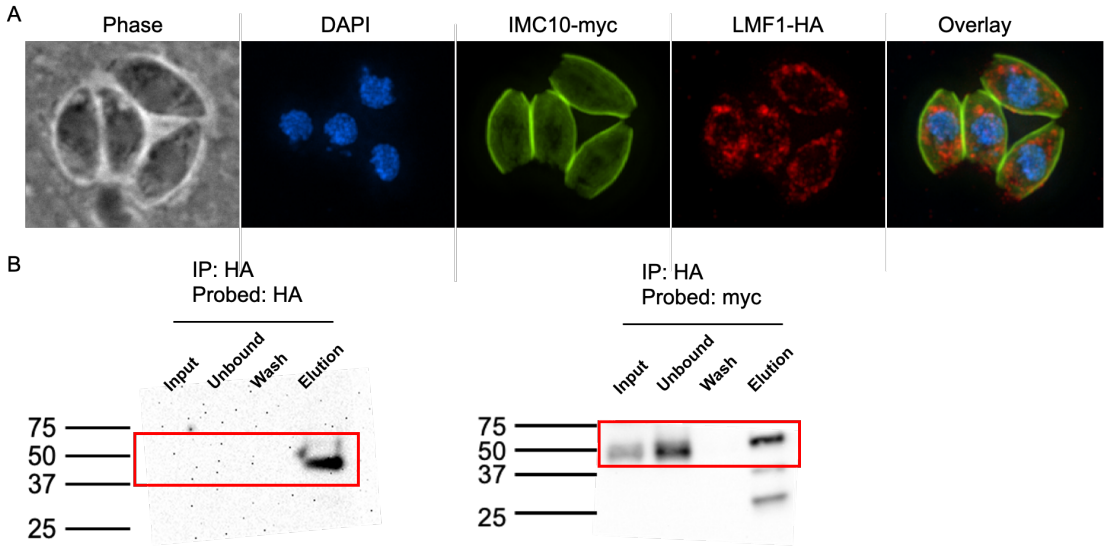

Figure 23. LMF1 and IMC10 are interacting partners. A. Representative image of parasites co-tagged with LMF1-HA(red) and IMC10(myc). B. Western blot of reciprocal co-IP where LMF1-HA was precipitated on HA magnetic beads and probed for HA (left panel) or myc (right panel). The predicted bands are outlined with a red box and the two bands in the myc elution lane are likely heavy and light chain.

Since IMC10 was shown to have the highest level of confidence of interaction by Y2H and a 11.3-fold change in the immunoprecipitation experiments, we decided to explore this potential interaction further. To determine if LMF1 and IMC10 are true interactors, we tagged IMC10 with a C-terminal endogenous myc tag in a parasite line in which LMF1 is endogenously tagged with a HA epitope tag. As expected, IMC10 localizes to the IMC and extends almost the entirety of the cortical cytoskeleton (Fig. 23A). With both proteins expressing different epitope tags, we were able to perform reciprocal co-immunoprecipitation experiments and determine interaction by Western blot. Briefly, LMF1-HA was pulled down on HA-magnetic beads and half of each sample was ran on a Western blot and probed for either HA or myc. Since LMF1 is not highly expressed, it is not surprising that LMF1 was not seen in the input sample, but was enriched in the elution from beads

(Fig. 23B). On the other hand, IMC10 is very highly expressed and was able to be seen in both the input and unbound fractions at the expected size (~60 kDa). We also saw an IMC10-myc band in the elution, indicating that IMC10 and LMF1 do in fact interact.

Chapter 4: Discussion and Future Directions

The single mitochondrion of the pathogen *Toxoplasma gondii* is highly dynamic, with its location and structure changing during various stages of the parasite's lytic cycle. As the last organelle to move from a live mother parasite into two nascent daughter cells, the morphology and position of the mitochondrion is tightly regulated during parasite division. Similarly, as the parasite moves from inside to outside host cells the mitochondrion morphology dramatically changes. While inside the host cell *Toxoplasma*'s mitochondrion forms a lasso with multiple points of contact with the parasite pellicle, then quickly retracts from the parasite periphery to a collapsed bundle at the apical end as the parasites move to the extracellular space. Our lab has shown that the mitochondrial morphology also changes under treatment with the anti-parasitic drugs atovaquone and monensin. Under drug treatment the mitochondrion's outer membrane becomes constricted causing the inner mitochondrial material to appear punctate. Importantly, this phenomenon is completely reversible and upon removal of monensin, the mitochondrion returns to its typical shape.

The morphological changes experienced by the mitochondrion under monensin treatment are likely a response to stress and might represent a mechanism by which the parasite protects the mitochondrion from irreversible damage. Mitochondria from numerous organisms alter their morphology to respond to specific stressors, such as UV radiation and nutrient starvation (40). In conditions that damage mitochondrial DNA, such as cycloheximide and UV radiation, mitochondria hyperfuse (40). This phenomenon most likely occurs to

complement damaged mitochondrial DNA and promote DNA mixing. Conditions that affect mitochondrial respiration, such as oligomycin and uncoupling agents, cause mitochondrial fragmentation (42, 43). Similarly yeast cultured in aerobic, respiratory conditions have more punctate mitochondria whereas anaerobic conditions result in branched and elongated morphologies (41). These data suggest that mitochondrial morphology is responsive to environmental conditions and stressors. Therefore, the phenotype observed under monensin treatment is likely a protective mechanism for the mitochondrion against the effects of the ionophore.

As the effect of monensin is a reversible constriction along the outer mitochondrial membrane, I hypothesize that this phenomenon would require the mitochondrial fission machinery. The yeast mitochondrial fission machinery is the most well characterized and it is comprised of the membrane anchored protein Fis1p, which actively recruits other proteins to the mitochondria during fission like Mdv1 (mitochondrial division protein 1), which acts as an adapter protein. Fis1p is then able to recruit a GTPase, dynamin (Dmn1), which is able to drive the final scission of the mitochondrion (45). No homologs for Mdv1 have been found in *Toxoplasma gondii*, but there is one Fis1 homolog (TGGT1_263323) and three dynamin-related proteins: DrpA, DrpB, and DrpC. Of these, DrpC, which lacks many of the features required for Drp function, has been associated with mitochondrial division (90). Nonetheless, we and other groups have shown that instead DrpC appears to be involved in vesicle trafficking and endocytosis (56, 90).

As the strongest homolog of any putative fission protein in *Toxoplasma,* we investigated the role of Fis1 in monensin driven mitochondrial rearrangement. We found that Fis1 localization to the mitochondrion is important for monensin-induced remodeling and the absence of Fis1 results in decreased sensitivity to the ionophore. Thus, it is plausible that Fis1 is recruiting proteins to the mitochondrion outer membrane during monensin treatment to induce a transient constriction, similar to the transient interaction Fis1 has with Drp1 (58, 91). As DrpC and Fis1 do not seem to interact and DrpC localization does not change upon monensin treatment, it is unlikely that DrpC is involved in this process (90). Interactome analysis of Fis1 identified some proteins with domains of interest that are also found in Fis1 interactors of other systems. For example, TGGT1_224270 contains WD40-like domains, which is common to the Fis1 adaptor proteins (58, 59), and localizes to the mitochondrion (Fig. 9A). TGGT1_304990 is a guanylate-binding protein that may be able to take the role of a dynamin-related protein in this system. While in yeast Fis1 is essential, mammalian cells appear to have several proteins able to recruit the fission machinery, which makes Fis1 dispensable in those organisms. Knockout of *Toxoplasma* Fis1 does not disrupt mitochondrial morphology (92) or affect parasite fitness (83, 92). These results have been corroborated by our lab through CRISPR/Cas9. Interestingly, we do observe a significant defect in the morphology of the mitochondrion when the endogenous Fis1 is mislocalized to the cytoplasm. In both mammalian cells and in yeast, either mislocalization or overexpression of Fis1 results in disruption of mitochondrial morphology (58, 93). In *Toxoplasma,* mislocalization of Fis1 resulted in aberrant

mitochondrial morphology in which they maintain their lasso shape, but it is stretched out and appears to have strenuous branches and material. The phenotype observed with mislocalized Fis1 could the consequence of Fis1 interacting with proteins that it would normally not come into contact with or of Fis1 pulling proteins away from the mitochondrial membrane where they are required. With this in mind we performed a yeast two-hybrid screen to identify putative interactors. Interestingly, among the 24 proteins identified, seven (TGGT1_215520, TGGT1_218560, TGGT1_265180, TGGT1_246720, TGGT1_304990, TGGT1_321370, and TGGT1_321450) likely localize to the mitochondrion, based on a proteomic analysis of the *Toxoplasma* mitochondrion, which used both *BirA (94) and APEX (95, 96) to identify novel mitochondrial proteins (97). Nonetheless, this proteome may not contain all the potential interactors that localize to the mitochondrion because the proteome was generated using a mitochondrial matrix protein, HSP70, thus excluding proteins that are localized to the outer mitochondrial membrane. Our lab has endogenously tagged TGGT1_304990 and found that it localizes to the ER, which is corroborated by the recent LOPIT data (82). *In silico* analysis of the putative Fis1 interactors using MitoProt, SignalP, and PSort (98–100) shows that an additional 5 proteins (TGGT1_226050, TGGT1_237015, TGGT1_247700, TGGT1_299670, and TGGT1_286470) may also localize to the mitochondrion based on the presence of mitochondrial signal. Another protein of interest is TGGT1_287980 has a forkhead-associated (FHA) domain, which is involved in a number of regulatory and signaling processes (101), modulates protein-protein interactions through a

phosphorylation-dependent mechanism, and was found to localize to the IMC (Fig. 8B). Further characterization of these proteins is needed to determine what role they may play in mitochondrial remodeling and dynamics.

In this study, I focused on one of the putative Fis1 interactors, TGGT1_265180, which we have dubbed LMF1. This protein was the only one to be identified through both the Y2H and immunoprecipitation assays. LMF1 localizes to the OMM despite the absence of any domain or modification that would predict mitochondrial or membrane localization, suggesting that its association with the mitochondrion is likely through protein-protein interactions. When Fis1 is mislocalized to the cytoplasm, LMF1 expression is significantly reduced and while some LMF1 is still deposited on the mitochondrion, some does not appear to be associated with the organelle. LMF1 may not colocalize with Fis1 in these parasites because either protein may be interacting with other proteins or membranes. In the case of LMF1, there are potentially redundant interactors on the mitochondrial surface or interactors localized to other parts of the parasite, like the IMC, that are important for maintaining the mitochondrial lasso shape. Additionally, the expression level of LMF1 is decreased significantly when Fis1 is mislocalized, which may be due to either a decrease in the transcript level of LMF1 or that the protein is being degraded in the absence of potentially a stabilizing interaction with Fis1.

Genetic disruption of LMF1 reveals its unexpected role in maintenance of mitochondrial morphology in intracellular parasites. LMF1 knockout results in loss of the typical lasso arrangement with the majority of parasites having either sperm-

like or collapsed mitochondria. Thus, it appears that in the absence of LMF1 the mitochondrion of intracellular parasites adopts morphology normally only seen in extracellular ones. These mitochondrial morphologies, sperm-like and collapsed, are proposed to be due to a retraction of the mitochondrion from the IMC as the parasite transitions to the extracellular environment (48). Therefore, it is possible that elimination of LMF1 has also eliminated these contact sites, causing a significant decrease in parasites with lasso morphology intracellularly. Membrane contact sites (MCSs) play important roles in signaling, lipid and ion exchange between organelles, and proper organelle positioning (37, 102). Whether any of these processes are affected in the LMF1 mutant strain is yet to be investigated. Nonetheless, the fact that parasites lacking LMF1 exhibit a propagation defect suggest that the proper morphology of the mitochondrion is important for parasite fitness.

Loss of LMF1 not only resulted in growth defects and alterations in mitochondrial morphology but also caused a number of defects in mitochondrial segregation and division. It was observed that the mitochondrion was not properly partitioned during division, leaving some parasites without mitochondrial material and some vacuoles with extraneous mitochondrial material outside of the parasites (Fig. 17). As the parasites continued through division, mitochondrial material appeared to accumulate in the residual body and there were abnormal numbers of parasites per vacuole (Figs. 17A and 18B). These defects were also seen when the LMF1 knockout parasites were analyzed by transmission electron microscopy. Ultrastructural analysis revealed abnormal mitochondrial morphology, the

presence of more than two daughter parasites per mother during endodyogeny, and mitochondrial material within the residual body of the vacuole (Fig. 18). These data confirm that genetic ablation of LMF1 results in defects in both division and mitochondrial segregation, which may account for the growth defects seen *in vitro*. We noted that complementation of the knockout strain with the wildtype LMF1 was incomplete. While the exogenous copy was under the control of the *LMF1* promoter, it is possible that the expression level from the ectopic site is not at the right level for complete complementation. Another possibility is that, in order to adapt to the lack of LMF1, the expression of other factors required for mitochondrial morphology was affected. It is also plausible that the addition of an epitope tag in the exogenous protein affects function or protein-protein interactions. Nonetheless, we have not observed any mitochondrial defect when epitope tags are added in the endogenous LMF1.

To ameliorate the potential adaptation of *Toxoplasma* to LMF1 deletion, I endogenously tagged LMF1 with a destabilization domain (DD) to mediate conditional knockdown. This system allows us to control the level of LMF1 in the parasite, which prevents the parasites from adapting to its absence. This system was employed in parasites that stably express SOD2-GFP and IMC1-TdTomato to observe the mitochondrion and IMC, respectively. Upon removal of the ligand SHLD-1, LMF1 is no longer stable and is sent for proteasomal degradation, which results in mitochondrial collapse (Fig. 20C). We examined the mitochondrial morphology of these parasites in four concentrations of SHLD-1 and compared the frequency of lasso, sperm-like, and collapsed mitochondria to the parental line.

LMF1-HA-DD parasites in the absence of SHLD-1 and the lowest concentration (50nM) had significantly lower percentages of parasites with lasso mitochondria than that of parasites maintained in 150nM and 300nM compared to the parental (Fig. 21A). Additionally, there was a significant difference in parasite growth *in vitro* between 0nM and 150nM SHLD-1. This indicates that the level of LMF1 in the parasite is important for mitochondrial lasso maintenance and parasite growth.

Mitochondrial dynamics in other parasitic species

Plasmodium falciparum, the etiological agent of malaria and close relative to *Toxoplasma gondii*, has a single mitochondrion that is dynamic during various life stages. During division within the red blood cell, termed schizogeny, the mitochondrion elongates and begins to branch into the forming daughter parasites (103). *P. falciparum* is lacking many traditional homologs of mitochondrial fission and fusion machineries. There are no apparent homologs to mitofusins, which would predict a canonical fusion pathway (104, 105). *P. falciparum* has two candidate dynamin-related proteins, dubbed DYN1 and DYN2, that are do not appear to serve a role in mitochondrial division, but may participate in hemoglobin uptake and endomembrane trafficking, respectively (105, 106). There is one Fis1 homolog that was found to localize to the mitochondrion, but upon further observation and genetic disruption is not essential for parasite survival nor mitochondrial division, which is in accordance with the TgFis1 homolog (107).

Unlike *Toxoplasma*, *T. brucei* is harbors homologs to both a dynamin-like protein (TbDLP) and a fusion protein (TbMFNL) that appear to regulate

mitochondrial dynamics of its single mitochondrion. TbDLP localizes to the mitochondrion and to the site of endocytosis and, upon genetic disruption, prevents proper parasite division and mitochondrial fission (108). Silencing of the candidate mitofusin-like protein, TbMFNL, causes mitochondrial fragmentation, which is in accordance with defects in mitochondrial fusion seen in yeast (108). Interestingly, *Trypanosoma brucei* is another parasite that alters its shape in different life stages (109). During the procyclic phase in the tsetse fly midgut, the mitochondrion elongates to form an elaborate network of mitochondrial branches. In the bloodstream form, the branches collapse to form one tubule that lacks the respiratory capability of the procyclic stage. This mitochondrial morphology change is dependent on a protein called TbLOK1, which is naturally downregulated in the bloodstream form (109).

There are many possible explanations for the retraction from the IMC toward the apical end of *Toxoplasma* during extracellular stress is to a) position the mitochondrion to the area of greatest energetic need and/or b) accommodate to the available nutrients. I propose that LMF1 interacts with Fis1 on the OMM and another or multiple proteins in the parasite pellicle to establish membrane contact sites to maintain the typical lasso shape (Fig. 24). Upon egress, LMF1 or its interactors is either post-translationally modified or downregulated as to eliminate these contact sites and position the mitochondrion towards the apical end. Once the parasite has reentered a host cell, the mitochondrion can then reattach to the pellicle and can extend to the parasite periphery. LMF1 knockout parasites cannot properly form this lasso and therefore have given us an incredible tool to study the

functional relevance of the mitochondrial morphodynamics and to identify the key players in this process.

Membrane contact sites

The mitochondrial shape change observed in extracellular parasites is proposed to be a loss of membrane contact sites between the mitochondrion and the parasite pellicle (48). Since this phenotype is reminiscent of the shape change observed upon LMF1 deletion, I propose that LMF1 mediates this membrane contact site in *Toxoplasma gondii*. Membrane contact sites (MCSs) are defined by two organelles in close apposition to each other (within 30nm) whose interaction results in changes to one or both organelles (37). Typically, certain proteins are enriched at these sites and the membranes do not fully fuse with each other. MCSs play important roles in exchange of lipids and calcium between organelles, intraorganellar communication and signaling, and organelle inheritance during division (37). The MCSs that form between the ER and the mitochondrion are some of the best studied. One such membrane contact site occurs between the inositol 1, 4, 5-triphosphate receptor (IP_3R) on the ER and voltage-dependent anion channel 1 (VDAC1) on the outer mitochondrial membrane. A cytosolic chaperone, glucose-regulated protein 75 (grp75), mediates the membrane contact site between these two proteins to allow for Ca^{2+} exchange between the ER and the mitochondria (110–112). Although the putative MCS between the ER and the mitochondrion has not been identified in *Toxoplasma gondii* or other apicomplexans, a contact between the acidocalcisome, a major Ca^{2+} store, and

the mitochondrion has been observed in *Trypanosoma brucei.* In the kinetoplastid parasite, *T. brucei,* the IP_3R homolog localizes to the acidocalcisome (113). Using super-resolution imaging, Ramakrishnan et al. (113) found that these organelles were in close apposition to each other in both the procyclic and blood stage forms. As of now, this membrane contact site is one of the few studied within parasitic protists, which demonstrates the knowledge gap in this field.

Within Apicomplexa, the membrane contact site between the mitochondrion and the apicoplast has been observed in both *Plasmodium falciparum* and *Toxoplasma gondii.* During *P. falciparum* asexual stages, the mitochondrion and apicoplast appear in close proximity to one another until late trophozoite stages, where this association is less apparent (103). During *Toxoplasma* endodyogeny, the mitochondrion transiently interacts with the apicoplast during its elongation, but this apposition is not maintained throughout the cell cycle (16). These interactions are proposed to allow for metabolite and lipid exchange between these organelles. The proposed MCS between the *Toxoplasma* mitochondrion and the parasite pellicle is of particular importance to this study. Ovciarikova et al. (48) observed these two structures in close proximity to each other during the intracellular life stages of *Toxoplasma* using electron microscopy. It was observed that the mitochondrion and IMC were typically within <50nm, with these contacts being more extensive in intracellular parasites (48). It is proposed that these putative contact sites are lost in the extracellular environment, causing the mitochondrial collapse in extracellular parasites. Upon reentry into a host cell, the mitochondrion can reform these connections and reestablish the typical lasso shape. Based on

these data and the data presented above, we propose that LMF1 mediates the membrane contact site between these two organelles.

In order to determine what other proteins may be involved in these potential contact sites, we employed both yeast two-hybrid (Y2H) and immunoprecipitation (IP) of LMF1. Comparing putative interactors of both lists produced two likely interactors, IMC localizing protein 1 (ILP1) and IMC10. Of these, I investigated IMC10 further because of its localization and confidence of interaction with LMF1 by both methods. It was observed to localize to the IMC (Fig. 23A), in accordance with previous studies (86). LMF1 was immunoprecipitated and the resulting elution was analyzed by Western blot and probed for both LMF1-HA and IMC10-myc, which confirmed interaction between these two proteins (Fig. 23B). Further analysis of this interaction and others within the parasite pellicle are a priority to study in the future.

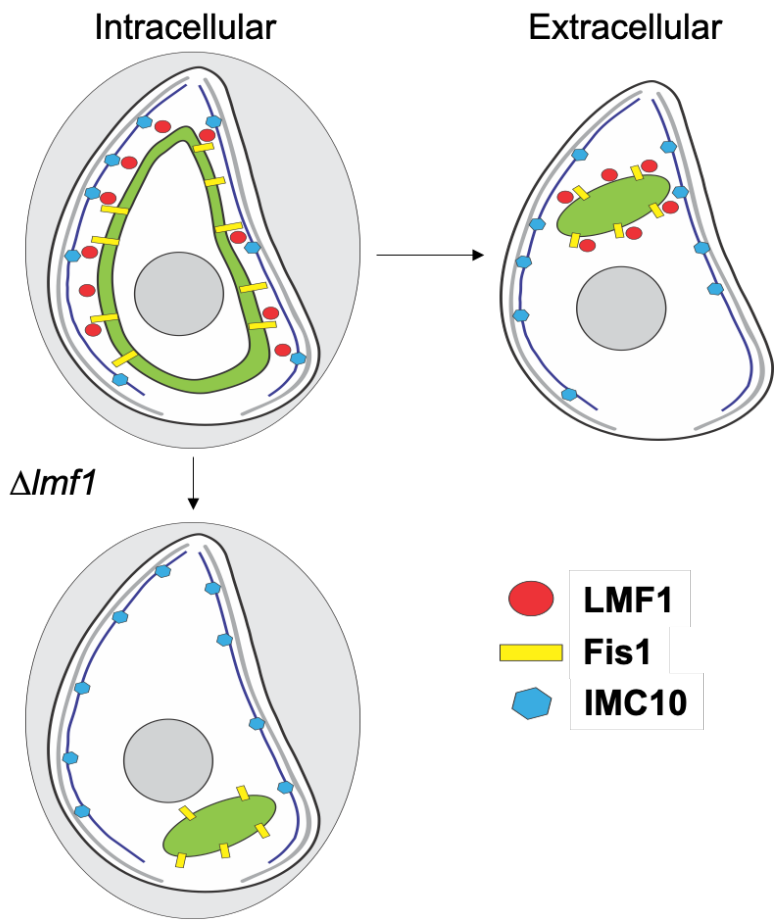

Figure 24. Model of the role of LMF1 and its interacting partners in mitochondrial morphodynamics. In this diagram, the mitochondrion of *Toxoplasma* is shown in green and extends to the parasite periphery. Fis1 is represented in yellow and is anchored to the OMM. LMF1, in red, interacts with Fis1 on the OMM and IMC10, in blue, on the IMC.

Our lab sought to determine the purpose of the mitochondrial retraction in extracellular parasites to the apical end of the parasites. To do this, we examined mitochondrial positioning throughout the lytic cycle of the parasite. The functional relevance of mitochondrial positioning is to position the mitochondria in areas of high energetic need. For example, mitochondria are positioned at the leading edge of lymphocytes to promote migration of the cell during chemotaxis (114). In *Toxoplasma*, mitochondrial movement to the apical end in the extracellular

environment may provide energetic support of secretion of the contents of the micronemes, rhoptries, and dense granules. These secretory organelles are essential for egress, attachment, invasion, and PV formation of *Toxoplasma gondii* and likely require energy while excreting their contents. To determine if mitochondrial position is important for these stages of the parasite lytic cycle, we observed the placement of the mitochondria of Δ*lmf1* and parental parasites while intracellular. Interestingly, we found that Δ*lmf1* mitochondrial positioning between the apical or basal end of the parasite was completely stochastic (Fig. 22A). Immediately after egress, the proportion of parasites that have apical or basal mitochondria does not change (Fig. 22B). However, directly after invasion, there is a significant difference between the percentage of parasites with apical mitochondria versus those with basal mitochondria, preferentially apical (Fig. 22C). It is unclear if this apical positioning allows *Toxoplasma* to be more efficient invaders or if parasites with basal mitochondria do not survive extracellularly. When we observed the levels of LMF1 in intracellular versus extracellular parasites, there was no apparent difference. This suggests that the mitochondrial shape change in extracellular parasites may be due to posttranslational modifications to LMF1 in extracellular parasites that eliminates mitochondrion-IMC contact sites.

Future directions

In this study, we have shown that a novel Fis1 interactor, LMF1, is required for maintaining mitochondrial shape and distribution to the periphery of the

Toxoplasma gondii. In the absence of LMF1, the mitochondrion collapses to from a lasso shape to a ball form. This aberrant morphology results in mitochondrial segregation defects and decreased parasite survival in tissue culture. Mitochondrial collapse also occurs when tachyzoites egress from the host cell and enter an extracellular environment. Currently, the functional significance of this shape change in extracellular parasites or in the absence of LMF1 is not known. One potential function is to move the mitochondrion to an area of higher energetic need in extracellular parasites. *Toxoplasma gondii* is metabolically flexible and is able to co-utilize glucose and glutamine (32, 115). However, extracellular parasites predominantly undergo glycolysis, which provides the energy necessary for parasite motility (115). To test if mitochondrial function is affected by the morphology change and contributes to parasite survival, I propose further examination of mitochondrial respiration and glycolysis of parental and Δ*lmf1* parasites. To determine if glycolysis or oxidative phosphorylation plays a role in parasite survival in the absence of LMF1, parasites will be cultured in the absence of glucose and/or glutamine. Additionally, parasites will be cultured in 2-deoxyglucose, to inhibit glycolysis, or atovaquone, to inhibit mitochondrial respiration (116, 117). These parasites will then be analyzed for oxygen consumption and extracellular acidification to examine changes in oxidative phosphorylation and glycolysis, respectively. Additionally, measuring ATP production of these parasites is of the utmost importance to understand the putative role of energy in mitochondrial collapse.

Our data demonstrated that the collapsed mitochondrial morphology in intracellular parasites results in a number of division defects, including parasites lacking mitochondrial material, extra mitochondrial material in the parasitophorus vacuole, and abnormal division of parasites (Figs. 17 and 18). I propose that these defects are due to the ablation of mitochondrion-IMC contact sites preventing the mother mitochondrion from interacting with the forming daughter IMCs. Therefore, the mitochondrion cannot migrate into the forming daughters and some parasites do not receive material and others are able to obtain some material. I propose using live imaging to better understand this connection between the two organelles during division. The LMF1-HA-DD parasite line stably expresses both SOD2-GFP and IMC1-TdTomato to observe the mitochondrion and IMC, respectively, which makes this line perfect for understanding the role LMF1 may play in mitochondrial segregation and division. We will observe these parasites in the presence and absence of SHLD-1 during division, egress, motility, and invasion. Additionally, we can use these parasites to observe the mitochondrial shape change in real time after removal of SHLD-1. These experiments will provide insight into mitochondrial dynamics of *Toxoplasma gondii* during the lytic cycle and how LMF1 affects these changes.

LMF1 deletion causes a mitochondrial shape change reminiscent to parasites exposed to the extracellular environment. However, it is not known what the natural trigger is to cause this shape change in the extracellular environment. A previous study demonstrated that high potassium, which mimic intracellular levels, still causes a mitochondrial collapse (48). Therefore, it is likely that there is

a different trigger in the extracellular environment than lowered potassium concentration. In addition to observe the mitochondrial shape change during the lytic cycle proposed above, I propose to also observe the mitochondrial shape in various conditions to determine the extracellular signal. For example, serum albumin is important for microneme secretion, motility, and invasion (118). Observing mitochondrial morphology in different concentrations of serum may alter the frequencies of lasso, sperm-like, and collapsed mitochondria extracellularly. In addition to different extracellular conditions, observing LMF1-HA-DD parasites in various concentrations of SHLD-1 in extracellular parasites may shift the mitochondrial morphology. For example, it is possible that parasites exposed to 300nM SHLD-1 in the extracellular milieu are able to maintain their lasso morphology longer than those maintained at 50nM SHLD-1. These experiments will determine if LMF1 levels are important for lasso maintenance and could explain differences between the endogenous and complemented morphology differences.

LMF1 protein levels did not differ between intracellular and extracellular parasites (Fig. 21D). Therefore, it is possible that the mitochondrial retraction from the IMC in extracellular parasites is due to differential posttranslational modifications (PTMs) of LMF1. In order to observe these differences, I propose mass spectrometric analysis of LMF1 extracted from intracellular and extracellular parasites. By comparing PTMs, such as phosphorylation, we can identify and mutate specific residues to observe if these modifications are essential to the mitochondrion-IMC membrane contact site and mitochondrial shape. *In silico*

analysis of LMF1 phosphorylation revealed that there are 12 phosphorylated residues, six of which are phosphorylated in either extracellular or intracellular parasites (ToxoDB). However, this experiment was done for all proteins and mass spectrometry of LMF1 specifically may yield different results. Interestingly, there is a patch of four phosphorylated residues within five amino acids. A similar phosphorylated patch is seen in the ceramide transport protein (CERT), which mediates the transport of ceramide from the ER to the Golgi (119, 120). When this patch is not phosphorylated, CERT mediates a membrane contact site between these organelles and promotes ceramide transport. However, when this patch is phosphorylated by protein kinase D and casein kinase 1, this connection is ablated and ceramide transport is repressed (119, 120). Therefore, I propose that the phosphorylated serine residues of the phosphorylated patch in LMF1 be mutated to either alanine or aspartic acid to inhibit and mimic phosphorylation, respectively. Mitochondrial morphology can then be observed in these mutants to determine if these phosphorylated residues are important for the mitochondrial-IMC MCS.

The mitochondrial-IMC membrane contact sites were shown to be more prevalent in intracellular parasites and are proposed to allow for peripheral distribution of the mitochondrion to its lasso shape (48). In this study, we have shown that LMF1 binds to Fis1 on the outer mitochondrial membrane and this interaction is essential for maintaining the typical lasso shape. We employed yeast two-hybrid and immunoprecipitations of LMF1 to determine potential interactors within the parasite pellicle (Tables 4 and 5). IMC10 and IMC-localizing protein 1 (ILP1) were the only proteins found in both of the generated lists. We have shown

by reciprocal co-IP that IMC10 is a LMF1 interactor (Fig. 23), but it is possible that IMC10 is redundant and LMF1 has multiple interacting partners on the IMC. Interestingly, ILP1 knockdown does have a mitochondrial morphology and segregation defect, although not quantified (86). Therefore, further study of ILP1 is warranted to determine if it is also a LMF1 interactor. Additionally, performing mass spectrometry of LMF1 in intracellular and extracellular parasites and identifying interactors in these conditions may reveal interactome differences. For example, it is plausible that LMF1 could have specific interactions with pellicle proteins in intracellular parasites, but these interactions are lost upon egress. Future work understanding the mechanism in which LMF1 mediates connections between the mitochondrion and parasite pellicle, proteins involved in these processes, and how these morphological changes affect parasite survival are important for determining the functional significance of mitochondrial morphology during the lytic cycle.

References

1. Dubey JP. 2008. The History of *Toxoplasma gondii* —The First 100 Years. J Eukaryot Microbiol 55:467–475.

2. Nicolle C, Manceaux. Sur une infection a` corps de Leishman (ou organismes voisins) du gondi. C R Seances Acad Sci 147:763–766.

3. Adl SM, Leander BS, Simpson AGB, Archibald JM, Anderson OR, Bass D, Bowser SS, Brugerolle G, Farmer MA, Karpov S, Kolisko M, Lane CE, Lodge DJ, Mann DG, Meisterfeld R, Mendoza L, Moestrup Ø, Mozley-Standridge SE, Smirnov AV, Spiegel F. 2007. Diversity, nomenclature, and taxonomy of protists. Syst Biol 56:684–689.

4. Cavalier-Smith T. 1993. Kingdom protozoa and its 18 phyla. Microbiol Rev 57:953–994.

5. Sibley DL, Charron A, Håkansson S, Mordue D. 2013. Invasion and Intracellular Survival by ToxoplasmaMadame Curie Bioscience Database [Internet]. Landes Bioscience.

6. Nichols BA, Chiappino ML. 1987. Cytoskeleton of Toxoplasma gondii. J Protozool 34:217–226.

7. Dubey JP, Frenkel JK. 1972. Cyst-induced toxoplasmosis in cats. J Protozool 19:155–177.

8. Dubey JP, Miller NL, Frenkel JK. 1970. THE TOXOPLASMA GONDII OOCYST FROM CAT FECES. J Exp Med 132:636–662.

9. Genova BMD, Wilson SK, Dubey JP, Knoll LJ. 2019. Intestinal delta-6-desaturase activity determines host range for Toxoplasma sexual reproduction. PLOS Biol 17:e3000364.

10. Blader IJ, Coleman BI, Chen C-T, Gubbels M-J. 2015. Lytic Cycle of Toxoplasma gondii: 15 Years Later. Annu Rev Microbiol 69:463–485.

11. Jones JL, Lopez A, Wilson M. 2003. Congenital Toxoplasmosis. Am Fam Physician 67:2131–2138.

12. Hill D, Dubey JP. 2002. Toxoplasma gondii: transmission, diagnosis and prevention. Clin Microbiol Infect Off Publ Eur Soc Clin Microbiol Infect Dis 8:634–640.

13. Derouin F, Pelloux H, ESCMID Study Group on Clinical Parasitology. 2008. Prevention of toxoplasmosis in transplant patients. Clin Microbiol Infect Off Publ Eur Soc Clin Microbiol Infect Dis 14:1089–1101.

14. Dobrowolski JM, Sibley LD. 1996. Toxoplasma Invasion of Mammalian Cells Is Powered by the Actin Cytoskeleton of the Parasite. Cell 84:933–939.

15. Anderson-White B, Beck JR, Chen C-T, Meissner M, Bradley PJ, Gubbels M-J. 2012. Cytoskeleton assembly in Toxoplasma gondii cell division. Int Rev Cell Mol Biol 298:1–31.

16. Nishi M, Hu K, Murray JM, Roos DS. 2008. Organellar dynamics during the cell cycle of Toxoplasma gondii. J Cell Sci 121:1559–1568.

17. Hg S, Ml M. 1968. The fine structure and reproduction of Toxoplasma gondii. J Parasitol 54:209–226.

18. Francia ME, Striepen B. 2014. Cell division in apicomplexan parasites. Nat Rev Microbiol 12:125–136.

19. Moudy R, Manning TJ, Beckers CJ. 2001. The loss of cytoplasmic potassium upon host cell breakdown triggers egress of Toxoplasma gondii. J Biol Chem 276:41492–41501.

20. Tomita T, Yamada T, Weiss LM, Orlofsky A. 2009. Externally Triggered Egress Is the Major Fate of Toxoplasma gondii during Acute Infection. J Immunol 183:6667–6680.

21. Scallan E, Hoekstra RM, Angulo FJ, Tauxe RV, Widdowson M-A, Roy SL, Jones JL, Griffin PM. 2011. Foodborne illness acquired in the United States--major pathogens. Emerg Infect Dis 17:7–15.

22. Furtado JM, Smith JR, Belfort R, Gattey D, Winthrop KL. 2011. Toxoplasmosis: A Global Threat. J Glob Infect Dis 3:281–284.

23. Tuazon CU. 1989. Toxoplasmosis in AIDS patients. J Antimicrob Chemother 23:77–82.

24. Chaudhry SA, Gad N, Koren G. 2014. Toxoplasmosis and pregnancy. Can Fam Physician 60:334–336.

25. Wallon M, Liou C, Garner P, Peyron F. 1999. Congenital toxoplasmosis: systematic review of evidence of efficacy of treatment in pregnancy. BMJ 318:1511–1514.

26. Goldstein EJC, Montoya JG, Remington JS. 2008. Management of Toxoplasma gondii Infection during Pregnancy. Clin Infect Dis 47:554–566.

27. McAuley J, Boyer KM, Patel D, Mets M, Swisher C, Roizen N, Wolters C, Stein L, Stein M, Schey W. 1994. Early and longitudinal evaluations of treated infants and children and untreated historical patients with congenital toxoplasmosis: the Chicago Collaborative Treatment Trial. Clin Infect Dis Off Publ Infect Dis Soc Am 18:38–72.

28. Garweg JG. 2016. Ocular Toxoplasmosis: an Update. Klin Monatsbl Augenheilkd 233:534–539.

29. Park Y-H, Nam H-W. 2013. Clinical Features and Treatment of Ocular Toxoplasmosis. Korean J Parasitol 51:393–399.

30. Grigg ME, Dubey JP, Nussenblatt RB. 2015. Ocular Toxoplasmosis: Lessons From Brazil. Am J Ophthalmol 159:999–1001.

31. Gould SB, Kraft LGK, van Dooren GG, Goodman CD, Ford KL, Cassin AM, Bacic A, McFadden GI, Waller RF. 2011. Ciliate Pellicular Proteome Identifies

Novel Protein Families with Characteristic Repeat Motifs That Are Common to Alveolates. Mol Biol Evol 28:1319–1331.

32. MacRae JI, Sheiner L, Nahid A, Tonkin C, Striepen B, McConville MJ. 2012. Mitochondrial Metabolism of Glucose and Glutamine Is Required for Intracellular Growth of Toxoplasma gondii. Cell Host Microbe 12:682–692.

33. Mazumdar J, Wilson EH, Masek K, Hunter CA, Striepen B. 2006. Apicoplast fatty acid synthesis is essential for organelle biogenesis and parasite survival in Toxoplasma gondii. Proc Natl Acad Sci 103:13192–13197.

34. Hu K, Johnson J, Florens L, Fraunholz M, Suravajjala S, DiLullo C, Yates J, Roos DS, Murray JM. 2006. Cytoskeletal Components of an Invasion Machine—The Apical Complex of Toxoplasma gondii. PLOS Pathog 2:e13.

35. Dubey R, Harrison B, Dangoudoubiyam S, Bandini G, Cheng K, Kosber A, Agop-Nersesian C, Howe DK, Samuelson J, Ferguson DJP, Gubbels M-J. 2017. Differential Roles for Inner Membrane Complex Proteins across Toxoplasma gondii and Sarcocystis neurona Development. mSphere 2.

36. Mann T, Beckers C. 2001. Characterization of the subpellicular network, a filamentous membrane skeletal component in the parasite Toxoplasma gondii. Mol Biochem Parasitol 115:257–268.

37. Helle SCJ, Kanfer G, Kolar K, Lang A, Michel AH, Kornmann B. 2013. Organization and function of membrane contact sites. Biochim Biophys Acta BBA - Mol Cell Res 1833:2526–2541.

38. Rowland AA, Voeltz GK. 2012. Endoplasmic reticulum–mitochondria contacts: function of the junction. 10. Nat Rev Mol Cell Biol 13:607–615.

39. Tamura Y, Kawano S, Endo T. 2019. Organelle contact zones as sites for lipid transfer. J Biochem (Tokyo) 165:115–123.

40. Tondera D, Grandemange S, Jourdain A, Karbowski M, Mattenberger Y, Herzig S, Da Cruz S, Clerc P, Raschke I, Merkwirth C, Ehses S, Krause F, Chan DC, Alexander C, Bauer C, Youle R, Langer T, Martinou J-C. 2009. SLP-2 is required for stress-induced mitochondrial hyperfusion. EMBO J 28:1589–1600.

41. Visser W, van Spronsen EA, Nanninga N, Pronk JT, Kuenen JG, van Dijken JP. 1995. Effects of growth conditions on mitochondrial morphology inSaccharomyces cerevisiae. Antonie Van Leeuwenhoek 67:243–253.

42. Mendl N, Occhipinti A, Müller M, Wild P, Dikic I, Reichert AS. 2011. Mitophagy in yeast is independent of mitochondrial fission and requires the stress response gene WHI2. J Cell Sci 124:1339–1350.

43. De Vos KJ, Allan VJ, Grierson AJ, Sheetz MP. 2005. Mitochondrial Function and Actin Regulate Dynamin-Related Protein 1-Dependent Mitochondrial Fission. Curr Biol 15:678–683.

44. Osellame LD, Singh AP, Stroud DA, Palmer CS, Stojanovski D, Ramachandran R, Ryan MT. 2016. Cooperative and independent roles of the

Drp1 adaptors Mff, MiD49 and MiD51 in mitochondrial fission. J Cell Sci 129:2170–2181.

45. van der Bliek AM. 2000. A Mitochondrial Division Apparatus Takes Shape. J Cell Biol 151:f1–f4.

46. Bleazard W, McCaffery JM, King EJ, Bale S, Mozdy A, Tieu Q, Nunnari J, Shaw JM. 1999. The dynamin-related GTPase Dnm1 regulates mitochondrial fission in yeast. Nat Cell Biol 1:298–304.

47. Friedman JR, Lackner LL, West M, DiBenedetto JR, Nunnari J, Voeltz GK. 2011. ER Tubules Mark Sites of Mitochondrial Division. Science 334:358–362.

48. Ovciarikova J, Lemgruber L, Stilger KL, Sullivan WJ, Sheiner L. 2017. Mitochondrial behaviour throughout the lytic cycle of Toxoplasma gondii. Sci Rep 7:42746.

49. Lavine MD, Arrizabalaga G. 2012. Analysis of monensin sensitivity in Toxoplasma gondii reveals autophagy as a mechanism for drug induced death. PloS One 7:e42107.

50. Besteiro S, Brooks CF, Striepen B, Dubremetz J-F. 2011. Autophagy protein Atg3 is essential for maintaining mitochondrial integrity and for normal intracellular development of Toxoplasma gondii tachyzoites. PLoS Pathog 7:e1002416.

51. Ghosh D, Walton JL, Roepe PD, Sinai AP. 2012. Autophagy is a cell death mechanism in Toxoplasma gondii. Cell Microbiol 14:589–607.

52. Charvat RA, Arrizabalaga G. 2016. Oxidative stress generated during monensin treatment contributes to altered Toxoplasma gondii mitochondrial function. Sci Rep 6.

53. van Dooren GG, Reiff SB, Tomova C, Meissner M, Humbel BM, Striepen B. 2009. An novel dynamin-related protein has been recruited for apicoplast fission in Toxoplasma gondii. Curr Biol CB 19:267–276.

54. Breinich MS, Ferguson DJP, Foth BJ, van Dooren GG, Lebrun M, Quon DV, Striepen B, Bradley PJ, Frischknecht F, Carruthers VB, Meissner M. 2009. A dynamin is required for the biogenesis of secretory organelles in Toxoplasma gondii. Curr Biol CB 19:277–286.

55. TgDrpC, an atypical dynamin-related protein in Toxoplasma gondii, is associated with vesicular transport factors and parasite division - Heredero-Bermejo - - Molecular Microbiology - Wiley Online Library.

56. Amiar S, Katris NJ, Berry L, Dass S, Shears MJ, Brunet C, Touquet B, Hakimi M-A, McFadden GI, Yamaryo-Botté Y, Botté CY. 2019. Division and adaptation to host nutritional environment of apicomplexan parasites depend on apicoplast lipid metabolic plasticity and host organelles remodelling. bioRxiv 585737.

57. Melatti C, Pieperhoff M, Lemgruber L, Pohl E, Sheiner L, Meissner M. 2019. A unique dynamin-related protein is essential for mitochondrial fission in Toxoplasma gondii. PLoS Pathog 15:e1007512.

58. Stojanovski D, Koutsopoulos OS, Okamoto K, Ryan MT. 2004. Levels of human Fis1 at the mitochondrial outer membrane regulate mitochondrial morphology. J Cell Sci 117:1201.

59. Zhang Y, Chan DC. 2007. Structural basis for recruitment of mitochondrial fission complexes by Fis1. Proc Natl Acad Sci 104:18526–18530.

60. Padgett LR, Arrizabalaga G, Sullivan WJ. 2017. Targeting of tail-anchored membrane proteins to subcellular organelles in Toxoplasma gondii. Traffic Cph Den 18:149–158.

61. Jacobs K, Charvat R, Arrizabalaga G. 2020. Identification of Fis1 Interactors in Toxoplasma gondii Reveals a Novel Protein Required for Peripheral Distribution of the Mitochondrion. mBio 11.

62. Charvat RA, Arrizabalaga G. 2016. Oxidative stress generated during monensin treatment contributes to altered *Toxoplasma gondii* mitochondrial function. Sci Rep 6:22997.

63. Donald R, Carter D, Ullman B, Roos D. 1996. Insertional tagging, cloning, and expression of the Toxoplasma gondii hypoxanthine-xanthine-guanine phosphoribosyltransferase gene Use as a selectable marker. J Biol … 271:14010–14019.

64. Huynh M, Carruthers V. 2009. Tagging of endogenous genes in a Toxoplasma gondii strain lacking Ku80. Eukaryot Cell 8:530–539.

65. Fox B, Ristuccia J, Gigley J, Bzik D. 2009. Efficient gene replacements in Toxoplasma gondii strains deficient for nonhomologous end joining. Eukaryot Cell 8:520–529.

66. Saeij JPJ, Arrizabalaga G, Boothroyd JC. 2008. A cluster of four surface antigen genes specifically expressed in bradyzoites, SAG2CDXY, plays an important role in Toxoplasma gondii persistence. Infect Immun 76:2402–10.

67. Donald R, Roos D. 1998. Gene knock-outs and allelic replacements in Toxoplasma gondii: HXGPRT as a selectable marker for hit-and-run mutagenesis. Mol Biochem Parasitol 91:295–305.

68. Arrizabalaga G, Ruiz F, Moreno S, Boothroyd JC. 2004. Ionophore-resistant mutant of Toxoplasma gondii reveals involvement of a sodium/hydrogen exchanger in calcium regulation. J Cell Biol 165:653–662.

69. Shen B, Brown KM, Lee TD, Sibley LD. 2014. Efficient Gene Disruption in Diverse Strains of Toxoplasma gondii Using CRISPR/CAS9. mBio 5:e01114-14.

70. Huet D, Rajendran E, Dooren GG van, Lourido S. 2018. Identification of cryptic subunits from an apicomplexan ATP synthase. eLife.

71. Gubbels M, Vaishnava S. 2006. A MORN-repeat protein is a dynamic component of the Toxoplasma gondii cell division apparatus. J Cell … 119:2236–2245.

72. LaFavers KA, Márquez-Nogueras KM, Coppens I, Moreno SNJ, Arrizabalaga G. 2017. A novel dense granule protein, GRA41, regulates timing of egress and calcium sensitivity in Toxoplasma gondii. Cell Microbiol https://doi.org/10.1111/cmi.12749.

73. Fromont-Racine M, Rain J-C, Legrain P. 1997. Toward a functional analysis of the yeast genome through exhaustive two-hybrid screens. Nat Genet 16:277–282.

74. Bartel PL, Chien CT, Sternglanz R, Fields S. Using the two-hybrid system to detect protein-protein interactions., p. 153–179. *In* Hartley, DA (ed.), Cellular Interactions in Development: A Practical Approach. Oxford University Press, Oxford.

75. Formstecher E, Aresta S, Collura V, Hamburger A, Meil A, Trehin A, Reverdy C, Betin V, Maire S, Brun C, Jacq B, Arpin M, Bellaiche Y, Bellusci S, Benaroch P, Bornens M, Chanet R, Chavrier P, Delattre O, Doye V, Fehon R, Faye G, Galli T, Girault J-A, Goud B, de Gunzburg J, Johannes L, Junier M-P, Mirouse V, Mukherjee A, Papadopoulo D, Perez F, Plessis A, Rossé C, Saule S, Stoppa-Lyonnet D, Vincent A, White M, Legrain P, Wojcik J, Camonis J, Daviet L. 2005. Protein interaction mapping: a Drosophila case study. Genome Res 15:376–384.

76. Fromont-Racine M, Rain JC, Legrain P. 1997. Toward a functional analysis of the yeast genome through exhaustive two-hybrid screens. Nat Genet 16:277–282.

77. Rodríguez-Negrete E, Bejarano ER, Castillo AG. 2014. Using the yeast two-hybrid system to identify protein-protein interactions. Methods Mol Biol Clifton NJ 1072:241–258.

78. Jayabalasingham B, Voss C, Ehrenman K, Romano JD, Smith ME, Fidock DA, Bosch J, Coppens I. 2014. Characterization of the ATG8-conjugation system in 2 Plasmodium species with special focus on the liver stage. Autophagy 10:269–284.

79. Xu C, Min J. 2011. Structure and function of WD40 domain proteins. Protein Cell 2:202–214.

80. Durocher D, Henckel J, Fersht AR, Jackson SP. 1999. The FHA domain is a modular phosphopeptide recognition motif. Mol Cell 4:387–394.

81. Praefcke GJK, McMahon HT. 2004. The dynamin superfamily: universal membrane tubulation and fission molecules? Nat Rev Mol Cell Biol 5:133–147.

82. Barylyuk K, Koreny L, Ke H, Butterworth S, Crook OM, Lassadi I, Gupta V, Tromer E, Mourier T, Stevens TJ, Breckels LM, Pain A, Lilley KS, Waller RF. 2020. A subcellular atlas of *Toxoplasma* reveals the functional context of the proteome. preprint, Cell Biology.

83. Sidik SM, Huet D, Ganesan SM, Huynh M-H, Wang T, Nasamu AS, Thiru P, Saeij JPJ, Carruthers VB, Niles JC, Lourido S. 2016. A Genome-Wide CRISPR Screen in Toxoplasma Identifies Essential Apicomplexan Genes. Cell 166:1423-1435.e12.

84. Anderson-White BR, Ivey FD, Cheng K, Szatanek T, Lorestani A, Beckers CJ, Ferguson DJP, Sahoo N, Gubbels M-J. 2011. A family of intermediate filament-like proteins is sequentially assembled into the cytoskeleton of Toxoplasma gondii. Cell Microbiol 13:18–31.

85. Choi CP, Moon AS, Back PS, Jami-Alahmadi Y, Vashisht AA, Wohlschlegel JA, Bradley PJ. 2019. A photoactivatable crosslinking system reveals protein interactions in the Toxoplasma gondii inner membrane complex. PLOS Biol 17:e3000475.

86. Chen AL, Kim EW, Toh JY, Vashisht AA, Rashoff AQ, Van C, Huang AS, Moon AS, Bell HN, Bentolila LA, Wohlschlegel JA, Bradley PJ. 2015. Novel Components of the Toxoplasma Inner Membrane Complex Revealed by BioID. mBio 6.

87. Morlon-Guyot J, Berry L, Chen C-T, Gubbels M-J, Lebrun M, Daher W. 2014. The Toxoplasma gondii calcium-dependent protein kinase 7 is involved in early steps of parasite division and is crucial for parasite survival. Cell Microbiol 16:95–114.

88. Brown KM, Sibley LD. 2018. Essential cGMP Signaling in Toxoplasma Is Initiated by a Hybrid P-Type ATPase-Guanylate Cyclase. Cell Host Microbe 24:804-816.e6.

89. Katris NJ, Yamaryo-Botte Y, Janouškovec J, Shunmugam S, Arnold C-S, Yang ASP, Vardakis A, Stewart RJ, Sauerwein R, McFadden GI, Tonkin CJ, Cesbron-Delauw M-F, Waller RF, Botte CY. 2020. Rapid kinetics of lipid second messengers controlled by a cGMP signalling network coordinates apical complex functions in Toxoplasma tachyzoites. bioRxiv 2020.06.19.160341.

90. Heredero-Bermejo I, Varberg JM, Charvat R, Jacobs K, Garbuz T, Sullivan WJ, Arrizabalaga G. 2019. TgDrpC, an atypical dynamin-related protein in Toxoplasma gondii, is associated with vesicular transport factors and parasite division. Mol Microbiol 111:46–64.

91. Yu R, Jin S, Lendahl U, Nistér M, Zhao J. 2019. Human Fis1 regulates mitochondrial dynamics through inhibition of the fusion machinery. EMBO J 38.

92. Melatti C, Pieperhoff M, Lemgruber L, Pohl E, Sheiner L, Meissner M. 2019. A unique dynamin-related protein is essential for mitochondrial fission in Toxoplasma gondii. PLOS Pathog 15:e1007512.

93. James DI, Parone PA, Mattenberger Y, Martinou J-C. 2003. hFis1, a Novel Component of the Mammalian Mitochondrial Fission Machinery. J Biol Chem 278:36373–36379.

94. Roux KJ, Kim DI, Raida M, Burke B. 2012. A promiscuous biotin ligase fusion protein identifies proximal and interacting proteins in mammalian cells. J Cell Biol 196:801–810.

95. Rhee H-W, Zou P, Udeshi ND, Martell JD, Mootha VK, Carr SA, Ting AY. 2013. Proteomic Mapping of Mitochondria in Living Cells via Spatially Restricted Enzymatic Tagging. Science 339:1328–1331.

96. Hung V, Zou P, Rhee H-W, Udeshi ND, Cracan V, Svinkina T, Carr SA, Mootha VK, Ting AY. 2014. Proteomic mapping of the human mitochondrial intermembrane space in live cells via ratiometric APEX tagging. Mol Cell 55:332–341.

97. Seidi A, Muellner-Wong LS, Rajendran E, Tjhin ET, Dagley LF, Aw VY, Faou P, Webb AI, Tonkin CJ, van Dooren GG. 2018. Elucidating the mitochondrial proteome of Toxoplasma gondii reveals the presence of a divergent cytochrome c oxidase. eLife 7:e38131.

98. Nakai K, Horton P. 1999. PSORT: a program for detecting sorting signals in proteins and predicting their subcellular localization. Trends Biochem Sci 24:34–36.

99. Claros MG, Vincens P. 1996. Computational method to predict mitochondrially imported proteins and their targeting sequences. Eur J Biochem 241:779–786.

100. Armenteros JJA, Tsirigos KD, Sønderby CK, Petersen TN, Winther O, Brunak S, Heijne G von, Nielsen H. 2019. SignalP 5.0 improves signal peptide predictions using deep neural networks. Nat Biotechnol 37:420–423.

101. Durocher D, Jackson SP. 2002. The FHA domain. FEBS Lett 513:58–66.

102. Eisenberg-Bord M, Shai N, Schuldiner M, Bohnert M. 2016. A Tether Is a Tether Is a Tether: Tethering at Membrane Contact Sites. Dev Cell 39:395–409.

103. Dooren GG van, Marti M, Tonkin CJ, Stimmler LM, Cowman AF, McFadden GI. 2005. Development of the endoplasmic reticulum, mitochondrion and apicoplast during the asexual life cycle of Plasmodium falciparum. Mol Microbiol 57:405–419.

104. Voleman L, Doležal P. 2019. Mitochondrial dynamics in parasitic protists. PLOS Pathog 15:e1008008.

105. Scarpelli PH, Tessarin-Almeida G, Viçoso KL, Lima WR, Borges-Pereira L, Meissner KA, Wrenger C, Raffaello A, Rizzuto R, Pozzan T, Garcia CRS. 2019. Melatonin activates FIS1, DYN1, and DYN2 Plasmodium falciparum related-genes for mitochondria fission: Mitoemerald-GFP as a tool to visualize mitochondria structure. J Pineal Res 66:e12484.

106. Li H, Han Z, Lu Y, Lin Y, Zhang L, Wu Y, Wang H. 2004. Isolation and functional characterization of a dynamin-like gene from Plasmodium falciparum. Biochem Biophys Res Commun 320:664–671.

107. Maruthi M, Ling L, Zhou J, Ke H. 2020. Dispensable Role of Mitochondrial Fission Protein 1 (Fis1) in the Erythrocytic Development of Plasmodium falciparum. mSphere 5.

108. Chanez A-L, Hehl AB, Engstler M, Schneider A. 2006. Ablation of the single dynamin of T. brucei blocks mitochondrial fission and endocytosis and leads to a precise cytokinesis arrest. J Cell Sci 119:2968–2974.

109. Povelones ML, Tiengwe C, Gluenz E, Gull K, Englund PT, Jensen RE. 2013. Mitochondrial shape and function in trypanosomes requires the outer membrane protein, TbLOK1. Mol Microbiol 87:713–729.

110. Szabadkai G, Bianchi K, Várnai P, De Stefani D, Wieckowski MR, Cavagna D, Nagy AI, Balla T, Rizzuto R. 2006. Chaperone-mediated coupling of endoplasmic reticulum and mitochondrial Ca2+ channels. J Cell Biol 175:901–911.

111. Csordás G, Várnai P, Golenár T, Roy S, Purkins G, Schneider TG, Balla T, Hajnóczky G. 2010. Imaging Interorganelle Contacts and Local Calcium Dynamics at the ER-Mitochondrial Interface. Mol Cell 39:121–132.

112. Csordás G, Renken C, Várnai P, Walter L, Weaver D, Buttle KF, Balla T, Mannella CA, Hajnóczky G. 2006. Structural and functional features and

significance of the physical linkage between ER and mitochondria. J Cell Biol 174:915–921.

113. Ramakrishnan S, Asady B, Docampo R. 2018. Acidocalcisome-Mitochondrion Membrane Contact Sites in Trypanosoma brucei. Pathogens 7.

114. Campello S, Lacalle RA, Bettella M, Mañes S, Scorrano L, Viola A. 2006. Orchestration of lymphocyte chemotaxis by mitochondrial dynamics. J Exp Med 203:2879–2886.

115. Nitzsche R, Zagoriy V, Lucius R, Gupta N. 2016. Metabolic Cooperation of Glucose and Glutamine Is Essential for the Lytic Cycle of Obligate Intracellular Parasite *Toxoplasma gondii*. J Biol Chem 291:126–141.

116. Lin SS, Blume M, von Ahsen N, Gross U, Bohne W. 2011. Extracellular Toxoplasma gondii tachyzoites do not require carbon source uptake for ATP maintenance, gliding motility and invasion in the first hour of their extracellular life. Int J Parasitol 41:835–841.

117. Baggish AL, Hill DR. 2002. Antiparasitic Agent Atovaquone. Antimicrob Agents Chemother 46:1163–1173.

118. Brown KM, Lourido S, Sibley LD. 2016. Serum Albumin Stimulates Protein Kinase G-dependent Microneme Secretion in Toxoplasma gondii. J Biol Chem 291:9554–9565.

119. Hanada K. 2018. Lipid transfer proteins rectify inter-organelle flux and accurately deliver lipids at membrane contact sites. J Lipid Res 59:1341–1366.

120. Kumagai K, Kawano M, Shinkai-Ouchi F, Nishijima M, Hanada K. 2007. Interorganelle trafficking of ceramide is regulated by phosphorylation-dependent cooperativity between the PH and START domains of CERT. J Biol Chem 282:17758–17766.

Curriculum Vitae

Kylie Jacobs

Education

Doctor of Philosophy

Major: Microbiology and Immunology

Minor: Individualized- Epidemiology

Indiana University-Purdue University Indianapolis (Indianapolis, IN)

February 2021

Thesis: Characterization of a novel Fis1 interactor required for peripheral distribution of the mitochondrion of *Toxoplasma gondii*

Mentor: Gustavo Arrizabalaga, Ph.D.

Bachelor of Science

Hope College (Holland, MI)

May 2016

Majors: Biochemistry/Molecular Biology

Research Experience

Graduate Student

Indiana University School of Medicine (Indianapolis, IN)

Department of Microbiology and Immunology

Mentor: Gustavo Arrizabalaga, Ph.D.

May 2017- December 2020

Area of study: Mitochondrial dynamics of *Toxoplasma gondii*

Undergraduate Researcher

University of Pittsburgh School of Medicine (Pittsburgh, PA)

Department of Neuropathology

Mentors: Drs. Clayton Wiley and Stephanie Bissel

June 2015- August 2015

Area of study: Examine the proliferative and pro-survival effects of YKL-40 on neuronal and glial cells

Hope College (Holland, MI)

Department of Biology

Mentor: Dr. Joseph Stukey

August 2014- May 2015

Area of study: Identify novel mycobacteriophage cytotoxic genes

Publications

Jacobs, K., Charvat, R., Arrizabalaga, G. (2020). Identification of Fis1 interactors in *Toxoplasma gondii* reveals a novel protein required for peripheral distribution of the mitochondrion. mBio 11:e02732-19. https://doi.org/10.1128/mBio.02732-19. *Editor's Pick.*

Shao, Y., Wichern, E., Childress, P. J., Adaway, M., Wellbrook, C., Burr, D. B., Wek, R.C., Mosely, A. L., Liu, Y., Robling, A. G., McClintick, J. N.,

Brustovetsky, N., Hamilton, J., **Jacobs, K**., Stayrook, K. R., Krishnan, V., Elliot, J., Allen, M. R., Wallace, J. M., Bidwell, J. P. (2019). Loss of Nmp4 optimizes osteogenic metabolism and secretion to enhance bone quality. Am J Physiol Endocrinol Metab. https://doi.org/10.1152/ajpendo.00343.2018.

Heredero-Bermejo, I., Varberg, J. M., Charvat, R., **Jacobs, K**., Garbuz, T., Sullivan, W. J., Jr., & Arrizabalaga, G. (2018). TgDrpC, an atypical dynamin-related protein in *Toxoplasma gondii*, is associated with vesicular transport factors and parasite division. Mol Microbiol. https://doi.org/10.1111/mmi.14138.

Funding

- T32 Immunology and Infectious Disease trainee (2T32AI060519-16) October 2017- November 2020
- IUPUI Travel Fellowship 2019 ($1000)

Honors and Awards

- IUSM Dean's List: Fall 2016-Fall 2018
- ASBMB Degree Certification
- Hope College Sigma Xi Senior Chemistry Research Award
- Hope College Dean's List: Fall 2012, Fall 2013, Fall 2015
- Hope College Presidential Scholarship

Selected Presentations

Kylie Jacobs, Gustavo Arrizabalaga. Understanding the role of mitochondrial pellicle membrane contact sites in Toxoplasma gondii. (Oral presentation) Molecular Parasitology Meeting; September 2020; Virtual.

Kylie Jacobs, Robert Charvat, Gustavo Arrizabalaga. Understanding the role of mitochondrial pellicle membrane contact sites in Toxoplasma gondii. (Oral presentation) International Toxoplasma Congress; June 2019; Quimbaya, Quindío, Colombia.

Kylie Jacobs, Robert Charvat, Tamila Garbuz, Gustavo Arrizabalaga. Characterizing novel Fis1 interactors to examine mitochondrial dynamics in Toxoplasma gondii. (Poster presentation) Molecular Parasitology Meeting; September 2018; Marine Biological Laboratories, Woods Hole, MA.

Kylie Jacobs, Robert Charvat, Tamila Garbuz, Gustavo Arrizabalaga. Characterizing novel Fis1 interactors to examine mitochondrial dynamics in Toxoplasma gondii. (Oral presentation) Biology of Intracellular Pathogens (BIP) Retreat; June 2018; Indiana University School of Medicine, Indianapolis, IN.

Teaching Experience

Experimental Design and Grant Writing Teaching Assistant

IUSM Department of Pharmacology and Toxicology

Summer 2020

- Moderated small group discussions and mock grant reviews in addition to evaluating grant materials and providing feedback to students.

Biochemistry Laboratory Teaching Assistant

Hope College Department of Chemistry

2015-2016

- Teaching assistant for a NSF-IUSE funded biochemistry lab experience that taught students biochemical methods and techniques while determining the function of uncharacterized proteins.

Organic Chemistry Laboratory Teaching Assistant

Hope College Department of Chemistry

2014-2016

- Aided students with organic chemistry laboratory techniques, answered questions pertaining to both lab and lecture, and maintained a safe environment for students.

Mentoring Experience

Summer Undergraduate Research Experience in the Biomedical Sciences (SUREBS) at IUSM

IUSM Department of Pharmacology and Toxicology

Summer 2019

- I guided an undergraduate student through a research project studying putative Fis1 interactors and their potential role in mitochondrial dynamics using techniques such as CRISPR/Cas9-mediated endogenous tagging and drug-inducible knockdown systems. Additionally, I served as a panelist to talk to SUREBS students about graduate school, work/life balance, and how to be an efficient researcher during their summer internship.

Organic Chemistry Laboratory Teaching Assistant

Hope College Department of Chemistry

Fall 2015

- I was asked by the department to be the sole TA of a student with severe learning disabilities. I assisted them in learning how to efficiently take notes during lab, kept the student on track, and was able to cut their time spent in lab from 10 hours per week to 5 hours.